Evaluating Temperature Impact On Solar Home Systems (SHS)

From the components to the systems level

Yunizar Natanael Pragistio

Technische Universiteit Delft

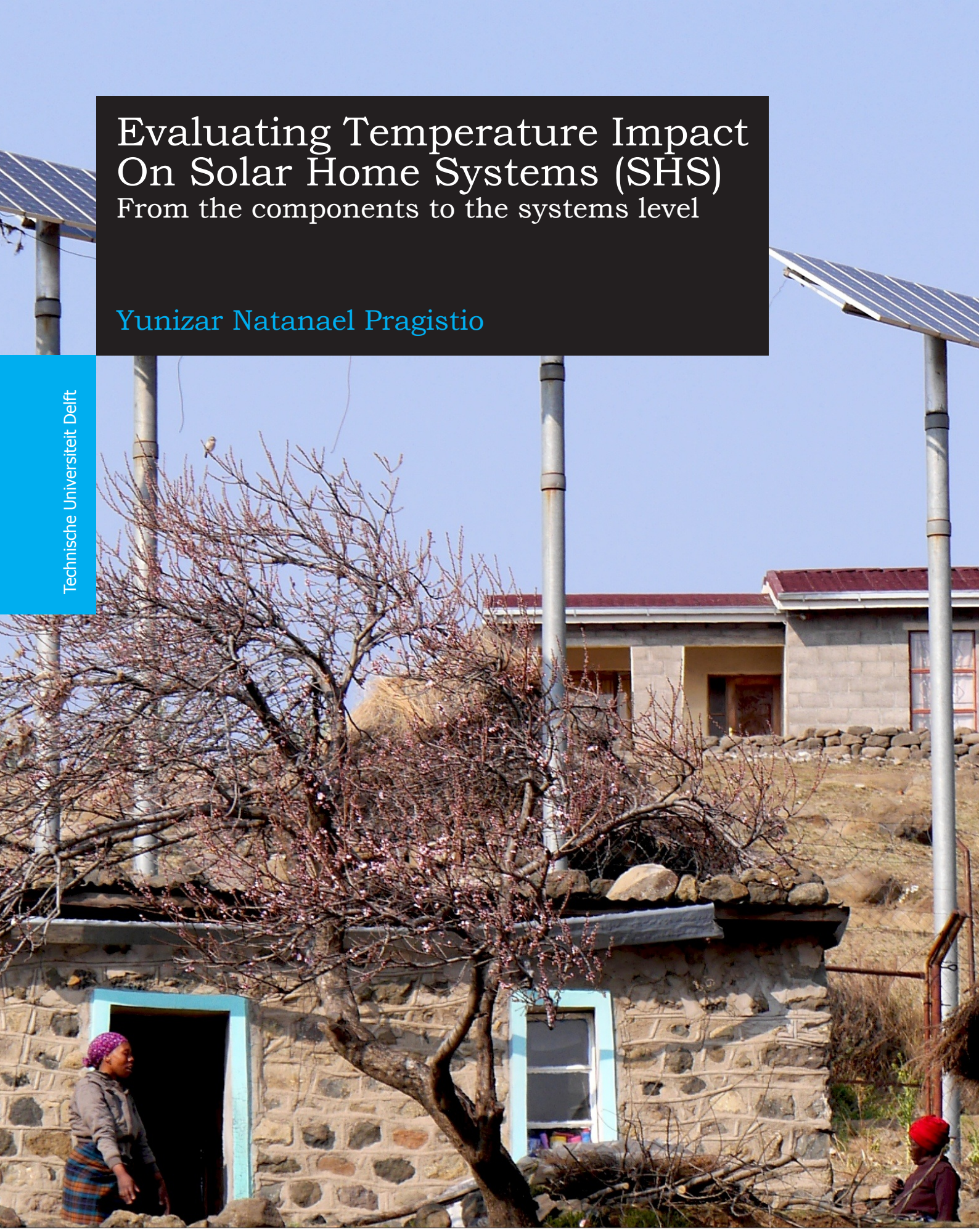

TU Delft Delft University of Technology

Challenge the future

Evaluating Temperature Impact On Solar Home Systems (SHS)

From the components to the systems level

by

Yunizar Natanael Pragistio

in partial fulfillment of the requirements for the degree of

Master of Science
in Sustainable Energy Technology

at the Delft University of Technology,
to be defended publicly on Thursday August 30, 2018 at 01:30 PM.

Supervisor:	Dr. ir. Z. Qin,	DCE&S - TU Delft
Advisor:	Nishant Narayan M.Sc.,	DCE&S - TU Delft
	Victor Vega-Garita M.Sc.,	DCE&S - TU Delft
Thesis committee:	Prof. dr. P. Bauer,	DCE&S - TU Delft
	Dr. ir. Z. Qin,	DCE&S - TU Delft
	Dr. O. Isabella,	PVMD - TU Delft

This thesis is confidential and cannot be made public until August 30, 2019.

TU Delft Delft University of Technology

Acknowledgement

This master thesis work represents the applied knowledge during my study in Sustainable Energy Technology (SET) at TU Delft. This work also represents my desire in alleviating the energy poverty through solar energy technology in the developing world, especially in my country, Indonesia. The ups and downs that I have been going through for the past nine months are a valuable learning process for me. I would like to thank some people who have contributed and drove me to go through all the learning experiences.

First of all, I would like to express my sincere gratitude to my parents who have given me the opportunity to study and who have supported me in everything.

Secondly, I would like to thank all the employees in DC Systems, Energy Conversion & Storage (DCE&S) group. I would like to acknowledge my main supervisor, Dr. ir. Zian Qin who has given me his guidance and positive feedbacks. Besides, I would like to thank my thesis committees, Prof. dr. Pavol Bauer and Dr. Olindo Isabella for the constructive discussion and comments.

Also, all of this thesis work cannot be done without my daily supervisors: Nishant Narayan and Victor Vega-Garita. Thank you for sparking the topic idea of my thesis where I find this is very enjoyable and meaningful. Also thank you for always building up my spirit, guiding me, and setting a high standard in writing scientifically.

I would like to give special gratitude to my Indonesian friends in Delft. Thank you for the delightful memories and lessons that we have shared during my study.

All of my friends in Sustainable Energy Technology (SET) deserve particular attention as they have contributed to my learning process at TU Delft through discussions and talks.

Lastly, I would like to thank all the people whose name are not on the list who have helped me during my study in Delft.

Yunizar Natanael Pragistio
Delft, August 2018

Nomenclature

Constants

σ	Boltzmann constant	1.38064852 $\times 10^{-23}$ $m^2 \cdot kg \cdot s^{-2} \cdot K^{-1}$
g	Gravity constant	9.81 m^2
G^{STC}	Irradiation at standard testing condition	1000 W/m^2
q	Electron charge	1.6021765 $\times 10^{-19}$ C
T^{STC}	Temperature at standard testing condition	25 °C

Number Sets

i	Number of arbitary events
t	Number of time steps

Subscript

amb	Ambient
back	Back
bb	Batteries
diffuse	Diffuse
direct	Direct
dw	Degradation-warranty
exp	Exponential region
forced	Forced
free	Free
full	Full region
ground	Ground
max	Maximum region
mpp	Maximum Power Point
m	Module (PV)
nom	Nominal region
pv	Photovoltaic
rated	Rated
ref	Reference
sky	Sky
s	Sun
thr	Throughput
top	Top

Meteorology

α Albedo (-)

cc Cloud coverage (okta)

G Irradiance (W/m2)

u Wind speed (m/s)

Photovoltaic Modules

α Thermal voltage (V)

γ Angle of incidence (-)

σ Emissivity of the glass surface (-)

θ Module tilt angle (°)

φ Absorption coefficient (-)

A Azimuth angle (°)

a Elevation angle (°)

D_h Hydraulic diameter (m)

Ea Activation energy (eV)

Gr Grashof number (-)

h_r Convection coefficient (W/(m^2·K))

I_o Saturation current (A)

I_{ph} Photocurrent (A)

$k_{I_{sc}}$ Thermal coefficient of short circuit current ($\%/^\circ C$)

k_p Thermal coefficient of power ($\%/^\circ C$)

$k_{V_{oc}}$ Thermal coefficient of open circuit voltage ($\%/^\circ C$)

n Diode ideality factor (-)

Nu Nusselt Number (-)

Pr Prandtl number (-)

Pr Reyonlds number (-)

R_D Degradation rate (%/year)

rh Relative Humidity (%)

Batteries

α Polarization constant thermal coefficient (-)

β Internal resistance thermal coefficient (-)

$\frac{dE}{dT}$ Voltage constant thermal coefficient (-)

$\frac{dQ}{dT}$ Battery capacity thermal coefficient (-)

A Exponential zone amplitude (V)

B Exponential zone time constant inverse (Ah^{-1})

D Battery degradation damage (-)

E Energy content (Wh)

E_o Voltage constant (V)

it Actual battery charge (Ah)

K Polarization constant (V Ah^{-1}) or polarization resistance (Ω)

N Battery equivalent (-)

n Battery cycle life (-)

Nb_{par} Number of batteries in parallel (-)

Nb_{ser} Number of batteries in series (-)

Q Charge throughput (Ah)

R Battery internal resistance (Ω)

Solar Home Systems

LLP Loss of load probability (%)

Other Symbols

η Efficiency (-)

ν Kinematic viscosity (m^2/s)

ρ Density (kg/cm^3)

c Heat capacity (J/K)

i current (A)

I_{sc} Short circuit current (A)

P Power (W)

T Temperature ($^{\circ}C$)

v voltage (V)

V_{oc} Open circuit voltage (V)

Accronym

AC Alternating Current

DC Direct Current

DHI Diffuse horizontal irradiation

DNI Direct normal irradiation

DOD Depth of Discharge

EOL End of life

ESH Equivalent Sun Hour

ESR Equivalent Series Resistance

FD Fluid Dynamic

GHI Global horizontal irradiation

Li-ion Lithium-ion

LLP Loss of Load Probability

MATLAB Matrix Laboratory

MPPT Maximum Power Point Tracking

MPP Maximum Power Point

MTTF Mean Time to Failure

NGO Non-Governmental Organization

NOCT Nominal Operating Cell Temperature

PMS Power Management Systems

PVM Point Value Model

PV PhotoVoltaic

SDM Single Diode Model

SEI Solid Electrolyte Interface

SF Scaling Factor

SHS Solar Home Systems

SLA Sealed Lead-Acid

SOC State of Charge

SOH State of Health

STC Standard Testing Condition

ZC Zero Crossing

Abstract

Access to electricity still lacks for a fifth of the world's population. Most of the areas are in the remote rural location. Due to the off-grid location, policies, and other social factors, the grid expansion in these areas is not economically viable. Installing Solar Home Systems (SHS) is considered to be a promising immediate solution, given that most of these areas are in the tropical region where it has the highest sun-hours in the world. SHS consists of PV modules for the energy generation, batteries for the energy storage, converters for the energy conversion, and load appliances for the energy consumption. However, its high ambient temperature can potentially harm the SHS in decreasing the performance and shortening the lifetime. The lower performance and lifetime can directly translate to have high capital expenses. Therefore a precise quantification of the performance and the lifetime is essential to all the stakeholders.

This thesis aims to evaluate and quantify the influence of temperature on the performance and the lifetime of SHS. In order to achieve the research goal, an integrated SHS model is proposed by considering the performance and the aging behavior of both PV modules and the batteries. Two different battery technologies: Li-ion and Lead-acid are involved in the evaluation. Moreover, the analysis was conducted for Sumba Island, Indonesia since it has great solar potential and also the potential market for the SHS. Furthermore, this work presents a comprehensive investigation of temperature impact from the PV module and battery component level to the system level.

Initial system design has been performed in which it requires a 330 Wp PV module, with a tilt and azimuth angle of 11° and 6° respectively, and 960 Wh of batteries to achieve the LLP of 9.5%. The simulation result of the PV component showed clearly that the PV energy yield reduces due to the higher ambient temperature is used. As for the battery, there is a converse behavior concerning the temperature impact in which an increase in temperature gives a positive impact on the capacity and internal resistance in the short term. However, in the long run, it has a severe aging rate.

By combining PV module and battery element in an integrated SHS model, it is shown that it achieves to have a 7.4% lower LLP compared to the initial sizing. However, as the aging plays a part, the LLP increases exponentially over the years, and can achieve almost doubled the initial LLP. As the ambient temperature increases, it results to have even higher LLP. Furthermore, it is seen that the system lifetime is limited by the battery lifetime. A decreasing trend of battery lifetime is observed as the ambient temperature increases.

Contents

1

Introduction

1.1. Background

It was recorded in 2015, nearly a fifth of the world's population have no access to the electricity, with around 85% of them living in the rural areas [1]. Technical factors, such as topography, and other social factors, such as policies and regional factors, limit grid-based electrification as an immediate solution to alleviate the energy poverty [2]. Installing SHS is considered to be a promising immediate solution, given that most of these regions lie in the highest sun-hours in the world. With the high percentage of un-electrified region, the potential market for renewable energy generators, especially solar home systems (SHS) is enormous. A solar home system is an integrated stand-alone solar system which is placed in a single household or shop. These systems range from 50 W to approximately 250 W rating [3].

One of the most significant barriers is the financial constraint which comes from the system costs. Given the rural area application, the high system costs affect both companies and consumers directly [4]. The costs can be seen as the upfront costs and the lifetime costs, such as the replacement and maintenance costs. Any reduction in performance, permanent degradation, or adding unnecessary components will directly impact the total system costs given that the energy price is the crucial parameter for rural off-grid market [5]. Therefore, any efforts to minimize the system's costs have been an important aspect to provide affordable SHS to rural households.

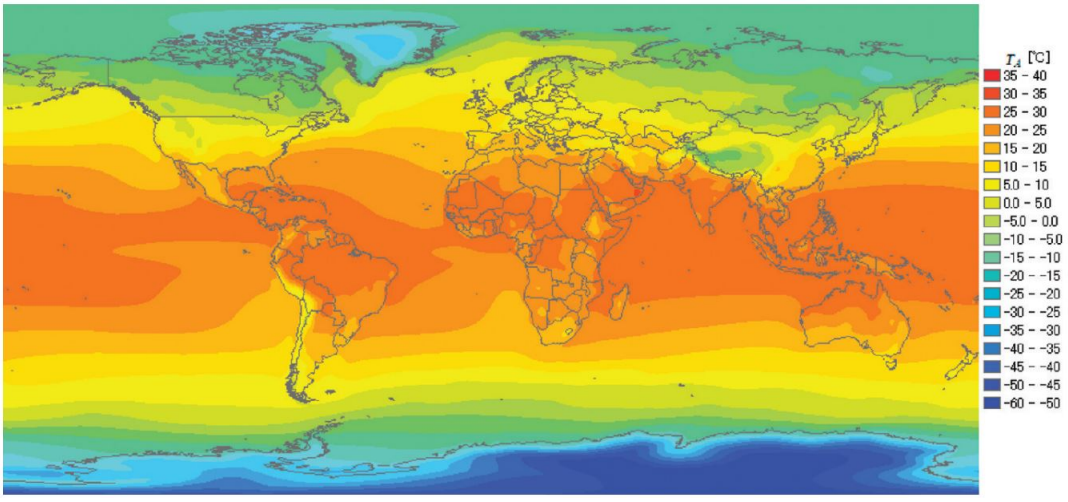

Figure 1.1: Global map of average ambient temperature [6]

Temperature plays a significant contribution to the performance, the aging, and the lifetime of SHS main components; PV modules, batteries, and power converters [7] [8] [9]. Moreover, most of the rural areas that are under-electrified lies in the (near) tropical region where the average ambient temperature are much higher than 25 °C as depicted in Figure 1.1. A higher temperature than the standard testing conditions (STC) will potentially harm the SHS components. Lower performance and lifetime translate

directly into less power produced and more replacement frequency [10]. Hence, it brings to the reduction of future cash flows. Therefore, A precise quantification of performance and lifetime is essential to all stakeholders.

Some researchers have developed models for determining the thermal effect on the performance and the lifetime of the PV systems. However, the models describe the analysis of the components of the PV systems (solar panels, batteries, or power converters) individually. There are still several gaps to fill in gaining the insight of the thermal implication on the performance of the whole PV systems. Therefore, in this research, an integrated model from the components level is built to describe the thermal effect on the performance and lifetime of the entire PV systems.

1.2. Research Goal

The main goal of this research is to **'Evaluate and quantify the influence of temperature profile on the performance and the lifetime of SHS**. The work focuses on investigating the performance, the aging, and the lifetime of SHS components concerning the temperature.

1.3. Research Questions

To achieve the research goal, several research questions are formulated:

1. How does the temperature affect the performance of the system? (*Ch. 6*)
   (a) To what extent the temperature will influence the dynamic performance of the PV module? (*Ch. 4*)
   (b) To what extent the temperature will influence the dynamic and aging performance of the battery? (*Ch. 5*)
2. How does the temperature impact the lifetime of the system? (*Ch. 6*)
   (a) To what extent the temperature will affect the lifetime of the PV modules? (*Ch. 4*)
   (b) To what extent the temperature will affect the lifetime of the batteries? (*Ch. 5*)

1.4. Scope and Structure

This report aims to provide readers the insight of temperature impact on a single SHS. This impact consists of the dynamic-aging performance and the lifetime of the systems. Besides that, the impact analysis is also made at a power level. A proposed comprehensive model is built by taking into account the main components, such as PV modules and batteries. However, the temperature dependence performance, aging, and lifetime of power electronics is not quantified in this research.

In the research approach, the analysis is divided into two stages. The first stage is the model construction and temperature impact assessment at the component level. The second stage is the integrated model construction by incorporating SHS components and temperature evaluation on a system level. The thesis workflow is illustrated in Figure 1.2. Moreover, the report is organized as follows:

- **Chapter 2**
  It provides the review of Solar Home Systems (SHS). It explains the definition of SHS, including the application, the system topology, and the design approach. A brief explanation of its components and their behavior against the temperature is described. Moreover, the state of the art of the temperature evaluation on SHS is widely described here.
- **Chapter 3**
  It presents the location details of Sumba Island, Indonesia which includes the meteorological data and the load profile.
- **Chapter 4**
  It elaborates more in-depth the behavior of a PV module as an energy generation with the influence of temperature, given a specific location and PV technology. The PV model consists of several submodels such as, the thermal model, the electrical model, and the aging model, that defines the performance and lifetime of PV modules. The power output of the PV model is used as a power generation in supplying the load and batteries.

- **Chapter 5**
  It describes further the dynamic behavior of a battery as energy storage with the dependency of temperature, given a specific location, battery technology, and load profile. The battery model contains the dynamic and aging model in which linking both models will determine the performance and lifetime aging of a battery. In this chapter, to evaluate the battery behavior, an off-grid PV system simulation is conducted together with the proposed initial system sizing methodology.

- **Chapter 6**
  It describes the overall temperature dependency at a system level, by taking into account the PV and battery model. Through the introduced case study, the SHS is evaluated by comparing different ambient temperature with a scaling factor.

- **Chapter 7**
  It draws the conclusions and the recommendations based on the simulation results.

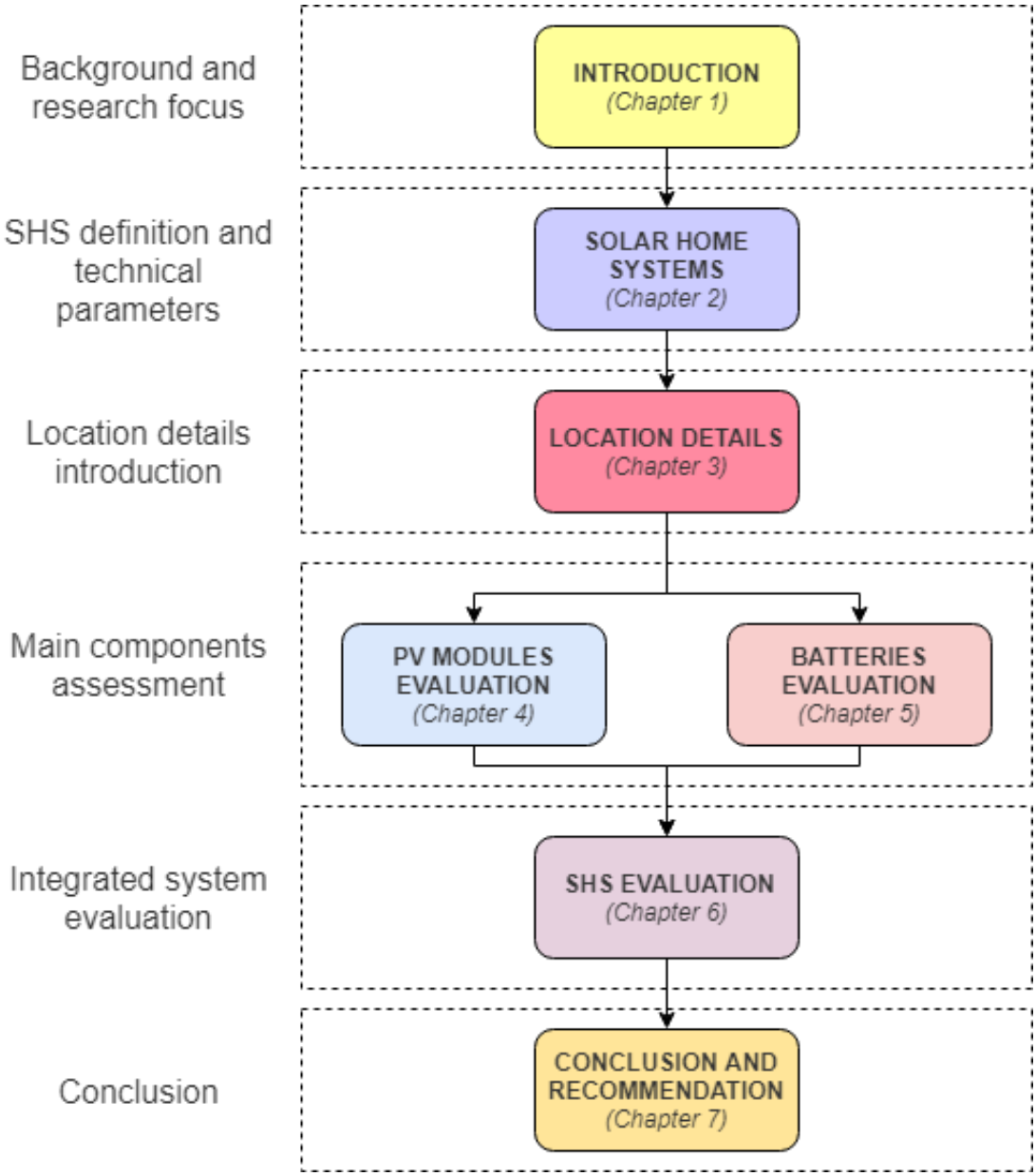

Figure 1.2: Thesis work flow

1.5. Research contribution

Apart from the research goal, this work has several unique contributions that can be used for other research in a broad application. More specifically, these contributions are:

- This work developed the battery model by incorporating the dynamic and the cyclic aging behavior in which both of them interact through a loop. As the battery generates the dynamic voltage, it can be implemented in the power management systems model or the battery management systems model. Furthermore, this battery model can potentially be used not only for off-grid PV systems application but also electric vehicles application.
- Secondly, this work provides an integrated model of SHS by taking into account the PV model and the battery model. It is indeed a practical model that requires only PV module and battery datasheet to work. Although the integrated model was meant to be developed for the SHS evaluation, it can also be used for the off-grid solar PV generator on a bigger scale by further correction. With its simplicity, the SHS product developer or off-grid PV designers can easily utilize the model to predict the lifetime of the battery and the performance under aging in an offline simulation. The lifetime and the degradation phenomenon are significant in predicting the total cost of the systems and its warranty in the end.

2

Solar Home Systems (SHS)

In this chapter, the underlying SHS concept is further explained. Section 2.1 to 2.3 explains the general overview of SHS, the application, and also the topology of the system. Then, the main components of SHS are presented in Section 2.4, which elaborates the technology selection together with its temperature impact. After that, Section 2.5 describes the power management system strategy of SHS. Lastly, Section 2.6 describes the state of the art of this thesis work.

2.1. General Overview

The Solar Home systems (SHS) provide a promising solution to boosting the electrification in remote rural areas in developing countries. Over 6 million SHS were estimated to have been installed and to be operating worldwide in 2015. Asia is the most extensive market so far [11]. The system size varies over a broad range depending on the needs and the technical design. A typical SHS has a capacity of 50 W to 100 W rating. However, a system with more than 150 W can occasionally be found [3]. Moreover, an interconnection of several such SHS could well lead to DC nano/micro-grids that have been discussed quite a lot in the scientific community recently.

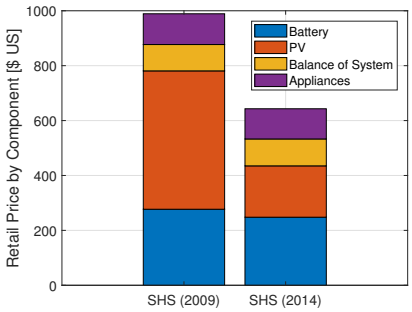

Figure 2.1: Retail purchase price for three SHS in 2009 and 2014 (adapted from [12])

Based on the findings showed in Figure 2.1, the initial cost of an SHS has declined considerably from 2009 to 2014. It was because of a substantial decline in the cost of PV modules, which dropped 62.5% [12]. The cost of batteries which is a lead-acid technology has declined slightly, making it a significant share of the total cost.

2.2. Application and working principle

Since the SHS are targeting off-grid rural households, the AC appliances, which commonly found in the west, are not essential. Since they run on DC systems and have a minimum electrical conversion, it might be considered to be the most efficient method in supplying the load. According to the definition, SHS is meant to power a single household with limited DC appliances such as lighting, a small fan, mobile telecommunication, a small fridge, and a television. These are the fundamental requirement of

a rural household in which the size depends on the buying capacity [13].

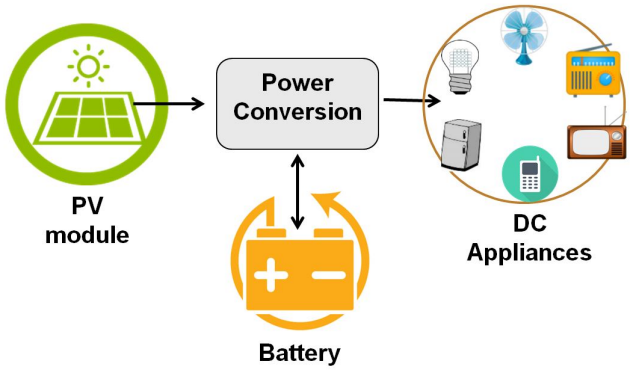

Figure 2.2: The Solar Home System concept

A typical SHS contains PV modules for the energy generation, batteries for the energy storage, and DC-DC converters for the energy conversion and load appliances for the energy consumption. They are illustrated in Figure 2.2. The working principle can be described as follows. The PV modules convert the solar power into electricity through the photovoltaic effect. The generated power can then be supplied to the load appliances or stored in the energy storage systems (batteries). The stored energy can be used in circumstances when the generated power is insufficient to supply the load appliances (e.g., during the evening or on cloudy days). The power flow between PV modules, batteries, and load appliances is controlled by the power electronics, namely, the charge controller.

2.3. System Topology

The proposed system topology for the SHS is a DC system stand-alone photovoltaics (PV) system. Figure 2.3 illustrates the block diagrams of typical components of SHS. The components are coupled in DC bus, in which they require DC-DC converters to transform the voltage level. For PV modules, they require an MPPT/ boost converter. It has two functions: (1) to regulate the voltage level on the systems and (2) to control the maximum power point of the PV modules. The batteries require a buck-boost bidirectional converter, depending on the discharging or charging state of the battery to maintain the voltage level between the output of the batteries and the DC bus. Lastly, the boost converter is needed to connect the DC load from the DC bus in which is the voltage level of the DC appliances.

2.4. SHS components

The SHS are built up from the main components: PV modules, batteries, and power converters/electronics. These components together with appliances are interconnected by the balance-of-system components (cables, switch gears, and other installation materials).

2.4.1. PV modules

PV modules contain many solar cells that electrically connected within each other (series and parallel) to achieve higher power. The light energy from the sun is converted into electricity through the photovoltaic effect. Three basic steps can explain this photovoltaic effect. (1) Charge carriers, namely electrons and holes, are generated due to the absorption of a photon in the materials that form a junction. (2) The photo-generated charge carriers are separated in the junction. (3) The photo-generated charge carriers are collected at the terminals of the junction. Within these steps, the chemical energy of the electron-hole pairs is converted to electric energy and pass through the electric circuit [14]. In general, the performance of PV modules depends on two main factors which are incident irradiance and the module temperature. The most important losses in PV modules are losses due to the interconnection of mismatched solar cells, the temperature, and the failure occurs in the modules [15].

Technology selection

The PV technology can be generally classified into three categories which are: Crystalline silicon (mono and poly), thin film (a-Si, CdTe, and CI(G)S) and the third generation solar cells (organic solar cells and dye-sensitized solar cells).

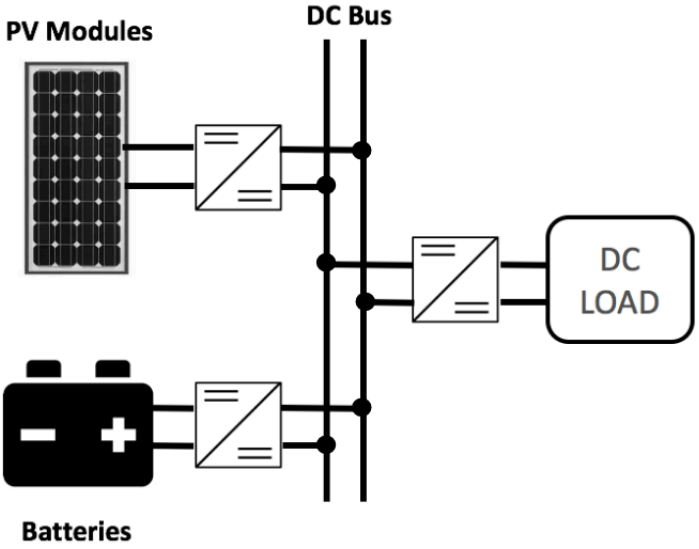

Figure 2.3: Topology of Solar Home Systems

Poly-crystalline silicon is selected as a suitable PV module due to several reasons. Firstly, it has a low degradation rate. Studies have shown that compared to other technologies such as; CdTe, CIGS, and a-Si, crystalline silicon-based PV modules have a low degradation rate. They do have 0.36%/year while other technologies have more than 0.85%/year [16]. Secondly, compared to monocrystalline silicon, it is less expensive due to the simpler and massive manufacture which reduces the cost of production [17]. Thirdly, compared with mono-crystalline silicon technology, the market share of poly-crystalline silicon technology is about 70% of total production [18].

Temperature influences

At the device level, the temperature has two contradictory effects on the solar cell. An increase in temperature decrease the band-gap and consequently the open circuit voltage (V_{oc}) of the solar cell. On the other hand, gain in temperature increases the short circuit current (I_{sc}) of the solar cell. In overall, the loss in voltage is the dominating effect, and it is eventually leading to a decrease in the output power [14].

Concerning its lifetime, typical crystalline silicon module has a lifetime of about 25 years. PV modules manufacturers typically guarantee a power between 80% of the initial power after 25 years. Temperature contributes a vital role to degrade the PV modules. It triggers the loss of adhesion and elasticity of the encapsulant, corrosion, and delamination which bring down the power generated. The fast changes of the temperature might also cause the PV modules to have broken cells and interconnections. It has been reported that typical poly-crystalline silicon PV modules experienced a lifetime-degradation rate of around 0.5-0.9%/year range in hot and humid climates [19].

2.4.2. Batteries

Batteries convert chemical energy into electrical energy. Batteries are the essential part of the SHS as they can store the energy produced by PV modules and provide electricity to the load appliances at the same time. During the operation of SHS, it is complementing the intermittent PV power production for two conditions. First, the (in)available of sun irradiation during day and night. Secondly, fluctuations due to the changes in weather, i.e., cloudy days and seasonal changes. Furthermore, batteries can be distinguished between primary (un-rechargeable) batteries and secondary (rechargeable) batteries. Most of the time, secondary batteries are suitable for SHS uses [20].

Technology selection

Lead acid batteries are one of the most mature technologies available. These batteries use the chemical reaction of lead and lead oxide with the sulfuric acid, as an electrolyte, to charge and discharge

the power. They are inexpensive and simple to be manufactured. It is obvious that the batteries have long been used for SHS [3]. Generally, lead-acid batteries require an upright orientation, ventilated environment, and periodic maintenance, which are the downside of the batteries. Sealed lead acid (SLA) batteries use a moistened separators and a sealed enclosure. By combining those features and the safety valves, which allow venting, the SLA batteries alleviate the downsides.

Lithium-ion batteries, however, offer new and up-and-coming technology in the future. Some key advantages and disadvantages are summarized in Table 2.1. It can be seen from the table that the important features of using lead-acid batteries are its high operating temperature range, safer during operation, and low investment cost. Lithium-ion batteries seem to offer more benefits over lead-acid batteries. They have higher (specific) energy density, can be deeper discharge, longer lifetime, higher efficiency, and faster-charging speed. Its high investment cost is still a barrier nowadays to be penetrated in the SHS market. However, as the technology gets more mature than before, the cost of lithium-ion batteries is reducing more rapidly than anyone expected [13].

Table 2.1: Comparative characteristics of lead-acid and lithium-ion battery technology [13]

Characteristic	**Unit**	**Lead-acid**	**Lithium-ion**
Specific energy	Wh/kg	40	90
Energy density	Wh/L	90	320
No. of cycles (@ 80% DOD)	-	200-300	500-1000
Charge time	h	8-16	1-2
Operation temperature range	°C	-20 to +50	0 to +45
Safety issues	-	Thermally stable	Protection circuit mandatory
Toxicity	-	High	Low
Recyclability	-	High	Very low
Cost	-	Low	High

Considering the number of advantages for Lithium-ion batteries, especially its aging and efficiency, some authors argue that in the longer run lithium-ion will replace lead-acid batteries [8] [21]. Therefore, this work will deal with these two type of batteries. The lead acid battery used is a sealed lead acid battery and the lithium ion battery used is a $LiFeMgPO_4$.

Temperature influences

Temperature is one of the important parameters as it affects several aspects of the battery such as reliability, lifetime, and life cycle cost. In general, the temperature has a very short-term positive and long-term negative influence on the battery performance. Temperature can increase or decrease the battery capacity and charge acceptance. Low temperature decreases the reaction rate of active materials and the ionic diffusion velocity of the batteries. Hence, it lowers the charge and discharge reaction which causes the capacity loss [22]. Zhang et al. demonstrated that the capacity of Li-ion batteries could decrease as much as 95% when the battery is operating at -10 °C compared to that at 20 °C [23]. Pesaran et al. also illustrated the changes in the capacity due to temperature. The extreme temperature condition, in which under -40 °C, the capacity of the battery can shrink to nearly zero (Figure 2.4. Further increase in temperature leads to achieving a saturation point in terms of capacity increase.

Besides that, the impact of the temperature is also addressed to the internal resistance of the battery. It is described in Figure 2.4 that the decrease in temperature leads to the increase in internal resistance [24]. This is because the diffusion slows down which results in a reduced average kinetic energy of the molecules. This phenomenon will increase the resistance of the chemicals [25].

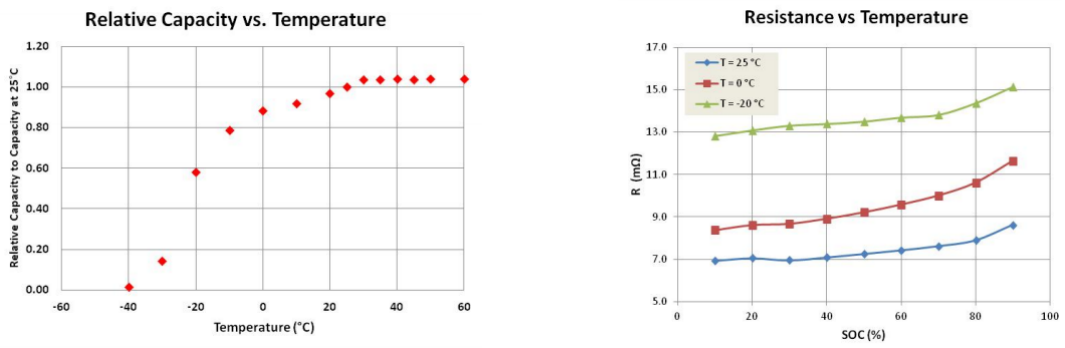

Figure 2.4: Relative capacity and internal resistance influenced by battery temperature [24]

In the long-run, higher temperature causes faster aging of the battery. For instance, the aging of lithium-ion batteries leads to internal resistance increase and a capacity decrease due to electrochemical and mechanical processes. This mechanism is strongly influenced by temperature, SOC, cycling depth and current rates [26]. Ning et al. reported that the capacity fading at high discharge current rates is because of the change in the carbon structure [27]. It can be worse as the temperature rises. The standard ISO 12405-2 defines battery end of life when the discharge capacity is reduced to 80% of the initial capacity. Moreover, the increase of the internal resistance triggered at high current rates is due to the cracks that result in the formation of a new solid electrolyte interface (SEI) layer. This layer becomes thicker and results in a significant increase in the internal resistance. Furthermore, the aging can be categorized into two mechanisms: cyclic aging and calendar aging. Cyclic aging is the degradation mechanism when the battery is discharging and charging. On the other hand, calendar aging is more related to the degradation when the battery is idle. Generally speaking, calendar aging plays an essential role in the case that the idle periods are dominant than the operation times.

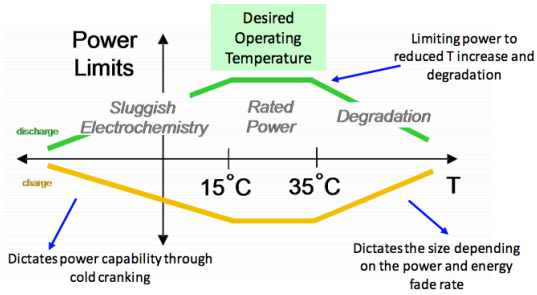

Figure 2.5: Desired operating temperature [28]

By taking into account both short-term and long-term effects, it is identified that the safe ambient temperature for Li-ion batteries is between 15 °C and 35 °C (Figure 2.5) [28]. A temperature lower than 15 °C will experience poor performance due to the increase in internal resistance and the decrease in capacity. On the other hand temperature higher than 35 °C will experience higher aging rate in which it limits the performance of the battery in the long run.

2.4.3. Power Converters

Power electronics are also important technologies associated with the PV systems. In PV systems, power converters are part of the power electronics which convert the electrical energy into different stages of the voltage level. The main challenge of power converters in SHS lies in optimizing power management system from the PV modules, batteries, and load appliances.

Technology selection

According to a system topology, as illustrated in Figure 2.3, there are three different converters used in regulating the power flow of the systems. First, the MPPT (maximum power point tracking) is interconnected directly with the PV module output. A boost converter is used to maximize the power of the PV which increase the voltage level to 48 V on the DC bus. Secondly, the charge controller is

interconnected with the battery. It regulates the current flow between the DC bus and the battery and also protects the battery from over-voltage and under-voltage conditions. Thirdly, the boost converters which raises the voltage level into the higher voltage level that is used by the appliances.

Temperature influences

To assess the performance of the power converter, one has to look power converter in a component level. Power converter presented in SHS generally is broken down into several components, such as switches, diodes, inductors, and capacitors. In practical, the losses are presented in each component during operation and will contribute to the increase of temperature of the component. Accordingly, the temperature will play a role in affecting the performance and losses of the components. Thus, it will influence the performance of the converter. The loss in the switch makes the junction temperature to increase. Hence, it will affect several parameters such as switch's drain-source resistor (R_{DS}), threshold voltage (V_{th}), and transconductance (g_{fs}) [29]. As for the diodes, the influence on the junction temperature can affect the diode reverse bias saturation current and diode voltage [30]. As for capacitor, it has a temperature dependent parameter which is equivalent series resistance and the capacitance. The capacitance rises while the internal resistance falls with an increase in temperature. Besides, the inductors have several elements which are influenced by temperatures, such as cores and windings. As the temperature of the ferrite cores increase to around 80 to 90°C, the loss increases [5].

Regarding failure, electrolytic capacitors and MOSFETs dominates in contributing to the degradation rate in the converter [9]. The failure of these components can be influenced by its operating conditions, such as voltage, current, frequency, and temperature. The degradation over a period will result in the failure of components which influences the performance of the overall system. As for capacitors, it can be broken down into equivalent series resistance (ESR) and the capacitance components. In contrast with the instantaneous performance, the temperature triggered degradation of capacitors will lead to capacitance decrease and ESR increase. In evaluating the degradation phenomenon, the degradation rate is often associated as a function of life-cycles. The life cycles are influenced by the thermal cycles that the power electronic component goes through [5]. As the component experiences the thermal cycle stress, the solder joint might achieve its fatigue point. Thus, it leads to the failure of the component.

2.5. Power Management Systems (PMS)

The control strategy used is based on the SOC of the battery in the previous time step. The power flow from the PV will prioritize to satisfy the load demand. When the load is satisfied, and there is still extra power from the PV, the extra power will be used to charge the battery.

It will dump the power when the maximum SOC is achieved, and the PV power is still oversupplied. Physically, there are various ways to define where the dumped power goes. The most common way is to shift the power curve of the PV, which done by the converter so that it always satisfies the load demand. In other words, during this condition, the PV is not working in the maximum power point [31].

On the other hand, when the minimum SOC is achieved, and the load demand is greater than the PV power the system is considered fail. This fail event will determine the Loss of Load Probability (LLP) which will be discussed in the next section.

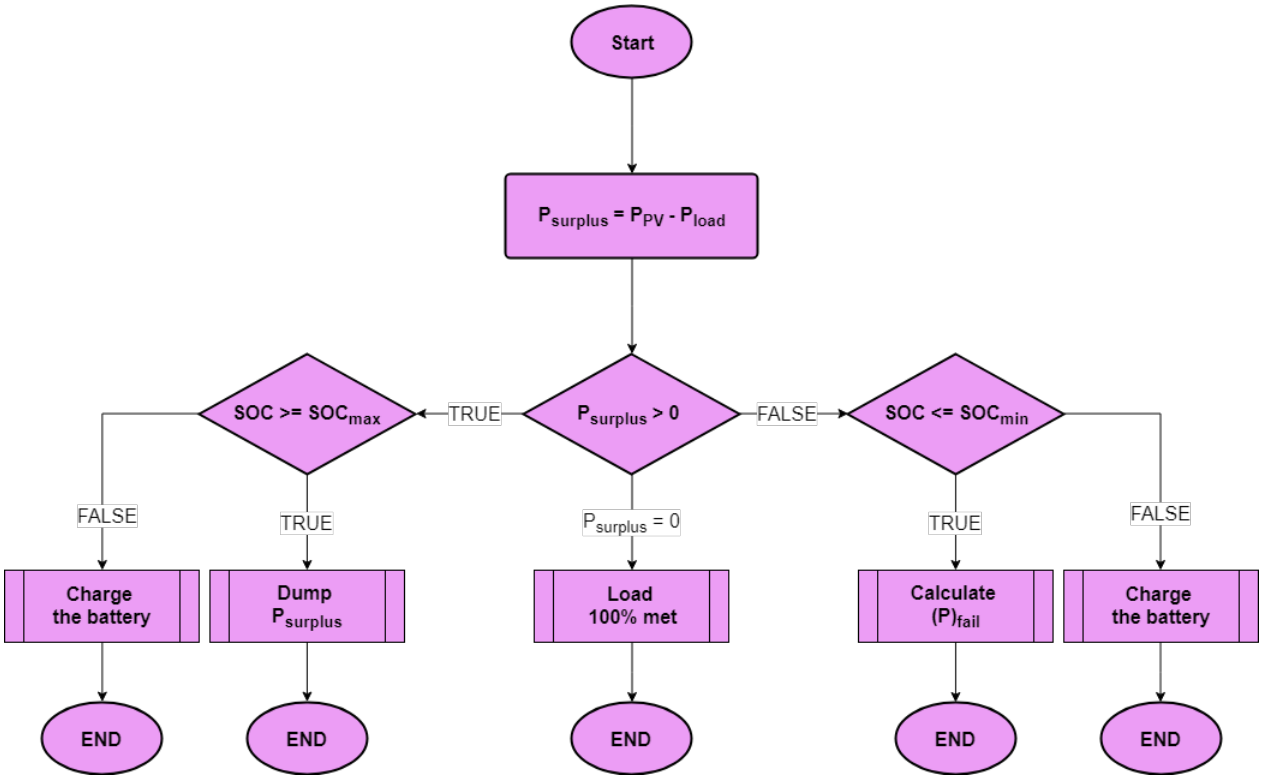

Figure 2.6: Off-grid PMS algorithm

2.6. Temperature Impact Assessment Approach

Current research and methodology

The current research of SHS is limited to the context of technical performance assessment for general stand-alone PV systems. Hence, the evaluation of the performance is taken into account the temperature effect at a particular location. Although there is a device developed for testing solar home systems [32], modeling/simulation approach offers more benefits in gaining the insight of long-term performance, such as aging and system sizing, and transient changes. Some system models have been developed to evaluate the performance of stand-alone PV systems by taking into account several components [14, 33–35]. Some of the authors are relying on various programming software such as MATLAB/Simulink and PVSyst [36, 37]. Some performance metrics that are often used are the loss of load probability (LLP), the efficiency of the system, and the power flow.

Moreover, several authors began to study more specifically for SHS. Mufiaty et al. assessed the performance and the lifetime of SHS practically in the field [38]. Nkhonjera et al. evaluated the SHS performance through simulation by using TRNSYS software [39]. Furthermore, Narayan et al. evaluated the temperature impact by quantifying the performance and lifetime of SHS components [5].

In the component level, several authors have been researching extensively about the thermal implication on the main SHS components. In some literature the PV model contains the thermal model and the temperature dependence electrical model [14, 40–42]. Krismadinata et al. developed an IV curve model of PV cell as a function of irradiance and temperature through a single diode model [40]. Moreover, a generic battery model provided by MATLAB/Simulink developed a battery model with regard to the temperature [43].

Proposed broad methodology

With many available explorations in components level it is interesting to involve these elements in assessing a more detailed the temperature impact regarding the SHS performance and lifetime. By adding the layer of components complexity, this work presents the temperature assessment of SHS through simulation. A comprehensive model is constructed composed of the main component models. The dynamic performance and lifetime-degradation of the components were modeled to determine the performance and lifetime of the components and therefore the system. For a given location, several

meteorological data and load profile are introduced to assess the behavior of the system.

However, in this work, not all the main components and behavior are taken into considerations. As the Figure 2.1 tells, in terms of cost, the batteries share a significant part of the total cost. It is followed by the PV modules as the second. Besides, regarding expected lifetime, the batteries can last for less than five years for lead-acid and 15 years for lithium-ion, compared to the lifetime of PV modules which around 25 years [21]. Therefore, as the batteries are usually found to be the first to fail and are the most expensive components, the lifetime of SHS can be determined by the lifetime of the batteries. However, the lifetime of PV modules can define the lifetime of SHS when the batteries achieve more than the lifetime of PV modules.

On the other hand, the performance of SHS can be determined by the loss of load probability. Therefore by this metric, one can know the effectiveness and the reliability of the system in delivering electricity to the appliances. Figure 2.7 illustrates the modeling approach of the SHS in this work.

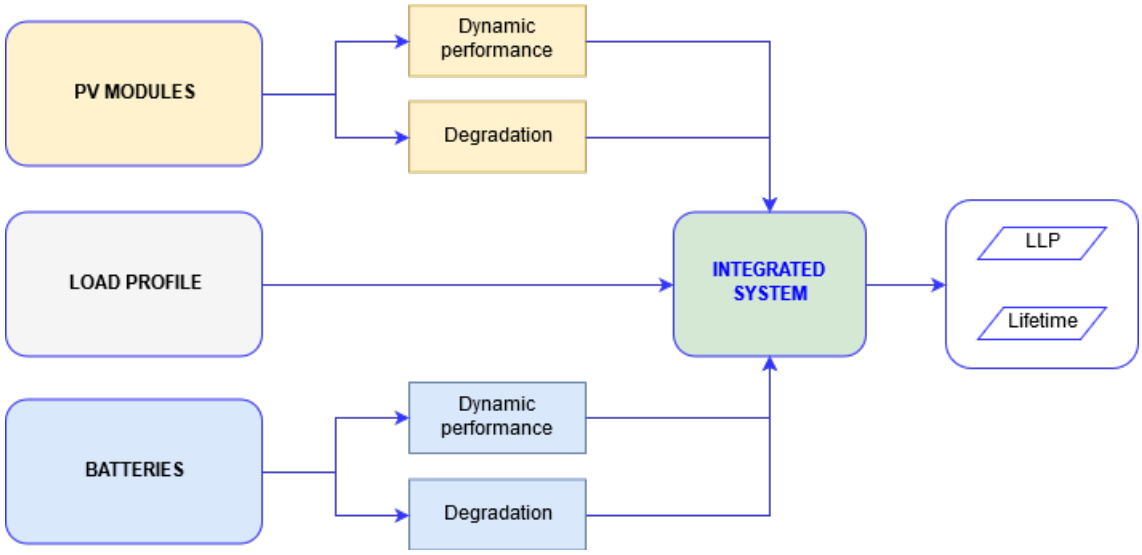

Figure 2.7: Proposed modeling approach for Solar Home System (SHS)

3

Location Details: Sumba Island, Indonesia

In this chapter, the details of the selected location are broadly explained. Sumba Island, Indonesia is chosen due to its solar potential and its necessity to install the SHS. The explanations can be found in Section 3.1 and Section 3.2. Then, Section 3.3 introduces the solar potential in Sumba Island. Section 3.4 describes the meteorological data including the irradiance and the ambient temperature. In this section scaling factor (SF) is introduced in evaluating the temperature effect of the systems. Lastly, the stochastic load profile is adopted and broadly explained in Section 3.5. This location details will be adopted for the evaluation in the upcoming chapters.

3.1. Introduction

Sumba Island is located in the southeastern part of Indonesia (9.726 °S, 120.037 °E), which is a part of East Nusa Tenggara Province (NTT). Waingapu is the largest town in the island. Generally speaking, Sumba is one of the poorest regions in Indonesia. Statistics Indonesia or Badan Pusat Statistik (BPS) recorded in 2017, approximately 32% of Sumba's population is categorized as poor [44]. The people tend to live together as one big family under one roof which can contain up to twelve members of the family [45]. In general, the people in Sumba depends on their economy in the agricultural sector. The income of typical rural households relies on the harvest season [46]. Besides, regarding telecommunication access, approximately 50% of the households in Sumba have telecommunication expenditures through their mobile phones [45].

Figure 3.1: Map of Sumba Island [47]

3.2. Necessity for Installing Solar Home Systems

As for the electricity access, there are still about 238 out of 433 villages which do not acquire electricity [45]. The electrification ratio is still low because some villages are located in a very off-grid area, and the local electricity grid expansion is not economically viable. Currently, rural households still use subsidized kerosene for lighting. Some of the villagers might use an expensive, polluting, imported resources diesel generators which is often limited to a few hours a day [48].

A program called Sumba Iconic Island, which initiated by a Dutch non-profit organization (Hivos), supports the island in boosting the electrification ratio while bringing the clean energy transition. The program aims to "ensure the provision and utilization of renewable energy sources that can encourage an inclusive economy and gender in order to improve the welfare of people in Sumba Island [49]." The program is supported by the Ministry of Energy and Mineral Resources of Republic Indonesia (MEMR) and State Electricity Company (PLN). An assessment of renewable energy potential in Sumba stated that the island could become a 'fossil fuel independent island.' It is observed that the island has remarkable renewable energy resources, ranging from hydro, solar, wind, and biogas [46]. There are already existing several renewable energy generators such as micro-hydro and wind turbines as it can be seen in Figure 3.1. On the other hand, Sumba Island is blessed with abundant solar insolation with ESH for about 5.0 hours.

Therefore, implementing SHS in Sumba island is considered one of the best solution in increasing the electrification ratio while improving the economy of the island. By considering the needs, the renewable energy resource, and the support from many stakeholders, installing SHS in Sumba island can be done right now. In this work, Waingapu town is selected as the case study location.

3.3. Solar Potential

As a tropical island, Sumba island is blessed with abundant solar radiation. The three different components of irradiance (DHI, DNI, and GHI) are taken from the Meteonorm software [50] and the irradiance plane of an array is computed as it is in a flat surface. It is calculated by using Equation 4.1 - 4.5. The results show that the irradiance varies with a small deviation within a year. It shows that in Figure 3.2 during March and September the irradiance is at its highest, and can achieve about 1300 W/m2. The total irradiance within a year is 1,856 kWh, or it can be translated to 5.09 ESH.

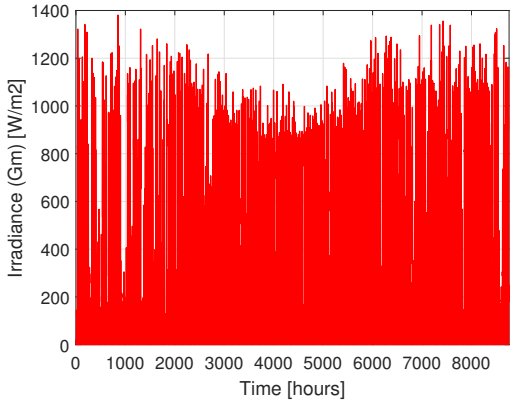

Figure 3.2: Total irradiance (G_m) on a flat surface for one year

3.4. Other meteorological data

In terms of the meteorological data, besides solar irradiance data, several factors are crucial for the performance estimation of SHS. Ambient temperature is the most significant factor for the SHS performance as well as in this study. As it can be seen from the Figure 3.3, the ambient temperature is ranging between 20 °C and 35 °C with the annual average temperature of 27 °C. In terms of wind speed, it is important in calculating the temperature of the PV module as FD model is adopted in estimating the module temperature. The wind speed occurs more frequently under 5 m/s with the average of 2.2 m/s. It can also be seen in Figure 3.4 that the Sumba Island has a frequent cloudy condition within a year.

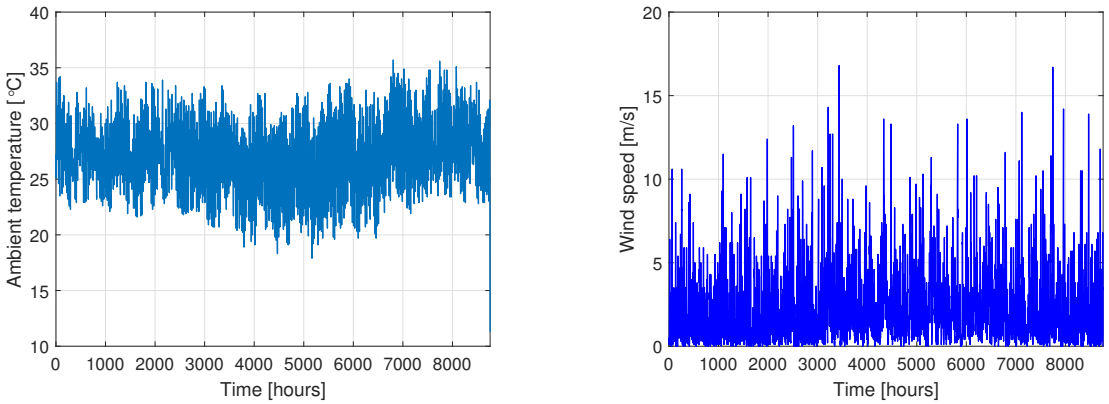

(a) Ambient temperature (b) Wind speed

Figure 3.3: Ambient temperature and wind speed of Sumba Island in a year

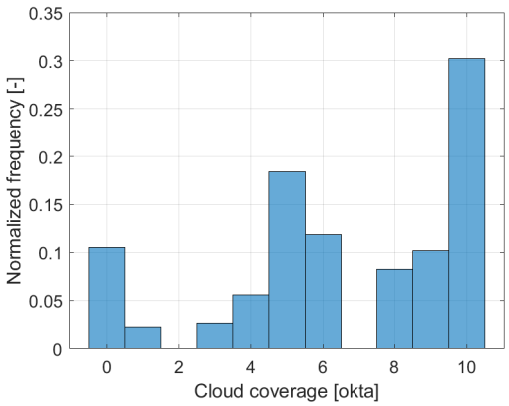

Figure 3.4: Histogram of cloud coverage which translates into normalized frequency

Scaling Factor (SF)

The scaling factor is introduced in this section to evaluate the temperature performance of the system. A coefficient is applied to the ambient temperature. For example, SF1.2 defines that the ambient temperature profile is scaled up to 20% more. SF0.8 defines that the ambient temperature profile is scaled down 20% more. The real ambient temperature in the location is always fluctuating. This scaling factor is used to evaluate the performance of the system to exhibit fairer comparison under the fluctuated ambient temperature. The average of these temperature profiles are calculated as it can be seen in Table 3.1.

Table 3.1: Variation of temperature profiles of Sumba island and its average

Name	Avg. Temp. (oC)	Definition
SF 0.8	21.57	0.8X Tamb
SF 1.0	26.96	Tamb
SF 1.2	32.36	1.2X Tamb

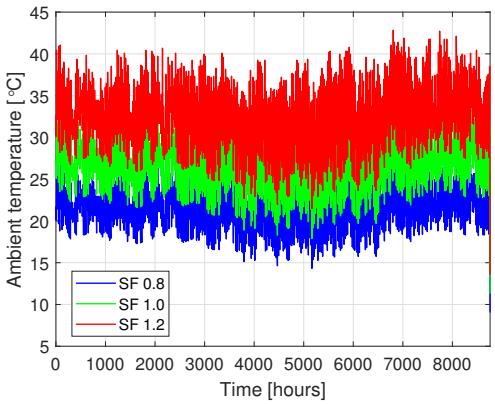

Figure 3.5: Scaling Factor (SF) illustration for ambient temperature

3.5. Load profile

The selected load profile from the Sumba Island study case will be further explained in this section. The World Bank in its research explained that the energy access definition must be multi-dimensional. The energy access was measured across five tiers and eight attributes of energy. Table 3.6 presents a simplified matrix of tiers and the evaluated attributes. Each tier represents the energy access to fulfill the appliances based on the living standard of a specific location. For instance, tier 1 only satisfy basic lighting and phone charging, and tier 2 consists of the needs of an electric fan and a television. Tier 3 fulfills even more demand which consists of mechanical applications, such as washing machines and food processors. Based on this definitions, Narayan, 2018, made a stochastic model which covers all the tiers [51].

Figure 3.6: Simplified multi-tier matrix of energy access according to World Bank [52]

Attributes of energy supply		Tier 0	Tier 1	Tier 2	Tier 3	Tier 4	Tier 5
Capacity	Household electricity	No electricity[a]	Very low power	Low power	Medium power	High power	
	Household cooking	Inadequate capacity of the primary cooking solution				Adequate capacity of the primary cooking solution	
Duration and availability	Household electricity	<4 hours	4–8 hours		8–16 hours	16–22 hours	>22 hours
	Household cooking	Inadequate availability of the primary cooking solution				Adequate availability of the primary cooking solution	
Reliability	Household electricity	Unreliable energy supply				Reliable energy supply	
Quality	Household electricity/cooking	Poor quality of energy supply			Good quality of energy supply		
Affordability	Household electricity	Unaffordable energy supply		Affordable energy supply			
	Household cooking	Unaffordable energy supply				Affordable energy supply	
Legality	Household electricity	Illegal energy supply			Legal energy supply		
Convenience	Household cooking	Time and effort spent sourcing energy cause inconvenience			Time and effort spent sourcing energy do not cause inconvenience		
Health and safety	Household electricity	Unhealthy and unsafe energy system				Healthy and safe energy system	
	Household cooking[b]	Level 0	Level 1	Level 2	Level 3	Level 4	Level 5

Based on the characteristics of the households in Sumba Islands, the energy access can be determined for Tier 3. It is due to firstly their needs of the mobile phone as their essential telecommunication tools. Secondly, as there are many donors given from NGOs to boost the economy of Sumba Island, TV, fan, radio, and fridge should be installed. Therefore, tier 3 is with an electricity demand of 0.914 kWh/day. Table 3.2 shows the appliances and the energy consumption details based on the other research done. This load profile varies between the days in a year. Figure 3.7 presents a typical 48 hours load profile in which the load power is usually high during night time.

Table 3.2: Load appliances for Tier 3 profile [51]

Load appliances	**Daily E. consumption [Wh]**
LED lighting	45.80
Fan	112.50
Tablet	79.63
Radio	23.22
TV	91.60
Mobile phone	48.44
Fridge	580.27

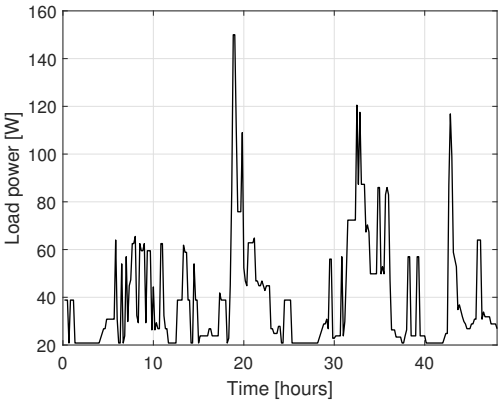

Figure 3.7: Tier 3 load profile, adapted from [51]

4

The Behavior of PV Modules Evaluation

This chapter aims to assess the behavior of PV module as the main power generator in the SHS. It starts from Section 4.1 which briefly explains the PV module behavior. Section 4.2 explains the integrated PV model which consists several models adopted from the literature. Then, Section 4.3 - 4.5 extensively describe the irradiance model, thermal model, and electrical model used in the simulation. The integrated PV model is then coupled with the degradation phenomenon which is explained in Section 4.6. Section 4.7 elaborates the input data used which is obtained from the previous chapter. Moreover, the simulation result is analyzed and discussed to evaluate the temperature impact on the PV performance and lifetime in Section 4.8. Finally, the conclusion is drawn based on the findings in Section 4.9. This integrated PV model will be applied to the integrated model of SHS by incorporating battery model element, power management systems (PMS), and meteorological data in Sumba Island, Indonesia through the case study in Chapter 6.

4.1. Introduction

Overview of the PV module behavior

PV modules have the technological parameters which play an important role in the power output. Besides the technological parameters, they are also affected by meteorological data. Irradiance, sun position, wind speed, and ambient temperature are the most important meteorological factors. These parameters are varied over time according to the location. Thus, in order to evaluate the effect of temperature on the PV modules, one could not neglect the effect of this meteorological factors. The irradiance is responsible for converting the solar power into the electrical power. Thus, it is necessary to model the irradiance on the PV modules given the sun position and irradiance data obtained.

It is clear that the temperature profoundly influences the PV power output. Hence, it is essential to have an accurate estimation of module temperature. Moreover, electrical performance is responsible for explaining the behavior of the PV module under various conditions such as irradiance and temperature changes. Furthermore, as this work involves in the lifetime evaluation of SHS, therefore it is necessary to incorporate with the degradation rate of the PV modules.

Relevance to the SHS

As it is discussed in the Chapter 2, PV modules are highly responsible for power generation in SHS application. Moreover, as locations are usually in the tropical climate, the module temperature can become 2 to 3 times higher than the ambient temperature due to the high irradiance. Thus, it can lead to having a more severe reduction due to the thermal stress.

4.2. PV Model Overview

Current research

Numerous studies have been done in predicting the energy yield of the PV modules [14, 42, 53], in which they include the irradiance model, thermal model and the electrical model in their prediction. Many authors proposed a different thermal model to predict the module temperature [41, 54]. As

for electrical performance, many works have been done in predicting the electrical behavior of the PV modules [14, 40, 55, 56]. As for the degradation phenomenon, there are several, but limited, works which tell about the degradation model of the PV modules [57, 58].

Integrated PV model

In this methodology, an integrated PV model is used in assessing the performance of the PV modules in the SHS. This model is constructed by adopting available models: irradiance model, thermal model, electrical mode, and degradation model. The block diagram of the integrated PV model is illustrated in the Figure 4.1. The output of the irradiance model is the total irradiance received on the plane of the PV module (G_{m}). The thermal model predicts the temperature of the PV cells (T_{m}) given the external factors such as ambient temperature, wind speed, and the total irradiance (G_{m}). Electrical model is used to calculate the DC electrical characteristics of the PV modules which can be translated into power. G_{m} and T_{m} are the primary input of this model. Finally, the degradation model is introduced as a de-rating factor of the electrical output characteristics of the PV modules.

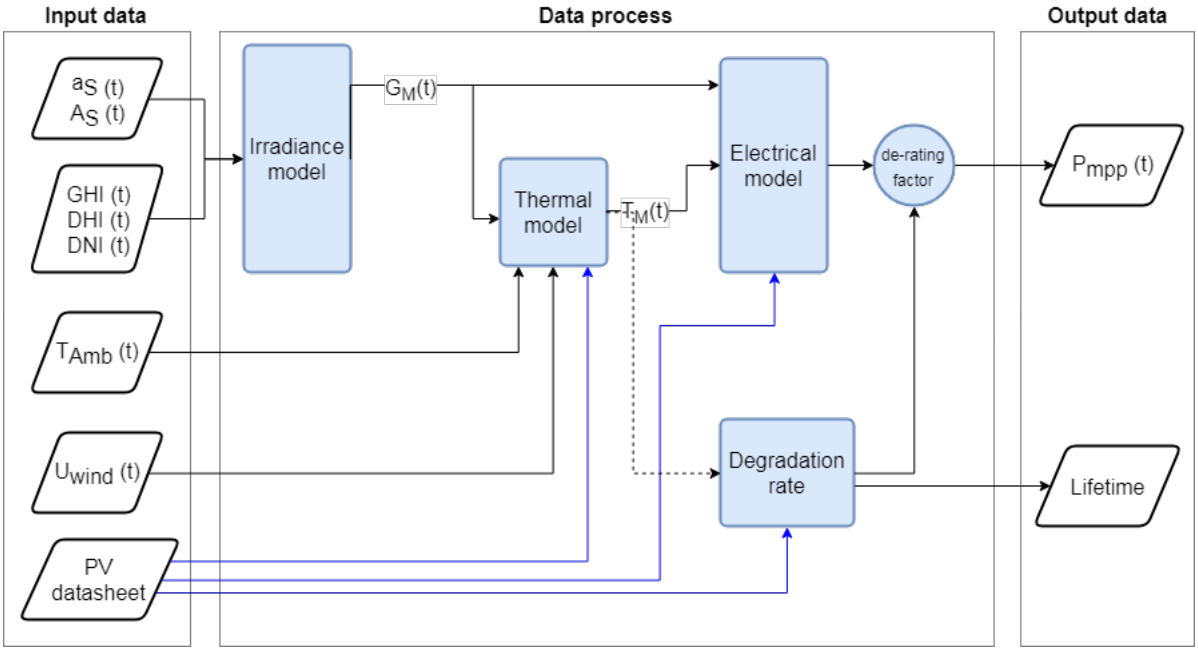

Figure 4.1: Block diagram of PV model

4.3. Irradiance model

4.3.1. Irradiance plane of array

The total irradiance received by an incline PV module contains three major components; direct (G_{direct}), diffuse (G_{diffuse}), and ground (G_{ground}). Those components are based on the irradiance data; Direct Normal Irradiance (DNI), Diffused Horizontal Irradiance (DHI), and Global Horizontal Irradiance (GHI), which are obtained from the Meteonorm database. The calculation of G_{m} is given by Equation 4.3 - 4.1 [5].

$$G_{\mathrm{m}} = G_{\mathrm{direct}} + G_{\mathrm{diffuse}} + G_{\mathrm{ground}} \tag{4.1}$$

Direct component

The direct component is influenced by DNI and the angle of incidence (γ) as described by using Equation 4.2. The angle of incidence is defined as "the angle between the surface normal and the incident direction of the sunlight" by taking into account the orientation of the module and the sun location [14] (Equation 4.3).

$$G_{direct} = DNI \times cos\gamma \tag{4.2}$$

$$cos\gamma = sin(a_s)cos(\theta_{\mathrm{m}}) + cos(a_s)sin(\theta_{\mathrm{m}})cos(A_{\mathrm{m}} - A_s) \tag{4.3}$$

Diffuse component

In general, the diffuse component depends on the condition of the sky such as the clouds movement, nearby surroundings, and other factors which are difficult to predict. In calculating the diffuse component, several models have been developed with different degrees of accuracy and complexity. The diffuse component model has one, two or three sub-components: isotropic, circumsolar, and horizon brightening. Isotropic radiation is the radiation that uniformly diffuses over the skydome. Circumsolar radiation depends on the forward scattering of radiation concentrated in the solar disk. Horizon brightening defines that when the is is near the horizon, the diffuse radiation increases. In this integrated PV model, the isotropic model is used in which it takes into account isotropic component only (Equation 4.4) [59].

$$G_{\text{diffuse}} = DHI \times \frac{1 + cos(\theta_{\text{m}})}{2} \tag{4.4}$$

Ground component

The ground component is an irradiance caused by the reflection of the ground and the surrounding which is influenced by the tilt of the modules. Albedo (α) is an important factor in calculating ground component which is defined as the ratio of reflected irradiance (GHI) on the ground. In the rural area, where the land covered are mainly: intensive agriculture, natural vegetation, and degraded savannah, the albedo varies in a range of 16% to 25% [60]. Therefore an average value of albedo of 20% is used.

$$G_{\text{ground}} = GHI \times \frac{1 + cos(\theta_{\text{m}})}{2} \times \alpha \tag{4.5}$$

4.3.2. Optimization

Having described that the total irradiation plane of array (G_{m}) is a function of PV modules orientation, therefore, selecting the optimum tilt and azimuth angle of the PV modules is considered first. The optimization of module's tilt and azimuth angle is done by tuning and iterating different pairs of module's tilt and azimuth angle using Equation 4.1 - 4.5. In general, the optimum angles are chosen so that the total integrated irradiation over a year is maximized, achieving the highest Equivalent Sun Hours (ESH). ESH is a term used by solar PV designer which defines how many hours the sun is shining at its maximum value. It has been agreed that the standard maximum solar irradiation is 1,000 W/m^2.

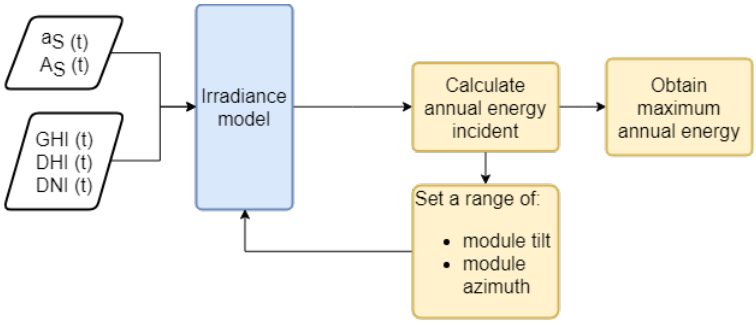

Figure 4.2: Module tilt and azimuth optimization block diagram

In this work, two layers of optimization is conducted to decrease the computational time. The first iteration is to set the tilt angle from 0° to 90° with a step of 10 ° and azimuth angle from 0° to 360° with a step of 36°. Once it obtains an optimal angles, the second iteration is to set the tilt angle with a limit of -20° to 20° from the first optimal angles. Hence it perform the iteration with a step of 1°. The same limit and angle step is done for the azimuth angle.

4.4. Thermal model

The temperature strongly affects the performance of PV modules. It is critical to have a good estimation of the cell temperature under operating conditions. In general, the input of the model is G_M and T_{amb}. However, in predicting the cell temperature accurately, more elements such as further meteorological data, technological parameters, and geometry of the modules, should be taken into account. An

accurate prediction also requires more computational time and information concerning physical parameters.

In this work, two thermal models based on the previous research are adopted in evaluating the module temperature; NOCT model [54] and Fluid-dynamic steady-state model (FD) [41]. A comparison of the two models will be assessed at a given tropical location. Each model has pros and cons concerning the complexity and accuracy. However, both model assumes that the PV module has a uniform temperature across the solar cells.

4.4.1. NOCT model

The NOCT model is mainly based on the sun irradiance as the heat generation. It is considered one of the simplest models in determining the module temperature. Equation 4.6 described a linear relationship between T_m - T_a and G_m which is based on the previous observation [54]. The nominal operating cell temperature (NOCT) is used as a reference point. NOCT is a temperature of a solar cell at 20°C ambient temperature, 800 W/m2 irradiance level, and 1m/s of wind speed [14, 41].

$$T_{\mathrm{m}} = T_{\mathrm{amb}} + \frac{T_{\mathrm{NOCT}} - 20^{o}}{800} G_{\mathrm{m}} \tag{4.6}$$

4.4.2. Fluid-Dynamic steady-state (FD) model

The fluid dynamic model is based on detailed thermal energy balance between the module and its surroundings. The main inputs for this model are T_{INOCT}, T_{amb}, G_M, u, thermal coefficients, and other module parameters. This model is proposed by Fuentes et al.[41] in which the transient model is developed. This model presents the simplified steady-state model. The time constant is 7 minutes in which it is the time lag between the change in irradiance and the change in module temperature [14]. Therefore as the simulation is conducted over 10 minutes time step, a simplified steady-state model is used.

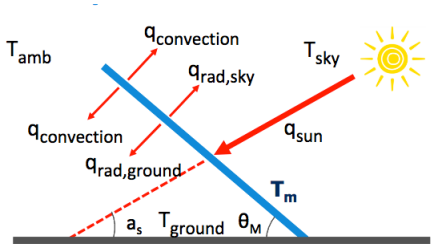

Figure 4.3: Illustration of heat transfers between a tilted PV module and the surroundings [14]

The heat balance is given as follows.

$$\dot{Q} = q_{\mathrm{irr.}} - q_{\mathrm{conv.}} - q_{\mathrm{rad.,gr.}} - q_{\mathrm{rad.,sky}} - q_{\mathrm{cond.}} \tag{4.7}$$

The heat generation is caused by the sun irradiance times the absorptivity of the module (φ). The convective heat transfer flow is a function of the convective coefficient, the temperature of the module and the ambient. The radiative heat transfer flow consists of the heat exchange between the upper module and the sky and between the rear module and the ground. The conductive heat transfer is neglected because the contact points are considered very small. As it is assumed to be in a steady state, the summation of all heat transfers is equal to zero.

$$mc\frac{dT_{\mathrm{m}}}{dt} = \varphi G_{\mathrm{m}} - h_c(T_{\mathrm{m}} - T_{\mathrm{amb}}) - \epsilon_{\mathrm{top}}\sigma(T_{\mathrm{m}}^4 - T_{\mathrm{sky}}^4) - \epsilon_{\mathrm{back}}\sigma(T_{\mathrm{m}}^4 - T_{\mathrm{gr}}^4) \tag{4.8}$$

$$mc\frac{dT_{\mathrm{m}}}{dt} = 0 \tag{4.9}$$

The radiation heat transfer can be simplified by linearizing the terms using relation below.

$$(a^4 - b^4) = (a^4 + b^4) \cdot (a + b) \cdot (a - b) \tag{4.10}$$

Therefore, the radiation terms can be defined by Equation 4.11 - 4.12.

$$h_{\mathrm{r,sky}} =_{\mathrm{top}} \sigma(T_{\mathrm{m}}^2 - T_{\mathrm{sky}}^2)(T_{\mathrm{m}} - T_{\mathrm{sky}}) \tag{4.11}$$

$$h_{\mathrm{r,gr}} =_{\mathrm{back}} \sigma(T_{\mathrm{m}}^2 - T_{\mathrm{sky}}^2)(T_{\mathrm{m}} - T_{\mathrm{gr}}) \tag{4.12}$$

The energy balance can be rewritten as illustrated in Equation 4.13. Thus, the temperature of the module can be determined as expressed in Equation 4.14.

$$0 = \varphi G_{\mathrm{m}} - h_c(T_{\mathrm{m}} - T_{\mathrm{amb}}) - h_{\mathrm{r,sky}}(T_{\mathrm{m}} - T_{\mathrm{sky}}) - h_{\mathrm{r,gr}}(T_{\mathrm{m}} - T_{\mathrm{gr}}) \tag{4.13}$$

$$T_{\mathrm{m}} = \frac{\varphi G_{\mathrm{m}} + h_c T_{\mathrm{amb}} + h_{r,sky} T_{\mathrm{sky}} + h_{r,gr} T_{\mathrm{gr}}}{h_{\mathrm{r,sky}} + h_{\mathrm{r,gr}} + h_c} \tag{4.14}$$

Convective heat transfer coefficients

The convective heat transfer flow of the PV module consists of convection in the top and the rear of the PV module as stated in Equation 4.15 [41]. This form of heat transfer is caused by the movement of the fluid. Hence, it highly depends on the fluid motion.

$$h_c = h_c^{\mathrm{T}} + h_c^{\mathrm{B}} \tag{4.15}$$

Top convective heat transfer. The convective heat transfer on the top surface consists of free or/and forced convection. These kinds of convection contribute to the overall mixed convective coefficient which can be obtained by solving Equation 4.16.

$$h_c^T = (h_{\mathrm{forced}}^3 + h_{\mathrm{free}}^3)^{1/3} \tag{4.16}$$

The free convection coefficient is estimated by using the dimensionless Nusselt number, which is the ratio between the convective and conductive heat transfer.

$$Nu = \frac{h_{\mathrm{free}} \cdot D_h}{k} = 0.21(Gr \times Pr)^{0.32} \tag{4.17}$$

It is a function of heat conductivity (k), Grashof number (Gr), and the hydraulic diameter (Dh). Grashof number is the ratio between the buoyancy and viscous forces,

$$Gr = \frac{g\beta(T - T_{\mathrm{amb}})D_h^3}{v^2} \tag{4.18}$$

While hydraulic diameter (Dh) is calculated by the length (L) and width (W) of the module,

$$D_h = \frac{2LW}{(L + W)} \tag{4.19}$$

For the forced coefficient, ones can distinguish between laminar or turbulent flow by using Reynolds number (Re) for evaluation,

$$h_{\mathrm{forced}}^{\mathrm{lam.}} = \frac{0.86 \cdot Re^{-0.5}}{Pr^{0.67}} \rho c_{\mathrm{air}} u \tag{4.20}$$

$$h_{\mathrm{forced}}^{\mathrm{turb.}} = \frac{0.028 \cdot Re^{-0.2}}{Pr^{0.4}} \rho c_{\mathrm{air}} u \tag{4.21}$$

Prandtl number it the ratio between the momentum diffusivity and the thermal diffusivity, which has a value of 0.71 for air. The Reynolds number determines the ratio of the inertial forces to viscous forces,

$$Re = \frac{u \cdot D_h}{v} \tag{4.22}$$

Rear convective heat transfer. Convective on the rear side of the module is always lower than on the top because of the mounting structure. Due to that, the scaling factor (R) will be determined by performing an energy balance at the INOCT conditions.

$$h_c^B = R \times h_c^T \tag{4.23}$$

$$\varphi G_{\mathrm{m}} - h_c^T(T_{\mathrm{INOCT}} - T_{\mathrm{amb}}) - h_{\mathrm{r,sky}}(T_{\mathrm{INOCT}} - T_{\mathrm{sky}}) = h_c^{\mathrm{B}}(T_{\mathrm{INOCT}} - T_{\mathrm{amb}}) + h_{\mathrm{r,gr}}(T_{\mathrm{INOCT}} - T_{\mathrm{gr}}) \tag{4.24}$$

R is defined as the ratio of the actual to the ideal heat loss from the back side,

$$R = \frac{h_c^B(T_{\text{INOCT}} - T_{\text{amb}}) + \epsilon_{\text{back}}\sigma(T_{\text{INOCT}}^4 - T_{\text{gr}}^4)}{h_c^B(T_{\text{INOCT}} - T_{\text{amb}}) + \epsilon_{\text{back}}\sigma(T_{\text{INOCT}}^4 - T_{\text{amb}}^4)} \tag{4.25}$$

Substituting Equation 4.25 to Equation 4.24 at INOCT conditions will make:

$$R = \frac{\varphi G_{\text{m}} - h_c^T(T_{\text{INOCT}} - T_{\text{amb}}) - h_{r,\text{sky}}(T_{\text{INOCT}} - T_{\text{sky}})}{h_c^B(T_{\text{INOCT}} - T_{\text{amb}}) + h_{r,\text{gr}}(T_{\text{INOCT}} - T_{\text{gr}})} \tag{4.26}$$

Sky temperature estimation

Sky temperature depends on ambient temperature, humidity, cloud coverage, and cloud elevation. As a rule of thumb, when the cloud cover is above six oktas, the sky temperature will approach the ambient temperature [41],

$$T_{\text{sky}} = T_{\text{amb}} \tag{4.27}$$

On a clear day (cloud coverage below or equal six oktas), the sky temperature can be estimated to be,

$$T_{\text{sky}} = 0.0552 \times T_{\text{amb}}^{3/2} \tag{4.28}$$

4.5. Electrical Performance

This section focuses on modeling the PV electrical performance as a function of irradiation and cell temperature in the module level. Two commonly used electrical models of solar cells, Single Diode Model (SDM) [40] and Point Value Model (PVM) [14] have been introduced.

4.5.1. Point Value Model (PVM)

Point Value Model is considered a simplified model, due to its estimation in power level [14]. It predicts the PV output power by combining two effects of temperature and irradiance. It can be directly applied by using data sheet provided by the manufacturer. The model starts by predicting the efficiency as a function of irradiance under STC temperature,

$$V_{oc}(25^oC, G_{\text{m}}) = V_{oc}(STC) + \frac{nk_BT}{q} ln(\frac{G_{\text{m}}}{G_{STC}}) \tag{4.29}$$

$$P_{\text{mpp}}(T_{STC}, G_{\text{m}}) = FF \times V_{oc}(T_{STC}, G_{\text{m}}) I_{sc}(T_{STC}, G_m) \tag{4.30}$$

$$\eta(T_{STC}, G_{\text{m}}) = \frac{P_{\text{mpp}}(T_{STC}, G_{\text{m}})}{G_{\text{m}} A_{\text{m}}} \tag{4.31}$$

The efficiency as a function of temperature and irradiance can be calculated as follows:

$$\eta(T_{\text{m}}, G_{\text{m}}) = \eta(T_{STC}, G_{\text{m}})[1 + K_p(T_{\text{m}} - T_{STC})] \tag{4.32}$$

Hence, the PV power can be determined by using the equation below,

$$P_{\text{mpp}} = \eta(T_{STC}, G_{\text{m}}) \cdot G_{\text{m}} \cdot A_{\text{m}} \tag{4.33}$$

K_p is the temperature coefficient of the maximum power point of the PV power output. This parameter can be obtained from the data sheet provided.

4.5.2. Single Diode Model (SDM)

Photovoltaics phenomenon is usually described in an electrical circuit model. Therefore PV cell models are often illustrated by the equivalent electrical circuit model which either consist of either four or five-parameters [55, 56]. The introduced model is considered as the simplified four-parameter model [40]. It contains light-generated current, diode reverse saturation-current, series resistance, and diode ideality factor. Due to the large value of shunt resistance [61], it is usually assumed to be neglected for simplification [62]. This model requires internal parameters of the PV modules that should be determined from the manufacturer's data sheet. Up-scaling this PV cell model into the module level can be made with several assumptions such as uniform temperature cell and electrical performance, and no cell

interconnection loss. In this work, the Single Diode Model (SDM) proposed by Krismadinata, et al. has been adopted [40].

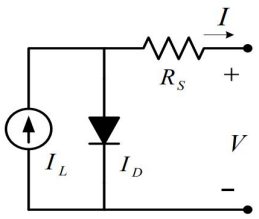

Figure 4.4: Simplified PV equivalent circuit [40]

The output voltage and current from the PV modules are described with the equation below:

$$i_{pv} = I_{ph} - I_o \cdot [exp(\frac{v_{pv} + i_{pv} \cdot R_s}{\alpha(T)}) - 1] \tag{4.34}$$

where,
i_{pv} = PV output current
I_o = Saturation current
v_{pv} = PV output voltage
R_{s} = Series resistance
α = Thermal voltage

Hence, the relationship of the output power of PV modules is defined as,

$$P_{\mathrm{pv}} = V_{\mathrm{pv}} \cdot I_{\mathrm{pv}} \tag{4.35}$$

The series resistance can be determined by using Equation 4.36 with the assumption that it is in the standard temperature (STC) [40]. Moreover, the thermal voltage can be calculated using Equation 4.37.

$$R_s = \frac{\alpha(STC) \cdot ln(1 - \frac{I_{\mathrm{mpp}}(STC)}{I_{sc}(STC)}) + V_{oc}(STC) - V_{\mathrm{mpp}}(STC)}{I_{\mathrm{mpp}}(STC)} \tag{4.36}$$

$$\alpha(STC) = \frac{kb * T(STC)}{q \cdot Ns \cdot n} \tag{4.37}$$

The value of I_{sc} and V_{oc} values depends on temperature and irradiance for the reference (STC) condition. The temperature constants (k_{Voc} and k_{Isc}) can be extracted from the module data sheet.

$$V_{oc}(T, G_{\mathrm{m}}) = V_{oc}(STC) + (n \cdot k_B \cdot T_M/q) \cdot ln(\frac{G_{\mathrm{m}}}{G(STC)}) + k_{Voc} \cdot (T_M - T(STC)) \cdot V_{oc}(STC) \tag{4.38}$$

$$I_{ph}(T, G_m) = \frac{G_M}{G(STC)} \cdot (I_{ph}(STC) + k_{Isc} \cdot T_M \cdot I_{sc}(STC) \tag{4.39}$$

The saturation current as a function of irradiance and temperature can be determined by using Equation 4.41 with the corrected thermal voltage under different temperature (Equation 4.40).

$$\alpha(T) = \alpha(STC) \cdot \frac{T_M}{T(STC)} \tag{4.40}$$

$$I_o(T, G_m) = \frac{I_{ph}(T, G_m)}{exp(\frac{V_{oc}(T, G_m)}{\alpha(T)}) - 1} \tag{4.41}$$

Finally, using Equation 4.34 one can compute the current flows from the output of the PV modules under a specified voltage by using iteration until it reached a convergent value. After that, to get the I_{mpp}, V_{mpp} can be used as an input voltage.

4.6. Lifetime-degradation

Generally, the degradation phenomenon of PV modules is evaluated by measuring the power loss during its lifetime with respect to the initial power. Various degradation modes take places at the same time in the PV module as it is exposed to the environment. Currently, the degradation models are still few and often explaining a part of all degradation modes. In this work, degradation rates from the datasheet and outdoor monitoring data were examined. Moreover, a degradation model influenced by temperature and humidity was introduced and evaluated. Despite the various lifetime estimation of the PV modules, in this work, the lifetime of the PV module is defined as 20% power reduction or when the SOH of the PV modules achieves 80%.

4.6.1. Degradation rate from warranty and outdoor monitoring

In terms of lifetime, crystalline silicon modules have been reported to experience a lifetime-degradation rate of around 0.51%/year on the average. Interestingly, it experienced 0.8%/year on the average due to the higher temperature in hot and humid climates [19] which is the potential target location for installing SHS. It is still debatable whether the degradation rate behaves linearly or non-linearly.

On the other hand, the PV module manufacturer, Jinko Solar, has also announced its linear performance warranty. It starts with the 97.5%, and it decreases to 95% in the first year until the fifth year. After that, it decreases to 90% until the 12th year. Finally, it reduces to 80.7% on the 25th year [63]. This definition of the warranty seems to be not linear. Based on this, the degradation from the warranty can be modeled by using the polynomials equation:

$$k_{dw} = p_{dw2} \cdot t^2 + p_{dw1} \cdot t + p_{dw0} \tag{4.42}$$

$$P_{pv}(t^*) = P_{pv}(t) \times k_{dw}(t) \tag{4.43}$$

Where k_{dw} is defined as the degradation coefficient according to the warranty datasheet. Besdies, t is described as a time step in second. Moreover the polynomials coefficients is determined from the fitting curve using MATLAB, which gives the result as follows:

Table 4.1: Fitting coefficient of the warranty curve

Coefficients	Value
p_{dw2}	-1.965E-05
p_{dw1}	-0.006535
p_{dw0}	0.9816

4.6.2. Peck's Model

In a hot and humid climate, PV modules experience high moisture that can penetrate through the back sheets or the EVA sheets and reach the solar cell. It will influence the degradation of the PV performance due to the delamination, loss of passivation and corrosion of solder joints. Among these possibilities, corrosion occurs frequently. Moreover, the high-temperature profile accelerates water vapor permeation into the module and the subsequent degradation reaction. The combination of these behaviors might bring significant losses in performance [57] [58].

Peck et al. originally proposed the degradation models of semiconductor devices as a function of temperature and relative humidity [64]. Several authors have implemented this model for the PV degradation model [57, 65]. The degradation rate based on the Peck's model is expressed as follows:

$$R_D = B \cdot exp(\frac{-Ea}{kT}) \cdot (rh)^n \tag{4.44}$$

B and n are two constant dependent on the failure mode. In order to obtain Ea, B, n, the equations can be represented on a logarithmic scale by a straight line,

$$ln(R_D) = ln(B) - (\frac{Ea}{kT}) + n \cdot ln(rh) \tag{4.45}$$

By plotting the results from a damp heat experiment with a variation of different relative humidity and temperature, ones can plot $ln(R_D)$ versus 1/T ($^{/circ}$C) and RH (%). Therefore, Ea, B, and n can be determined using curve fitting. Park et al. [57] conducted a damp heat experiment which observed

the degradation rate from different temperature and humidity. The samples setup mimics a typical PV module available in the market which consists of glass, EVA, cell, and back sheet (Figure 4.5).

(a) Test samples for Damp Heat tests; PV module with glass/EVA/cell/EVA/back sheet [57]

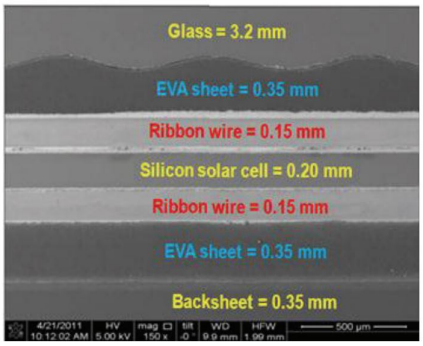

(b) SEM result of test samples [57]

Figure 4.5: Test samples structure for DH tests

Table 4.2: Experimental results for damp heat tests [57]

Temp. (oC)	RH (%)	R_D (%/h)	R_D (%/year)
85	85	0.00611	63.523
65	85	0.00208	18.221
45	85	0.00087	7.6212
65	75	0.00132	11.563
65	65	0.00079	6.9204

By plotting the experimental results from the damp heat tests, the Peck's parameters could be determined by using Matlab's curve fitting.

Table 4.3: Activation energy and constants for Peck's model determined from curve fitting

Ea (eV)	B	n
0.442	1.594×10^8	4.012

Several assumptions of this Peck model are as follows. Firstly, the temperature and relative humidity are assumed to be uniform and in the steady-state condition in a PV module. In practice, the relative humidity inside the PV modules could not achieve the equilibrium condition due to several parameters such as water vapor transmission rate (WVTR) and diffusivity. Thus, it will offer a very pessimistic approximation of degradation rate because of its high relative humidity inside the PV modules. Secondly, the experimental data available is assumed to have a linear degradation extrapolation [57].

For the degradation simulation, the Peck's model was adopted, and the coefficients were extracted based on the damp heat experiments [57]. Then, the %RH and module temperature for every time step, which was taken from meteorological data and thermal model, are used to compute the degradation for that particular time step. In implementing the Peck's model, the PV module temperature profile was first computed using Fluid-Dynamics (FD) model. The relative humidity of certain location was extracted from Meteonorm software. The state-of-health (SOH) of PV modules is introduced from the power reduction of the PV module due to degradation. 100% SOH means that the PV module is in the initial condition. As time goes by, the degradation as a function of %RH and temperature is introduced. The dynamic accumulation of the power degradation is estimated as follows:

$$SOH(t) = SOH(t-1) - SOH(t-1) \times R_D(t-1) \tag{4.46}$$

$$P_{PV}(t^*) = P_{PV}(t^*) \times SOH(t) \tag{4.47}$$

The Peck's model indeed can be used to quantify the effect of varying temperature and relative humidity on the rate of property change. However, it could not provide a complete picture of the long-

term degradation of PV modules, as other stress factors such as light-induced degradation (LID) and temperature cycling are involved.

4.7. Data characteristics

Before performing the simulation to evaluate the PV modules, the input data should be collected first. The input data covers irradiance components, ambient temperature, wind speed, and PV modules size with its technological parameters. In general these parameters are explained in details in Chapter 3.

- **Irradiance components data**
  The GHI, DNI, and DHI are taken from Meteonorm software. The irradiance plane of array is calculated by using Equation 4.1 - 4.5. The module tilt and azimuth angle used is 11° and 6°. This is based on the optimization which further explained in Section 6.3.
- **Ambient temperature**
  This profile is further explained in Section 3.4. Furthermore, this analysis required a Scaling Factor that is explained previously.
- **Wind speed**
  This profile is further explained in Section 3.4
- **PV modules size and its technological datasheet**
  The size of the PV module used is 330 Wp by using Jinko solar JKM330-P [66].

4.8. PV Model Insight

Analyzing the module temperature

For a specific day, it can be seen that the module temperature rises above the ambient temperature. The solar irradiation influences the rising in module temperature. It can rise for more than twice the ambient temperature depending on which thermal model used. The NOCT thermal model offers a higher module temperature approximation as it neglects the convection heat transfers and mounting configuration. However, the FD thermal model offers a lower module temperature approximation since it takes into account convection and irradiative heat transfers which makes the heat flows out from the PV modules.

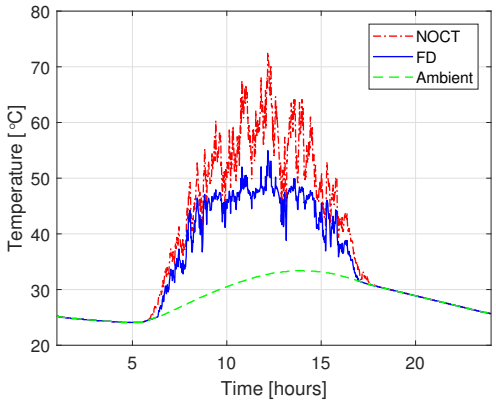

Figure 4.6: Comparison of module temperature by various thermal models with the ambient temperature

The impact of temperature on the PV module performance

In this work, the PV module performance is defined as the instantaneous power and the energy yield over a year. In order to obtain the insight of temperature influences on the PV modules, an electrical circuit model simulation was made. It is shown in Figure 4.7 that an increased module temperature makes a shift in the I-V curve. As temperature increases, the short circuit current increases slightly while the open circuit voltage decrease drastically. Therefore, it resulted to reduce the PV power generated and its efficiency. Thus it can be concluded that a lower temperature gives the highest power generated in the PV module and consequently makes the highest energy yield over a year.

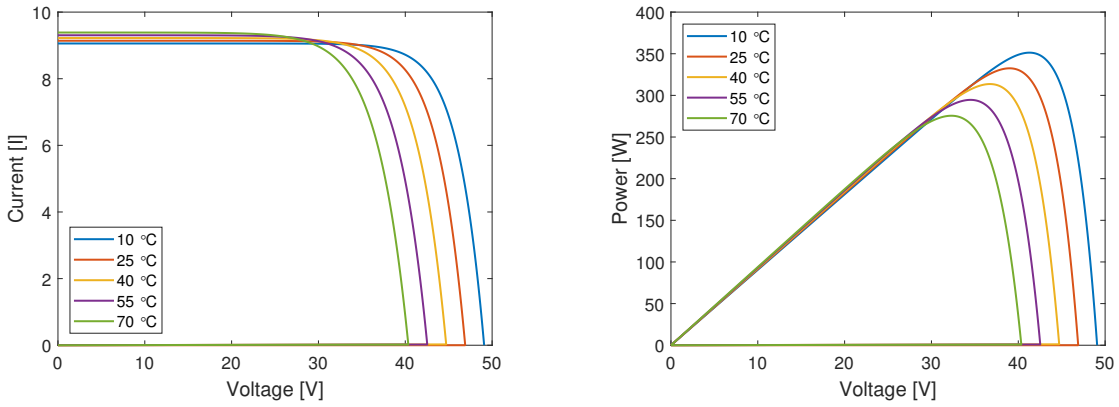

(a) I-V curve (b) P-V curve

Figure 4.7: Temperature impact on a PV module performance at 1000 W/m2 estimated using SDM

The PV energy yield is also influenced by the thermal model used. In this simulation, the tilt and azimuth angle of 11 ° and 6 ° respectively is used. This is an optimal orientation of the PV module in which it will be further discussed in Chapter 6. As it can be seen in the simulation result (Figure 4.8a), the energy yield generated is directly affected by the estimated module temperature used. PVM was used in estimating the PV energy yield by using various thermal model. The NOCT model gives the lower energy yield compared with FD model as it resulted from the higher estimated module temperature, as it can be observed in Figure 4.6. Compared with the standard testing condition (STC), in which that the temperature of the module and ambient is neglected, the FD and NOCT model affects the energy yield for 7.45% to 10.41%. However, with respect to the ambient temperature, the FD and NOCT model influences the energy yield for 5.78% to 8.80% respectively. It can be concluded that different thermal model influence to different energy yield produced for up to 10.41%.

Regarding the field data evaluation, A research has been done to find the most suitable thermal model in predicting the temperature in Delft, The Netherlands. It is observed that FD has a better performing model for predicting the temperature of modules compared with NOCT model. It is proven in which FD model resulted to have higher R-squared (0.866) than NOCT model (0.861) [53]. A higher R-squared means that the model explains better fits to experimental data.

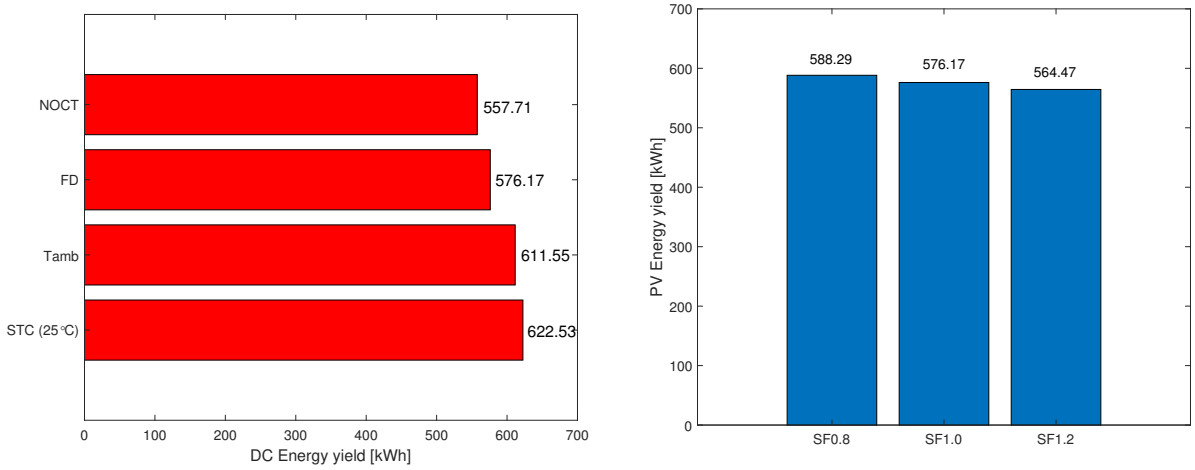

(a) Annual PV yield evaluated under different prediction of module temperature

(b) Annual PV yield evaluated under different temperature profiles

Figure 4.8: Annual PV yield comparison under different temperature profiles and prediction models

If different temperature profile is used, the result might changes. Here, the ambient temperature is

multiplied by the Scaling Factor (SF), which is introduced in Section 3.4, ranging from 0.8 to 1.2. SF1.0 means the ambient temperature Figure 4.8b tells the energy yield for different ambient temperature profile or Scaling Factor (SF). It can be observed that the lowest temperature profile (SF0.8) will result to have the highest energy yield. It decreases as the temperature profile increases. Compared to ambient temperature (SF1.0), the energy yield for SF1.2 is reduced by 2.03%, while the energy yield for SF1.2 is increased by 2.10%. It can be potentially judged that the decreased in the energy yield as the ambient temperature increases is slightly exponential.

The impact of temperature on the PV module lifetime-aging

Based on the damp heat experimental data conducted by Park et al. [57], the degradation of the PV modules depends on temperature and greatly depends on relative humidity. The relationship between temperature, humidity, and degradation rate can be extended further from the experiment's data by using the Equation 4.44. The result is presented below,

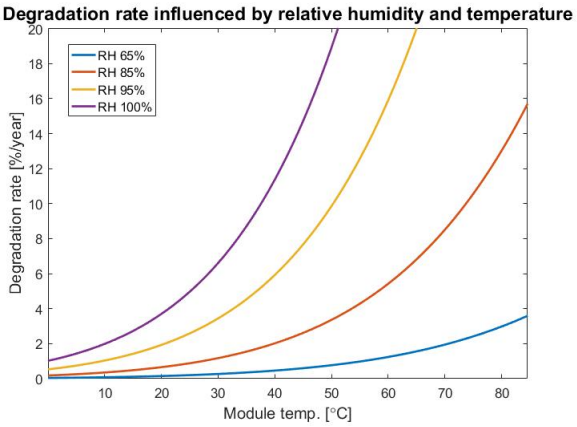

Figure 4.9: Power degradation rate as a function of temperature and relative humidity

Figure 4.9 shows the relationship between the module temperature, the relative humidity, and the yearly degradation rate. Based on the Figure 4.9, it is seen that the degradation increases exponentially as a function of module temperature. Moreover, when higher relative humidity is introduced, the exponential slope increases adequately. It can achieve 20% power reduction a year under 100% RH and 50 °C of module temperature. It means that the PV modules might achieve its end of life for only a year when is exposed to that constant environment.

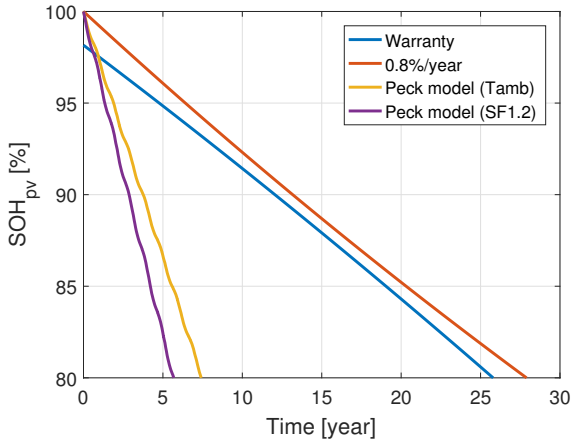

(a) Comparison of relative power degradation of the module

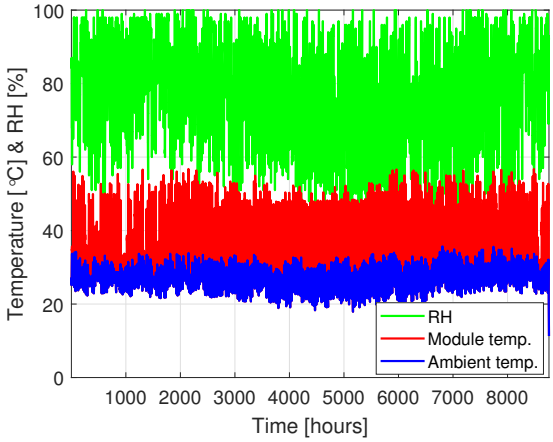

(b) Meteorological data for Peck's model

Figure 4.10: Comparison of relative power degradation of the module for different models and meteo data

The Peck's model was implemented in a hot and humid location (Sumba Island, Indonesia) in which the relative humidity varies in a range of 40% to 95%. The average of the relative humidity is 76.7%. The module temperature are calculated which gives a module temperature profile which varies between 20 °C to 60 °C (Figure 4.10b). The average of the module temperature is 31.3 °C. The computed result gives the most severe degradation compared to the warranty and the hot and humid degradation rate obtained from the reference. It gives 7.41 years of PV modules lifetime while the warranty can achieve 25.3 years and the hot and humid degradation rate can achieve 25.6 years (Figure 4.10a). This very pessimistic result might be due to some critical parameters that are neglected. One of them is the diffusion phenomenon. The diffusion phenomenon contains several factors such as diffusivity, saturation concentration, and maximum Water Vapor Transmission Rate (WTVRmax) [67]. By using these factors, the relative humidity on the PV cells can be evaluated first. This model is adopted based on the damp heat experiment data in which the condition is set constant for 1,000 hours [57]. Hence, it is not the same as at the outside where the relative humidity fluctuates over time. Therefore, the moisture diffusion phenomenon can be quite different. With the further evaluation of relative humidity inside the PV modules (on the cells), the correction from this experimental data can be made.

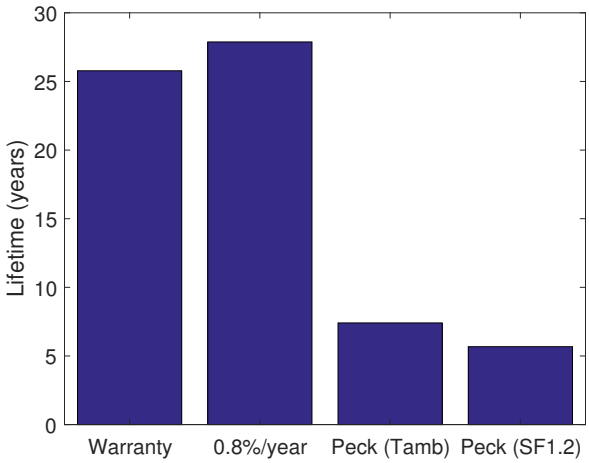

Figure 4.11: Estimated PV module lifetime by using various methods

Figure 4.11 provides a PV module lifetime comparison for various lifetime estimation: warranty, hot-humid average degradation rate, and Peck's model. It is observed based on the definition of EOL, in which the SOH achieves 80%, the degradation rate of hot-humid climate lasts the longest year which is 27.9 years. The degradation rate from warranty achieves the PV modules lifetime for 25.8 years, while the degradation from Peck's model achieves only 7.409.

Although the model has an inaccuracy in predicting the real lifetime of PV modules due to neglecting the diffusion phenomenon, the influence of temperature can be evaluated using Peck's model. If the ambient temperature is increased 20% (SF1.2) and the relative humidity stays the same, the lifetime of the module decreases from 25.13% to 5.68 years as it is seen in Figure 4.11.

4.9. Conclusion

It is important to have an insight of the PV module behavior in evaluating the SHS performance and lifetime since the PV module is the only power generator in the system. A simulation model is constructed by taking into account the irradiance model, thermal model, electrical model by incorporating degradation phenomenon of the PV module. By using this integrated PV model, the performance of the PV module is evaluated concerning temperature impact.

In this chapter, the following research questions are addressed:

To what extend the temperature will influence the dynamic-performance of the PV modules?

The temperature will change several parameters of PV modules such as Voc and Isc. Under 1000

W/m2, the Isc slightly increases (0.06%/°C) while the Voc reduces remarkably (0.31%/°C) as the temperature rises. The combination of these changes results in the reduced PV power output by 0.41%/°C. By taking into account the irradiance (G_m) and the module temperature estimation (T_m), the PV yield is affected by 7.45% to 10.41% compared with the condition where the temperature impact is neglected. Hence, as the higher ambient temperature (SF 1.2) is introduced, it is seen that the energy yield decreases slightly exponentially.

To what extend the temperature will influence the lifetime of the PV modules?

By using Peck's model, the PV modules lifetime as a function of temperature can be evaluated. By selecting a hot and humid location, the ambient temperature is varied: normal ambient temperature and 1.2 higher ambient temperature. Thus as the average ambient temperature increases by 20% the lifetime decreases by 25%. However, the Peck's model overestimates the degradation rate in which it gives 71% lower lifetime than the warranty. The overestimated value is due to the water vapor diffusion behavior which is neglected in the Peck's model.

In the next chapter, FD thermal model, PVM, and degradation rate obtained from the warranty are used for the integrated PV model. This model will be coupled with the batteries model and Power Management Systems (PMS) in performing the simulation of the SHS.

5

The Behavior of The Batteries Evaluation

This chapter focuses to evaluate the batteries for the energy storage in the SHS. It begins in Section 5.1 by explaining the battery behavior. Then, the state of the art and the research gap is well explained in Section 5.2. Based on that, an integrated battery model is proposed which is explained in Section 5.2. The two elements of the integrated battery model are explained comprehensively in Section 5.3 - 5.4. The input data is introduced in Section 5.5 which is obtained from the previous chapters. Having carried on the simulation, the temperature impact on the battery performance and the lifetime is presented and analyzed in Section 5.6. Lastly, Section 5.7 draws the conclusion based on the findings. This battery model will be applied to the integrated model of SHS by incorporating PV model element, power management systems (PMS), and meteorological data in Sumba Island, Indonesia through the case study in Chapter 6.

5.1. Introduction

Battery is one of the most vital components in the SHS. It is strongly influenced by the environment and the operating condition of the systems. Thus, it is important to predict the behavior of the battery. In general, the behavior of the batteries consists of two parts: the dynamic performance and the degradation behavior.

Overview of the battery behavior

Dynamic performance explains the dynamic response of the battery when it is connected to the load. It also depends on the certain conditions, such as temperature, C-rate, and SOC. Battery voltage is one of the examples of the dynamic response during the charging and discharging operation. It also contributes to the efficiency of the battery calculation. As the battery behaves dynamically, modeling the dynamic performance is very important to obtain an accurate state of the battery at a given specific temperature and C-rate during operation.

Degradation phenomenon describes the battery behavior in the long term resulted from the operation and environment that the battery undergoes. As the time goes, the battery performance is getting worse compared to its initial condition. There are various degradation mechanisms studied for both lithium-ion and lead-acid battery [22, 24, 68, 69]. These degradation behaviors can be modeled in many different ways, as it is generally called an aging model. There are two types of aging models: calendar aging and cyclic aging. Calendar aging explains that the capacity fades when the battery is not operated. On the other hand, Cyclic aging occurs due to the active operation; discharging or charging, of the battery. Both calendar and cyclic aging are strongly influenced by temperature. Cyclic aging plays a significant role when the active operation periods are larger than the idle period. However, when the active periods are much shorter and, often, the shallow cycling and low C-rates, the calendar aging plays a dominant role.

Relevance to the SHS

For SHS application in which it highly depends on the battery, knowing the dynamic performance of the battery is essential. The battery performance provides the dynamic behavior in terms of charged

stored and the voltage in the current-voltage level. Thus, by interconnecting to the load, it directly affects the system performance and also its lifetime. Furthermore, as the SHS depend on the batteries to back up the PV power generation, it can be observed that cyclic aging plays a dominant role during the operation.

5.2. Battery Modeling Overview

Current research

Numerous computationally mathematical models have been developed in which they capture battery behavior in sufficient details. There are three types of battery models available in general: Experimental, electrochemical or physical, and electric circuit equivalent model [70, 71]. The experimental model illustrates the parameters of the battery performance using simple equations derived from experiments. It makes the model not flexible and only suitable for specific case [72]. The electrochemical model offers a deeper physical phenomenon of the battery inside the cell which requires high computational time and many parameters. On the other hand, an electric circuit based model offers a useful insight in representing the behavior of the batteries [73]. However, it has several parameters needs to be assessed, which can be done by the experiment. Thus it cannot be universally used.

A generic battery model developed by Tremblay [71] offers a more straightforward and more flexible approach compared to the other battery models. It also offers a universal battery model which can be used for different battery technology using data sheet provided. The model is originally derived from Shepherd model [74]. It models the battery behavior of a battery which covers: terminal voltage, open-circuit voltage, internal resistance, discharge current and state-of-charge based on the datasheet. Moreover, A generic battery model proposed by the Simulink [43] explains the dynamic behavior derived from Tremblay with temperature effect. However, these models are lacking in describing the degradation phenomenon.

Concerning degradation phenomenon, Narayan et al. [75] proposed a degradation model which practically estimates the battery lifetime by using data sheet from the manufacturer under a given application. The model offers a dynamic capacity fading model, as a function of temperature and DOD, which is derived from the micro-cycles of the battery during operation by using Miner's rule.

Integrated battery model

In order to guarantee the long-term dynamic performance of the batteries, one needs to incorporate the dynamic behavior and the degradation model. By interlinking both models, the evolution of the battery behavior can be estimated dynamically in terms of cycle numbers or time. Therefore for a system such as SHS, the lifetime and the degradation-performance can be determined dynamically as the battery is operated. The proposed model should give a combination of dynamic performance and lifetime-degradation models at a voltage and current level of the component.

The link between dynamic and aging models is where the main contribution took part in this work. This proposed model linked dynamic and aging models in which several parameters: Capacity and internal resistance, were updated every time due to the degradation model. As it is illustrated in Figure 5.1, it offers a detailed behavior of the battery in order to evaluate the effect of temperature on its performance over the years. The dynamic-performance model concept was taken from Tremblay et al. [71] with a modification based on Simulink battery block [43]. It is combined with the degradation model proposed by Narayan et al. [5] in which it takes into account the capacity fading as a function of depth-of-discharge (DOD) and temperature of the battery during cyclic operation. Finally, the last step is to update the battery parameters in which the capacity fades and the internal resistance increases due to degradation. The last step is part of contribution in this thesis project. Hence, from this proposed integrated battery model, one can evaluate the behavior of the battery dynamically by taking into account the degradation. Finally, when it is connected to the SHS application, the performance and the lifetime of SHS can be assessed over time with the temperature influence to achieve the research goal.

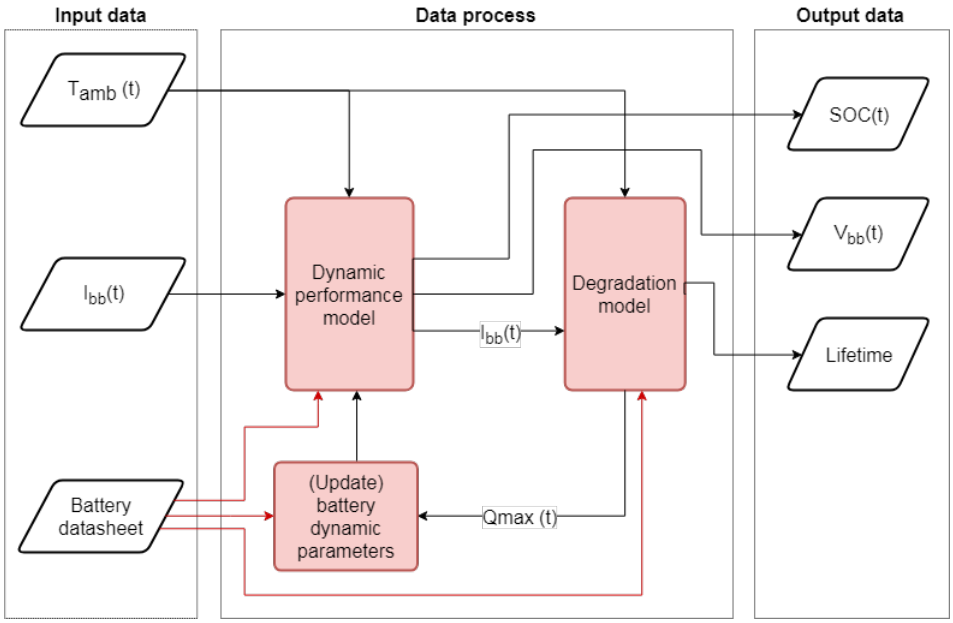

Figure 5.1: Block diagram of battery model

5.3. Dynamic Performance

Generic battery model

A generic battery model proposed by Tremblay [76] is the improved Shepherd model [74] which can represent the voltage dynamics more accurately when the current varies. It also models the Voc as a function of SOC. Polarization voltage term is included, and the polarization resistance is slightly modified to represent the Voc well. In determining the relationship between the voltage and the discharged capacity of the battery, two regions are modeled: exponential and nominal area, as it is shown in Figure 5.2. Four points from the discharge curve were selected based on the shape of the idealized curve. They are the capacity and the voltage at various points: full, exponential, nominal, and maximum. Figure 5.2 illustrates the points which are lying in different regions. The pairs are used to determine the parameters for the battery charge or discharge model.

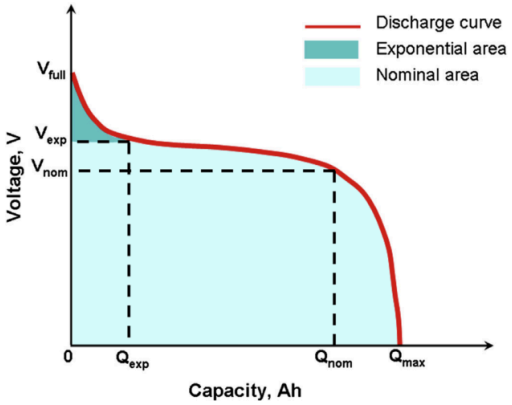

Figure 5.2: Discharge curve of an idealized battery [77]

Charge and discharge model

In the generic battery model [76], the battery voltage is distinguished between charging and discharging mode. It is given by the following equation:

Charging ($i(t) < 0$)

$$V_{\text{bb}} = E_o - K\frac{Q_{\max}}{Q_{\max} - it}it - K\frac{Q_{\max}}{it + 0.1Q_{\max}}i + A.exp(-B.it) - R \cdot i \tag{5.1}$$

Discharging ($i(t) > 0$)

$$V_{\text{bb}} = E_o - K\frac{Q_{\max}}{Q_{\max} - it}it - K\frac{Q_{\max}}{Q_{\max} - it}i + A \cdot exp(-B \cdot it) - R \cdot i \tag{5.2}$$

Where,
E_o = battery constant voltage [V]
K = battery polarization voltage [V Ah^{-1}] and [Ω]
$Q_{\max}$ = battery maximum capacity [Ah]
R = battery internal resistance [Ω]
A = exponential voltage amplitude constant [V]
B = time constant inverse [Ah^{-1}]
it = discharged capacity [Ah]
i = battery current [A]

According to Tremblay [71], the first term (E_0) represents the open circuit voltage (Voc) of a battery at the full capacity. Polarization constant (K) is associated with the polarization ohmic voltage loss and could also represent for the internal resistance loss. Therefore, parameter K has two dimensions respectively: [V Ah^{-1}] and [Ω]. The internal resistance of the battery is represented as a constant resistance as a function of state-of-charge. The time constant inverse (B) can be determined to $3/Q_{exp}$ [71].

It is understood that the battery voltage varies given the different number of C-rate. The C-rate factor is given as $i(t)$ in the dynamic calculation of the battery voltage in the equations above. C-rate refer to the rate of constant current that will cause the battery to discharge in a certain amount of hours [78].

Extracting the parameters

In this model, only four points on the discharge curve provided by the manufacturer (Figure 5.2) are needed to determine the parameters. With these four points, the parameters (E_o,K, and A) can be calculated by solving Equation 5.4 - 5.6 [71]. These equations are the battery voltage on the fully charged, the exponential zone, and the nominal zone. These equations can be solved by using linear programming function in MATLAB.

$$B = \frac{-3}{Q_{\text{exp}}} \tag{5.3}$$

$$V_{\text{full}} = E_o - R \cdot i + A \tag{5.4}$$

$$V_{\text{exp}} = E_o - K\frac{Q_{\max}}{Q_{\max} - Q_{\text{exp}}} \cdot (Q_{\text{exp}} + i) - R \cdot i + A \cdot exp(-B \cdot Q_{\text{exp}}) \tag{5.5}$$

$$V_{\text{nom}} = E_o - K\frac{Q_{\max}}{Q_{\max} - Q_{\text{nom}}} \cdot (Q_{\text{nom}} + i) - R \cdot i + A \cdot exp(-B \cdot Q_{\text{nom}}) \tag{5.6}$$

The internal resistance can usually be found in the battery datasheet. The internal resistance can be derived analytically from the nominal voltage and the rated capacity of the battery [76]. Internal resistance affects the output voltage of the battery which influences the efficiency according to the Equation as follows:

$$\eta = 1 - \frac{I_{\text{nom}} \cdot R \cdot I_{\text{nom}}}{V_{\text{nom}} \cdot I_{\text{nom}}} \tag{5.7}$$

The nominal current (I_{nom}) can be estimated as,

$$I_{\text{nom}} = Q_{\text{nom}} \cdot \text{C-rate} \tag{5.8}$$

Where C-rate is the rated C-rate used for the discharge curve. Hence, the internal resistance can be

calculated as follows:

$$R = V_{\text{nom}} \cdot \frac{1-\eta}{\text{C-rate} \cdot Q_{\text{nom}}} \tag{5.9}$$

LithTable 5.1 is the example of the points from different temperatures from both lithium-ion and lead-acid battery used in this work. The points are according to the battery datasheet [79, 80].

Table 5.1: Parameters from discharge curve in different temperatures

	Lithium-ion		**Lead acid**	
	T_1 (T= 20°C)	T_2 (T = 10°C)	T_1 (T = 20°C)	T_2 (T = 0°C)
Q_{max} [Ah]	19.96	19.94	1.1	0.984
V_{full} [V]	26.55	26.55	6.450	6.400
Q_{exp} [Ah]	0.238	0.300	1.000E-3	0.980E-3
V_{exp} [V]	26.13	25.84	6.440	6.395
Q_{nom} [Ah]	18.50	16.06	0.770	0.637
V_{nom} [V]	24.10	24.73	6.250	6.240

Temperature effect

A generic battery model developed by the MATLAB/Simulink [43] explains that the temperature influences the model parameters (E_0, K, Q, R). These parameters change as a function temperature in various relationships: exponential and linear. They are represented by the equations below.

$$E_o(T) = E_{o,\text{ref}} + \frac{dE}{dT}(T - T_{\text{ref}}) \tag{5.10}$$

$$K(T) = K_{ref} \cdot exp[\alpha(\frac{1}{T} - \frac{1}{T_{\text{ref}}})] \tag{5.11}$$

$$Q(T) = Q_{\text{ref}} + \frac{dQ}{dT}(T - T_{\text{ref}}) \tag{5.12}$$

$$R(T) = R_{\text{ref}} \cdot exp[\beta(\frac{1}{T} - \frac{1}{T_{\text{ref}}})] \tag{5.13}$$

The parameters are needed to be calculated by comparing the discharge curve of the battery from different battery temperatures (Table 5.1). α and β can be calculated by determining K and R. $\frac{dE}{dT}$ can be defined using calculated voltage constant from different temperature. Finally, as for $\frac{dQ}{dT}$, the relationship of maximum capacity and the temperature can be taken directly from the datasheet.

$$\alpha = \frac{log(\frac{K_{T_2}}{K_{T_1}})}{(\frac{1}{T2} - \frac{1}{T_1})} \tag{5.14}$$

$$\beta = \frac{log(\frac{R_{T_2}}{R_{T_1}})}{(\frac{1}{T_2} - \frac{1}{T_1})} \tag{5.15}$$

$$dE/dT = \frac{E_{o,T_2} - E_{0,T_1}}{T_2 - T_1} \tag{5.16}$$

5.4. Cyclic Degradation

Zero-crossing (ZC) approach

The zero crossing approach model is proposed by Narayan et al. [8] which evaluates the capacity loss caused by cycling degradation at the power level. In this work, a modification is made, so the analysis is done at a current and voltage level. In the ZC approach, micro-cycles, when the battery operates, are defined in which the current crosses a zero. In other words, this method only takes into account the active battery periods as illustrated in Figure 5.3. The simulation starts with the initial 100% SOH which relates to healthy battery capacity.

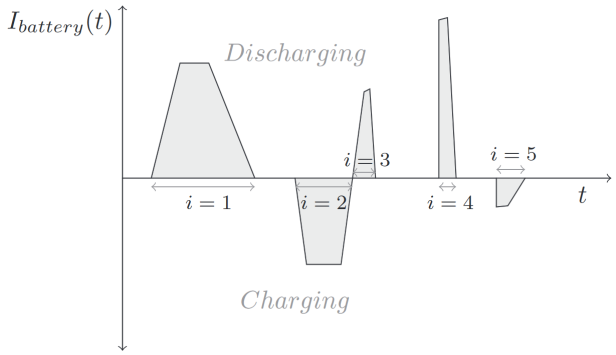

Figure 5.3: An illustration of battery current waveform where zero-crossing approach is applied [8]

In the first step, it evaluates the charged throughput, the average ZCi DOD, and the average ZCi temperature. With the micro-cycle zero-crossing data extracted from the battery simulation, the average active DOD can be calculated as shown [8],

$$\overline{DOD} = \frac{\sum_{i=1}^{N} \overline{DOD_i} \cdot Q_{thr_i}}{\sum_{i=1}^{N} Q_{thr_i}} \tag{5.17}$$

Moreover the average temperature can be determined based on the duration of the ZCs as follows,

$$\overline{T} = \frac{\sum_{i=1}^{N} \overline{T_i} \cdot t_{ZC_i}}{\sum_{i=1}^{N} t_{ZC_i}} \tag{5.18}$$

Polynomial approximations

In determining the cycle of life as a function of DOD, it can be observed that the cycle life of the battery shows a linear temperature correlation. This method is initially proposed in [8]. This relationship can be found in several data sheets provided by manufacturer [79–81]. This linearity can be incorporated to create a 4th order polynomial function,

$$n(T, DOD) = n(T_{ref}, DOD) - f(T_{avg}) D_n(DOD) \tag{5.19}$$

$$n(T_{ref}) = p_4 d^4 + p_3 d^3 + p_2 d^2 + p_1 d + d_0 \tag{5.20}$$

$$f = p_{l_1} T_{avg} + p_{l_0} \tag{5.21}$$

$$D_n = p_{d_4} d^4 + p_{d_3} d^3 + p_{d_2} d^2 + p_{d_1} d + p_{d_0} \tag{5.22}$$

By using Equation 5.19 - 5.22 and data sheet, the polynomials coefficients were estimated by the previous work [82] for lithium-ion and sealed lead acid battery technology. The estimated polynomial coefficients are shown in Appendix C.2. These polynomial functions are used to estimate the damage that the battery takes. The reconstructed curves for Sealed Lead Acid (lead acid) and LiFeMgPO4 (lithium-ion) battery technology by taking into account polynomial coefficients are described in Figure 5.4. The cycle life as a function of temperature and DOD are limited to DOD 20% until DOD 80%.

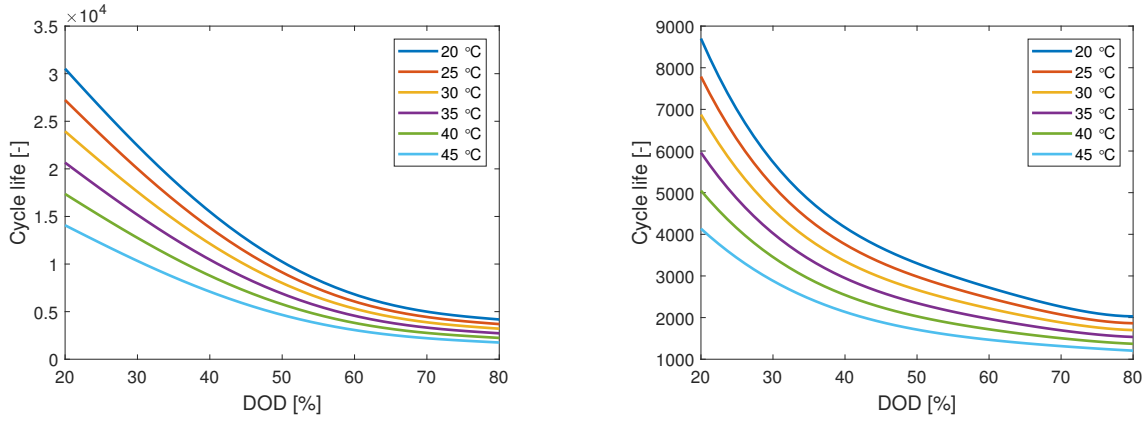

(a) Lithium-ion battery

(b) Sealed lead acid battery

Figure 5.4: Reconstructed of battery cycle-life curves as a function of DOD and temperature for various battery technology (adapted from [82])

Damage calculation

The damage calculation method is adopted from [75]. Having the energy throughput (Q_{thr}), the average battery DOD ($\overline{DOD}$), the average temperature ($\overline{T}$), and the estimated cycle life ($n(\overline{T}, \overline{DOD})$) calculated for each time step of ZCs micro-cycle, one can proceed to the next step which is to evaluate the damage. The equivalent number of cycles (N) can be calculated as a function of the charged throughput and the rated capacity of the battery as shown in Equation 5.23. Note that this fraction is also a proportional number under the same average DOD at a given ZCs time.

$$N_i = \frac{Q_{thr_i}}{2 \times Q_{\max}} \tag{5.23}$$

The damage (D) given to the battery life is then calculated using the Palmgren-Miner rule. The PM rule tells that a finite fraction corresponding to each of the load events will reduce the lifetime of a component. This fraction is determined as a ratio of the number of cycles the element has done to the total expected cycles until EOL under stress factor. However, in this battery degradation model, the equation is slightly modified according to the definition of EOL in the battery. The damage magnitude is scaled so that the EOL is defined when the battery reaches the 80% of SOH.

$$D = \frac{N_i}{n(\overline{T_i}, \overline{DOD_i}) \times \overline{DOD}} \times 0.2 \tag{5.24}$$

Hence, the damage (D_i) is subtracted from the current SOH at every ZCs time step until the EOL is reached (80%).

Updating battery parameters

In the previous explanation, SOH is defined as the capacity ($Q_{\max}$) of the battery which is dynamically reduced. Hence for the next ZCs iteration, the parameters should be updated. The updated parameter consists of battery capacity and internal resistance. It is known previously that under the cyclic degradation, the capacity is always interlinked with the internal resistance. It is known as well that due to degradation, the $Q_{\max}$ reduces and the internal resistance (R) increases. Therefore, the internal resistance can be re-calculated by using the following steps.

Firstly, it is known that the damage makes the capacity reduced as illustrated in Equation 5.25. It is assumed that the capacity in the nominal point is reduced at the same rate (Equation 5.26).

$$Q_{\max}(t^*) = Q_{\max}(t^* - 1) - D \times Q_{\max}(t^* - 1) \tag{5.25}$$

$$Q_{\text{nom}}(t^*) = Q_{\text{nom}}(t^* - 1) - D \times Q_{\text{nom}}(t^* - 1) \tag{5.26}$$

Secondly, the internal resistance can be re-calculated by using Equation 5.9 taking into account the degraded Q_{nom}. The voltage at this specific region might changes. It can be estimated by using Equation 5.28. Lastly, using these equations and an iteration process, one can estimate approximately both the

updated voltage and internal resistance (R).

$$R = V_{\text{nom}} \cdot \frac{1 - \eta_{\text{bb}}}{\text{C-rate} \cdot Q_{\text{nom}}} \tag{5.27}$$

$$V_{\text{nom}} = E_o - K\frac{Q_{\max}}{Q_{\max} - Q_{nom}}Q_{nom} - K\frac{Q_{\max}}{Q_{\max} - Q_{\text{nom}}}i + A \cdot exp(-B \cdot Q_{\text{nom}}) - R \cdot i \tag{5.28}$$

The overall steps of the proposed degradation model can be explained by the flowchart as illustrated in the figure below.

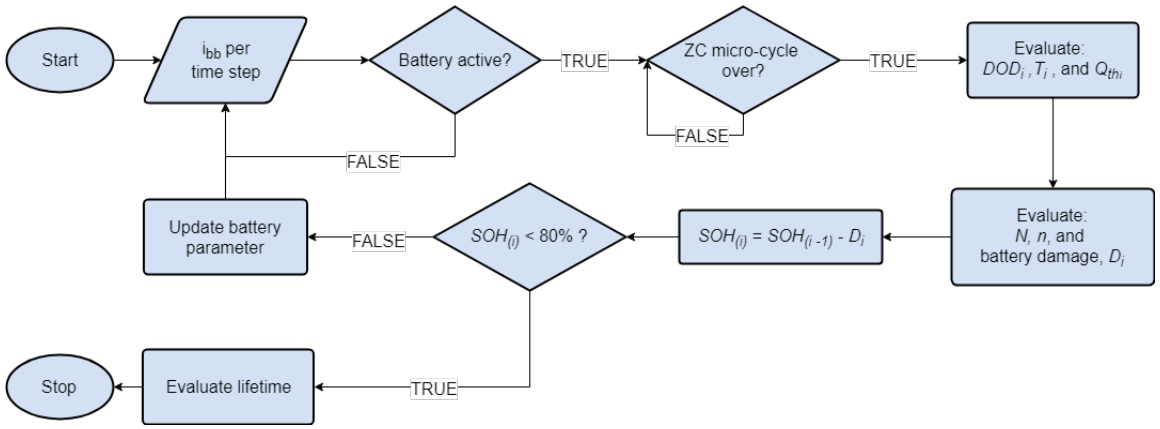

Figure 5.5: Flowchart of cyclic degradation model (adapted from [75])

5.5. Data characteristics

Before performing the simulation in evaluating the batteries, the input data should be obtained first. In this chapter, the battery is simulated for SHS application. Therefore this integrated battery model is placed into the general simulation workflow (Figure 6.1). However, this chapter is focusing on the battery component. Therefore, the input data is designed in order to evaluate the battery by taking out the temperature effect of PV modules. The input data covers the current profile, the ambient temperature/battery temperature, the battery energy capacity with its technological parameters.

- **Battery temperature**
  Since the evaluation of temperature effect on the battery is the focus of attention in this chapter, the temperature of the battery is kept constant under 5 °C, 20 °C, and 35 °C. With these different values, the temperature impact on the battery is assessed.

- **Current profile**
  The current profile used in this battery evaluation is divided into two types. The first one is the constant current which will be used in evaluating the dynamic performance of the battery.

  The second one is the dynamic current. This current profile is obtained by performing the SHS simulation together with the PV power, the Power Management System (PMS), and the load profile. This general simulation work flow is illustrated in Figure 6.1. The PV power is described based on the Chapter 4. The important note is that the PV power is generated under FD of ambient temperature without taking into account the PV power degradation. Furthermore, the power management system is explained in Section 2.5. Moreover, the load profile is introduced in Section 3.5.

- **Battery size and the technological datasheet**
  The lithium-ion and lead-acid battery is used based on the specified component datasheets [79] [80]. The size of the battery used is 960 Wh for both the battery technologies. This is based on the system sizing which is explained further in Section 6.3. The simulation is performed under specific SHS application which can be explained further in Figure 6.1. As it is shown in Table 6.2, the SOC limit used in the degradation simulation is between 20% to 80%.

Table 5.2 summarized the evaluation approach for the dynamic and the degradation performance in this chapter.

Table 5.2: Summary of battery evaluation

Subsection	Evaluation	Current profile	SHS simulation
5.6.1	Dynamic performance	Constant	NO
5.6.2	Degradation performance	Dynamic	YES

5.6. Battery Model Insight

The simulation results are presented as follows. Firstly, the dynamic performance result of the battery is introduced. Secondly, the degradation behavior of the battery, together with the correlation of its dynamic performance, is presented. Lastly, the lifetime of the battery with regard to the temperature is demonstrated. In this work, the analysis is made in a single battery bank.

5.6.1. Dynamic performance

C-rate influence on the charge and discharge curve

The battery shows different behaviors when they are on discharging mode and charging mode. Figure 5.6 shows the discharge and charge curve for Li-ion battery. In this figure, two things can be identified. First, when the batteries are charged under the same current rate, the voltage is higher than when they are discharged. It is because when the batteries are charged, the current direction becomes negative. Therefore, according to the Equation 5.1 - 5.2, it results to have a more positive value of the voltage due to the internal resistance and the polarization resistance of the battery.

Secondly, when a higher current is introduced, on the discharging mode, the voltage decreases. However, on the charging mode, the voltage increases. It is because as the higher current is introduced during discharging, the internal and polarization resistance which is multiplied by the positive current makes the voltage drops. On the other hand, during charging, a negative current makes the voltage of the battery increases.

The SLA battery uses 0.05 C-rate for its rated C-rate, but the Li-ion battery uses 0.5 C-rate. Concerning the trend discussed previously for Li-ion battery, the same trend can be identified for various C-rate for discharge and charge curve of the SLA battery as it is observed in Figure 5.7. However, it can be seen that as the battery is charged or discharge with lower C-rate, i.e., 0.05 C-rate, the voltage increases very lightly. It can be observed as well that the lead-acid battery has different cut-off voltage depends on the C-rate used. This is based on the datasheet of the lead-acid [80].

In general, the battery evaluation does not perform the initial voltage at time zero where there is no current involved. In reality, the voltage of the battery came from the same point under the same SOC level, in which it is called an open circuit voltage. Once the load is connected to the battery, the voltage increases or decreases suddenly, depending on the charge or discharge mode. When the battery is disconnected from the load, the voltage is moving to the open circuit voltage for some time (relaxation time).

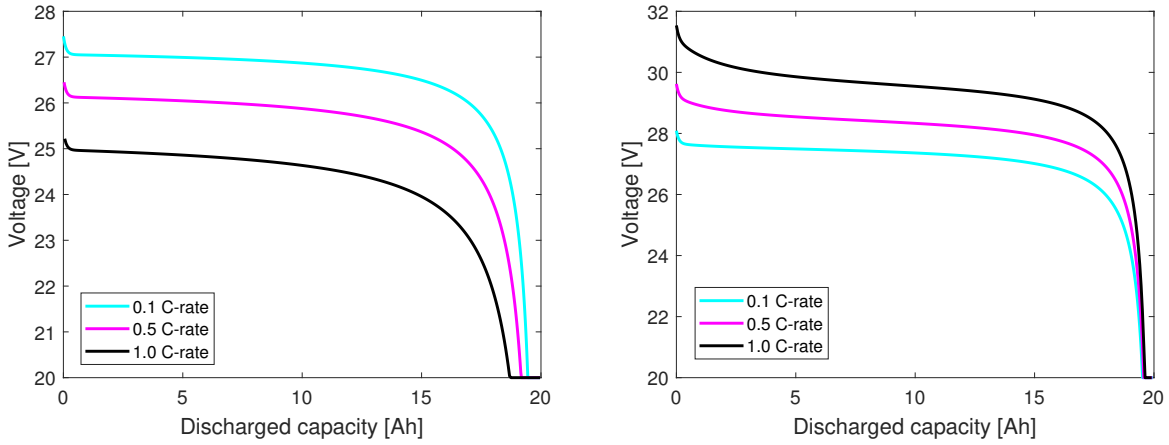

(a) Discharge curve (b) Charge curve

Figure 5.6: Charge and discharge curve for Lithium-ion battery technology at various C-rate using 20 °C

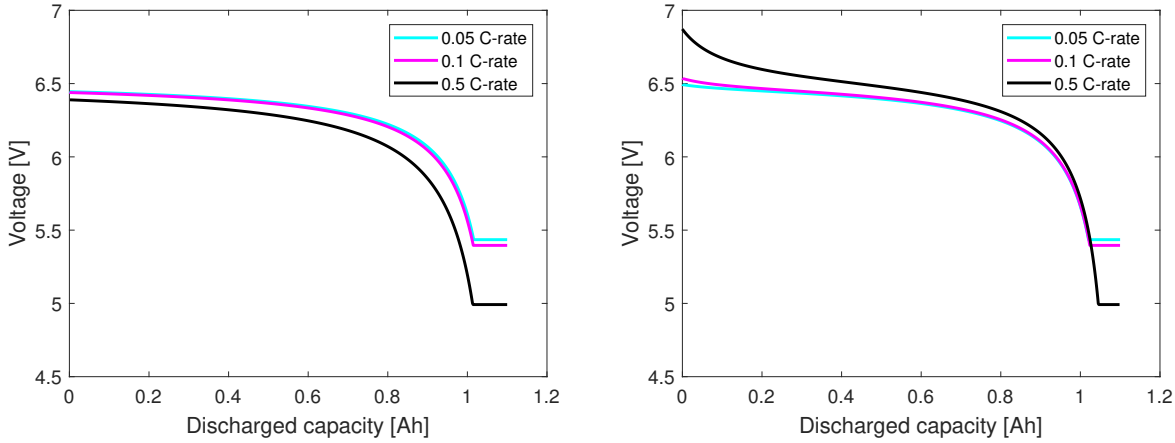

(a) Discharge curve (b) Charge curve

Figure 5.7: Charge and discharge curve for lead acid battery technology at various C-rate using 20 °C

Temperature impact on the battery model parameters

Based on the Equation 5.10 - 5.13, the temperature impact of the battery parameters can be evaluated for both lithium-ion (Li-ion) and lead acid (SLA) battery technology. The relationship between the maximum capacity and the temperature can be obtained directly from the battery datasheets [79, 80]. However, the internal resistance, the polarization constant, and the voltage constant as a function of temperature are predicted by calculating the thermal coefficient of the internal resistance using Equation 5.15. In this part, battery model parameters are evaluated with regard to the parameters at the reference temperature (20°C).

It can be observed from Figure 5.8a that as the temperature rises, the capacity increases even above its rated capacity for both lithium-ion and lead-acid battery technology. However, the capacity drops exponentially when a lower temperature is introduced. It can achieve around 90% at 0°C. The capacity of the lead acid battery is higher than the lithium-ion battery when it comes to the high temperature.

As for internal resistance, as the temperature decreases the internal resistance increase exponentially up to 106% of the internal resistance at the reference temperature (Figure 5.8b). The exponential increase can also be seen in the polarization resistance (Figure 5.9a) as a lower temperature is introduced. As for voltage constant, a decrease in temperature makes the voltage constant value decrease by around 1% at 0°C as it is shown in Figure 5.9b.

In general, it can be observed from these figures that the SLA battery is more temperature sensitive than Li-ion battery. It is shown that, in terms of capacity, internal resistance, and voltage constant, the SLA battery is very responsive with regard to the temperature changes. However, in terms of polarization constant, Li-ion battery is more sensitive with against the temperature.

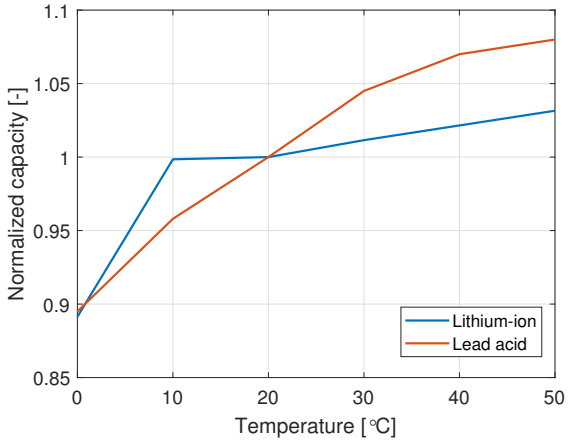

(a) The impact of temperature on capacity (taken from manufacturer's data sheet [79] [80])

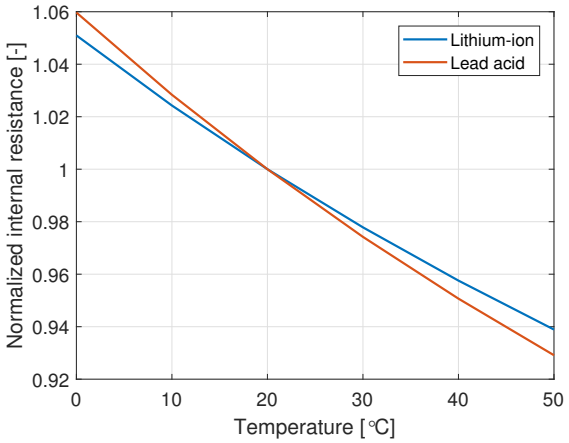

(b) The impact of temperature on internal resistance

Figure 5.8: The influence of temperature on capacity and internal resistance

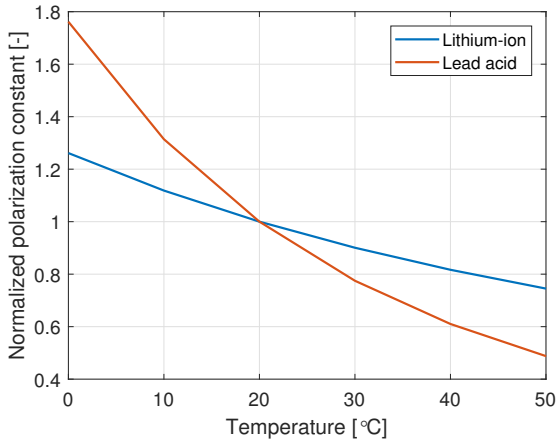

(a) The impact of temperature on polarization constant

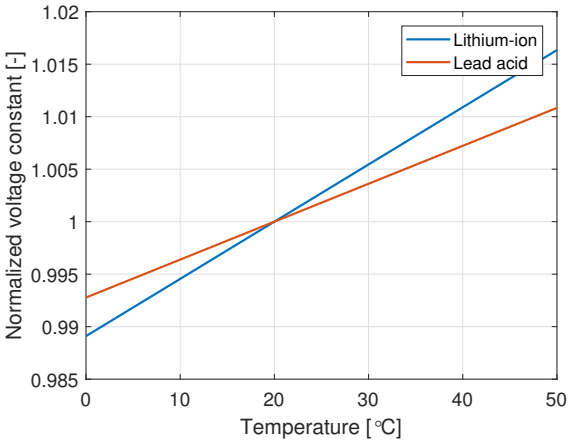

(b) The impact of temperature on voltage constant

Figure 5.9: The influence of temperature on polarization constant and voltage constant

Temperature influence on the discharge and charge curve

The previous subsection explained that due to temperature changes, several battery model parameters change. Thus, combining the effect of temperature on the parameters, the dynamic voltage of the battery as a function of temperature can be evaluated.

Figure 5.10 - 5.11 shows the charge and discharge curve simulation result of Li-ion and SLA battery under 5°C, 20°C, and 35°C. It can be analyzed that as the temperature increases, the voltage and the capacity of the battery increases. The same trends appear for SLA batteries. However, it can be observed that the rate of increase in capacity for 35°C for SLA is higher than the Li-ion batteries. This follows the capacity-temperature relationship based on Figure 5.8a in which that the SLA battery is more sensitive against the temperature.

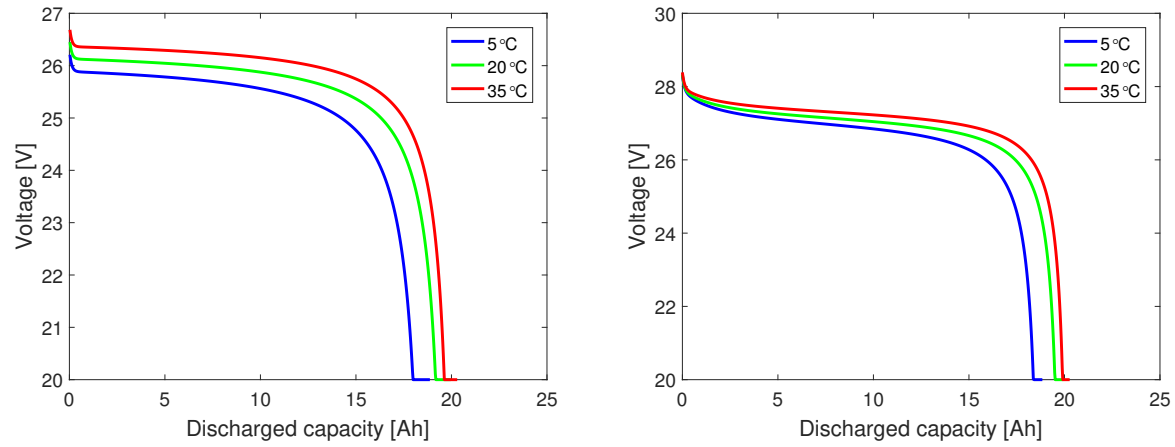

(a) Discharge curve (b) Charge curve

Figure 5.10: Charge and discharge curve for Lithium-ion battery technology at various temperature using 0.5 C-rate

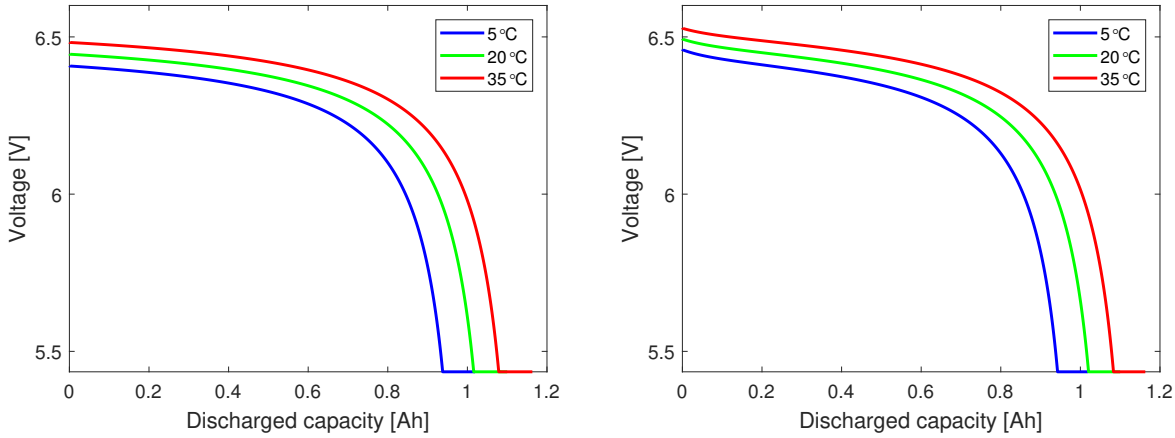

(a) Discharge curve (b) Charge curve

Figure 5.11: Charge and discharge curve for lead acid battery technology at various temperature using 0.05 C-rate

5.6.2. Degradation performance

In this subsection, the battery is simulated under the SHS application so that the current is dynamic. According to the aging model, battery parameters change as the accumulated cycle counts increases (N_{total}). As it can be seen from the results, under the cyclic aging, there are two significant changes in the battery's characteristics.

Temperature impact on capacity and internal resistance degradation

Firstly, due to cyclic degradation, the battery capacity ($Q_{\max}$) fades. This capacity fading is irreversible. The battery capacity fades at various rates depending on the damage imposed. According to the Equation 5.23 - 5.24, the damage is a function of temperature and DOD at every time step. Thus, if the DOD and the temperature of the battery increases, the degradation accelerates faster. On the other hand, it is known that the increase in temperature makes the increased capacity in the short term, as it is explained in the Section 2.4.2. However, by combining both short term and long term effect, the battery capacity with higher temperature can potentially drop very fast even though it has a slightly higher capacity in the short term.

Figure 5.12a illustrates the combination of a short-term capacity changes and a long-term capacity fading, for the Li-ion battery, as the battery undergoes cycling under different temperature. The higher temperature starts at high capacity, but it is imposed to have a faster capacity fading. It results at a

certain moment, i.e., after 1,000 or 2,500 cycles, the battery at 35 °C has the same (or lower) capacity compared to at 20 °C and 5 °C respectively. As for SLA battery (Figure 5.13a), the battery decreases sharply due to the degradation. It can be noticed that at 35 °C, the battery starts with higher relative capacity than the Li-ion battery. On the other hand, at 20 °C, the SLA battery starts with lower relative capacity than the Li-ion battery. As a result, even after near its EOL, there is no intersection of the capacity level between the temperatures given.

Secondly, the internal resistance (R) increases due to the degradation. The increase in resistance behaves irreversibly. The increase in resistance is originally based on the damage imposed counted from the Equation 5.23 - 5.24. Thus the rate of increase is a function of temperature as well. Compared to the rate of capacity fading, the rate of increase for the internal resistance is slightly higher as it can be noticed in the Figure 5.12b. As for SLA battery, the increase in the internal resistance is faster than the Li-ion. Hence, the intersection between internal resistance at 35 °C and 20 °C can be found when the battery is degraded after 700 cycles.

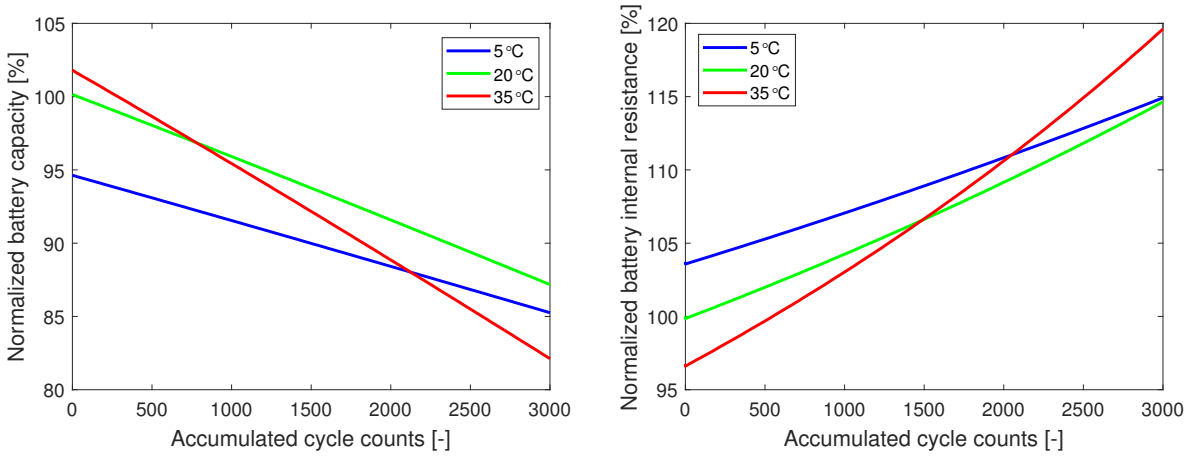

(a) Capacity degradation (b) Internal resistance rise

Figure 5.12: The impact of cyclic degradation on battery parameters for Lithium-ion battery technology at various temperature

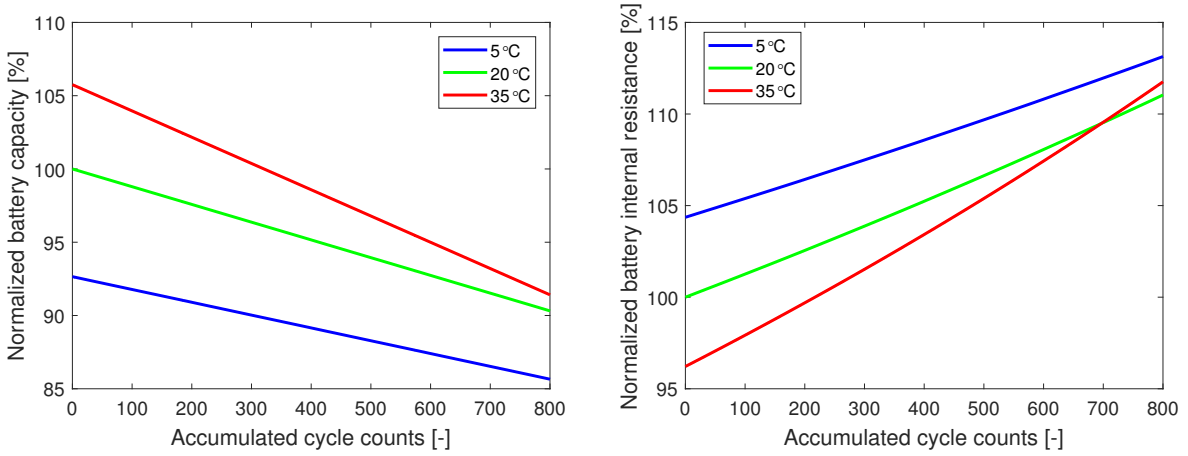

(a) Capacity degradation (b) Internal resistance rise

Figure 5.13: The impact of cyclic degradation on battery parameters for lead acid battery at various temperature

Temperature impact on discharge and charge curve under cyclic aging

In this section, the discharge and charge curve of the Li-ion and the SLA battery are evaluated under cyclic aging. As for the Li-ion battery, the battery after 3,000 cycles is chosen, while for SLA battery,

the degraded battery after 800 cycles is chosen.

As for the Li-ion battery, after 3,000 cycles, there are several shifts in the discharge and charge curve. It can be seen in Figure 5.14. It can be observed from both of discharge and charge curve; they have a lower maximum capacity in which the maximum capacity of the battery under 35°C become less than under 20°C. It is due to the capacity fading which is explained in Figure 5.12a. Moreover, in the discharge curve, the voltage slightly decreases while in the charge curve, the voltage increases. They are resulted from the internal resistance rising due to the degradation.

In terms of the SLA battery, a decrease in capacity can be found after 800 cycles as it is illustrated in Figure 5.15. different from the Li-ion battery, the full capacity of the battery under 35°C does not overlap the capacity of the battery under 20°C as it can be seen in Figure 5.13a. The effect of internal resistance degradation is not clearly observed on both charge and discharge curve for the lead-acid battery.

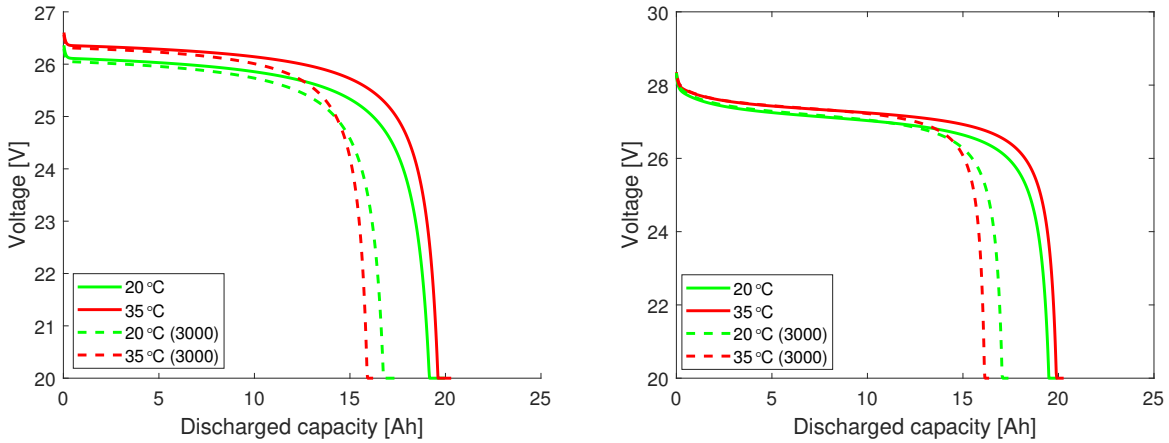

(a) Discharge curve (b) Charge curve

Figure 5.14: Charge and discharge curve for Lithium-ion battery technology after 3000 cycles at various temperature using 0.5 C-rate

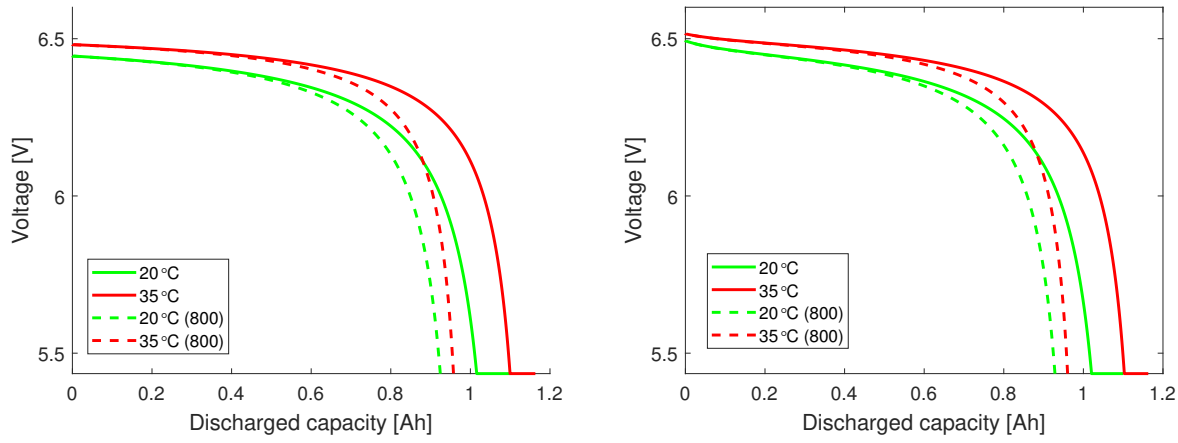

(a) Discharge curve (b) Charge curve

Figure 5.15: Charge and discharge curve for lead acid battery technology after 800 cycles at various temperature using 0.05 C-rate

In general, the effect of internal resistance aging is minimal compared to the effect of capacity fading. It is because the current that is used is small (0.5 C for Li-ion and 0.05 C for SLA battery). Hence, based

on generic battery model equation (Equation 5.1 - 5.2), the voltage is indeed dominantly influenced with the capacity aging. It reflects the same situation under SHS operation where it tends to use relatively small current.

5.6.3. Battery Lifetime

By putting together all the battery results, the performance and the aging behavior of the battery can be observed. In this evaluation, the PV power at a given location is generated to supply a specific load profile. The PMS which is discussed in Section 2.5, is used to control the power flow. In this subsection, the battery is performed under a constant temperature of 5°C, 20°C, and 35 °C.

The result shows a predictable behavior. It can be seen in Figure 5.16, as the temperature increases, the aging rate of the battery increases. Hence it leads to have a decreased battery lifetime. From the simulation, it can be seen that the battery can achieve 35 years for lithium-ion battery and 12.5 years for lead-acid battery under 5 °C. The lifetime decreases as the temperature rise with the rate of 0.59 years/°C or 1.65%/°C. As for the lead-acid battery, it decreases with the rate of and 0.19 years/°C or 1.54%/°C in which that the rate of decrease in the lifetime as a function of temperature is slightly lower than the lithium-ion battery.

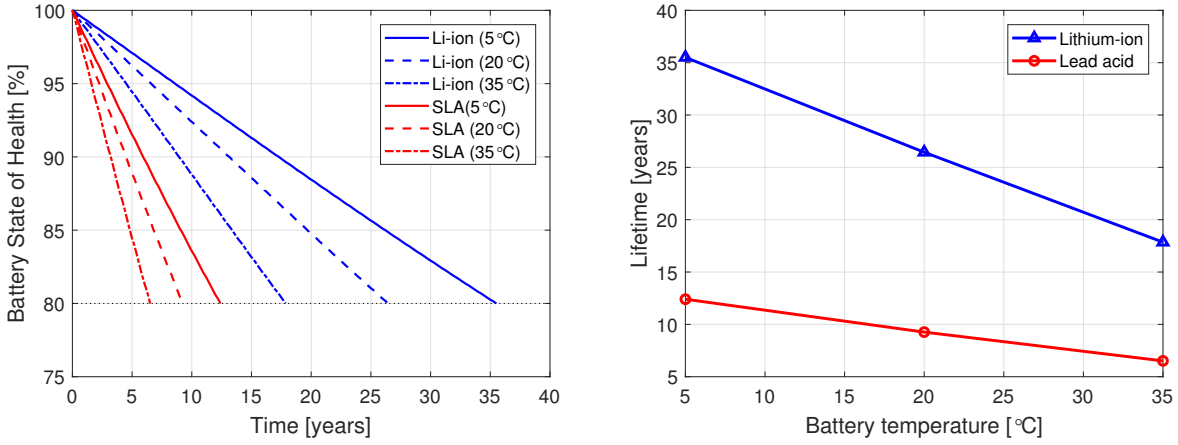

(a) Discharge curve

(b) Charge curve

Figure 5.16: Battery State-of-Health and lifetime for 5°C, 20°C, and 35 °C

5.7. Conclusion

The knowledge of the battery behavior is essential in evaluating the SHS performance and lifetime. A comprehensive battery model is proposed by taking into account the dynamic performance and the cyclic aging of the battery. The main contribution of this chapter is to interlink both dynamic performance and cyclic aging of the battery in a closed loop. Therefore, using this model, the battery can be evaluated dynamically by focusing on the temperature impact.

In this chapter, the following research questions are addressed:

To what extend the temperature will influence the dynamic and aging performance of the batteries?

The temperature influences several parameters of the battery model: capacity, internal resistance, polarization constant, and the voltage constant. The relationship of these parameters changes might be described linearly and exponentially. The influence is based on the battery technology used. As the temperature increases, the maximum capacity can increase up to 103.5% to 108%, and the internal resistance can decrease exponentially up to 92% to 91% at 60°C. The polarization constant decreases exponentially up to 40%. As for the voltage constant, it increases linearly up to 102%. This phenomenon will affect the discharge and charge curve of the battery in terms of the capacity and the voltage. Generally speaking, it can be concluded that the SLA battery is more temperature sensitive than the battery voltage.

The temperature also affects the rate of aging of the batteries. In the Li-ion battery, the capacity fades with a rate 0.0037% per cycle at 20 °C. The rate of fading increases for 54.54% as the temperature increases to 35 °C. Furthermore, the internal resistance rises at a similar rate but slightly higher. Compared to the Li-ion battery, the aging rate in the SLA battery is more extreme. At the 20 °C, the capacity fades with a rate 0.0094% per cycle which is 154.05% more severe than the lithium-ion battery at the same temperature. These parameters changes affect the discharge and charge curve of the battery.

To what extend the temperature will influence the lifetime of the batteries?

The battery simulation is performed by taking into account the SHS application in the integrated system model. The result shows that as the temperature rises, the lifetime decreases with a linear rate of 0.59 years/°C for Li-ion battery and 0.19 years/°C for SLA battery. Therefore, it is clear that an increase in temperature will give a positive effect on the lifetime of the battery in the SHS application.

In general, it is observed that there is a converse behavior of the battery with regard to the temperature impact. An increase in temperature will improve the performance in terms of capacity and internal resistance in a short time. However, in the long run, the aging plays a part so that the capacity decrease faster and eventually will come to a lower value than the battery with lower temperature. These phenomena will directly affect the performance of the entire Solar Home Systems.

6

The Solar Home Systems Evaluation in Sumba Island, Indonesia

This chapter provides the SHS performance evaluation in Sumba Island, Indonesia. The evaluation adopted the proposed integrated SHS model which consists of several models: PV model (Chapter 4), battery model (Chapter 5), and the PMS (Section 2.5). Section 6.1 briefly explains the proposed integrated SHS model. Eight cases are introduced in Section 6.2 which covers various temperature profiles, battery technologies, and model considerations. Before carrying out the simulation, the initial system design should be performed in which it tells the PV module orientation and the size of the system (Section 6.3. Section 6.4 addresses the simulation result in evaluating the temperature impact. The result covers the power flow performance, LLP, and the battery lifetime. Lastly, Section 6.5 draws the conclusion based on the simulation results.

6.1. Integrated Model Overview

A simple constant DC-DC converter efficiency of 0.96 is introduced. The main output of this integrated model is the performance which includes the LLP every year and also the lifetime of the system. Moreover, the simulation used a time-step of 10 minutes. Figure 6.1 illustrates the integrated model overview in assessing the temperature impact of the system. The main variable of its input is multiple temperature profiles which are then to be assessed.

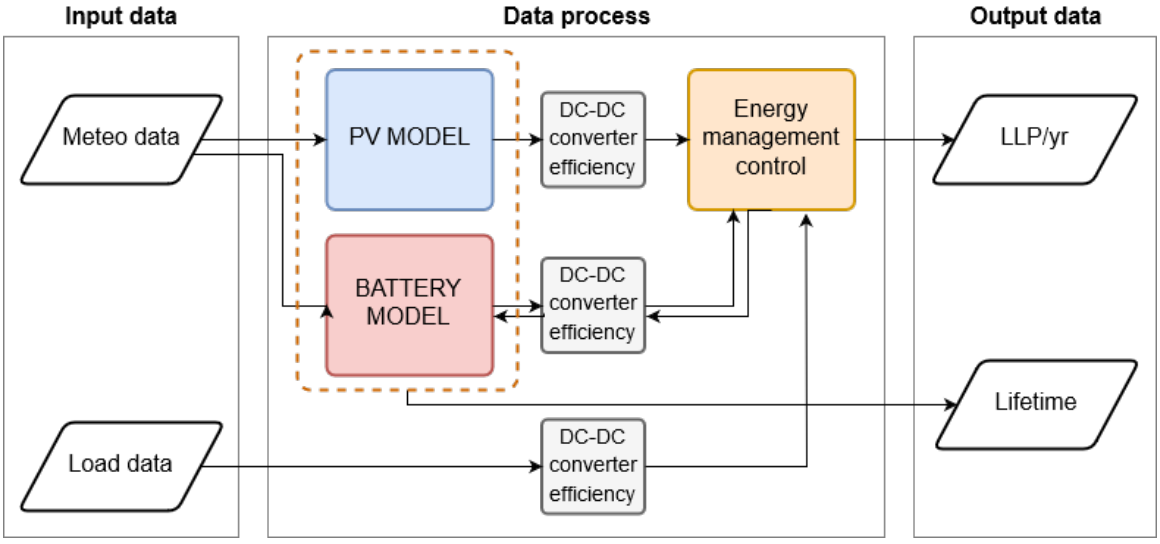

Figure 6.1: Block diagram of integrated model

6.2. Cases Explanation

In this integrated SHS evaluation, eight study cases were performed. They are divided concerning the ambient temperature used, and the feature of the model used. Each division is contributed to the

analysis of the temperature impact concerning many features that the integrated model is incorporated.

- Firstly, they are divided with regard to the battery technology used: Li-ion and SLA batteries.
- Secondly, they are divided by the ambient temperature considered: Ambient temperature (SF1.0), SF1.2, and SF0.8 which is explained earlier in the previous Chapter 3. This is used to compare the performance and aging under the fluctuated temperature profile.
- Lastly, another two cases are introduced by neglecting/considering the thermal behavior of the PV. These cases are introduced firstly in the initial system sizing.

The details of the cases including the considerations adopted are summarized in Table 6.1.

Table 6.1: Overview of the cases

Case	Ambient temp.	PV			BB		
		Thermal	Electrical	Deg.	Dynamic	Aging	Technology
Li-ion (SF1.0)	Amb. temp.	FD Model	PVM	Warranty	Yes	Yes	Li-ion
Li-ion (SF1.2)	1.2 × Amb. temp.	FD Model	PVM	Warranty	Yes	Yes	Li-ion
Li-ion (SF0.8)	0.8 × Amb. temp.	FD Model	PVM	Warranty	Yes	Yes	Li-ion
SLA (SF1.0)	Amb. temp.	FD Model	PVM	Warranty	Yes	Yes	SLA
SLA (SF1.2)	1.2 × Amb. temp.	FD Model	PVM	Warranty	Yes	Yes	SLA
SLA (SF0.8)	0.8 × Amb. temp.	FD Model	PVM	Warranty	Yes	Yes	SLA
Initial FD	Amb. temp.	FD Model	PVM	No	No	No	Li-ion/SLA
Initial T25	25°C	No	PVM	No	No	No	Li-ion/SLA

SHS Assessment Metrics

A perfect design is more critical for SHS (off-grid systems) than for on-grid systems due to independence on the electricity grid. Two assessment metric is developed to assess the performance and the lifetime of SHS in the designing phase.

The first metric is Loss-of-Load Probability (LLP) which is related to the performance of SHS. LLP is determined as a function of the number of failed events. A failed event is defined when the power required by the load appliances cannot be delivered by the PV system (PV modules or/and batteries). It is calculated as follows:

$$LLP = \frac{\text{Total number of failed events}}{\text{Total number of events the system is designed for}} \tag{6.1}$$

In this work, the LLP is calculated for every year. This performance metric will determine how optimal the system is. For example, if the LLP is below the acceptable value, the PV modules power or the capacity of the batteries should be increased.

The second metric is the lifetime of the components of SHS. The primary focus of attention is to analyze the lifetime of the battery. It is because the batteries have a shorter lifetime than the PV modules. The lifetime is defined as when the SOH achieves 80%. The term SOH is determined by the percentage of degraded capacity with respect to the initial capacity.

6.3. Initial System Design

The system design optimization consists of PV modules orientation selection and system sizing. It is necessary to maximize the PV module output by considering the sun position and also to maximize the performance of SHS in delivering the power to the appliances.

PV module orientation

The optimization result by using the methodology explained in Section 4.3.2 tells that a maximum yearly total irradiation can be achieved by placing a PV module with a tilt and azimuth angle of 11° and 6° respectively. The orientation results to have the sun irradiation (G_m) received on the module boosted

1.56% from 1,856 kWh/m2 to 1,885 kWh/m2 annually. It makes to have an ESH of 5.16.

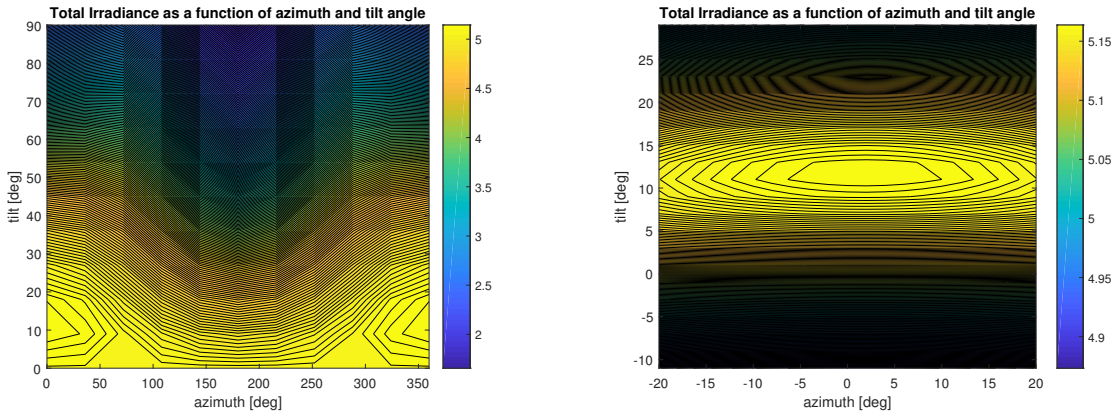

(a) first step (b) second step

Figure 6.2: Two-step optimization result in determining maximum annual irradiation (G_m) or ESH

LLP approach system sizing

In sizing the system, LLP optimization methodology is used. The methodology is based on the mismatch between PV output power and the load profile under the described energy management control strategy (Section 2.5). For a specific PV module rated power, the SHS is simulated by using various battery size. The output of this simulation is LLP which can be used for the sizing methodology. The sizing simulation began with 120 kWh battery as a starting point. Then with the increments of 120 kWh until 3000 kWh, the simulation is carried.

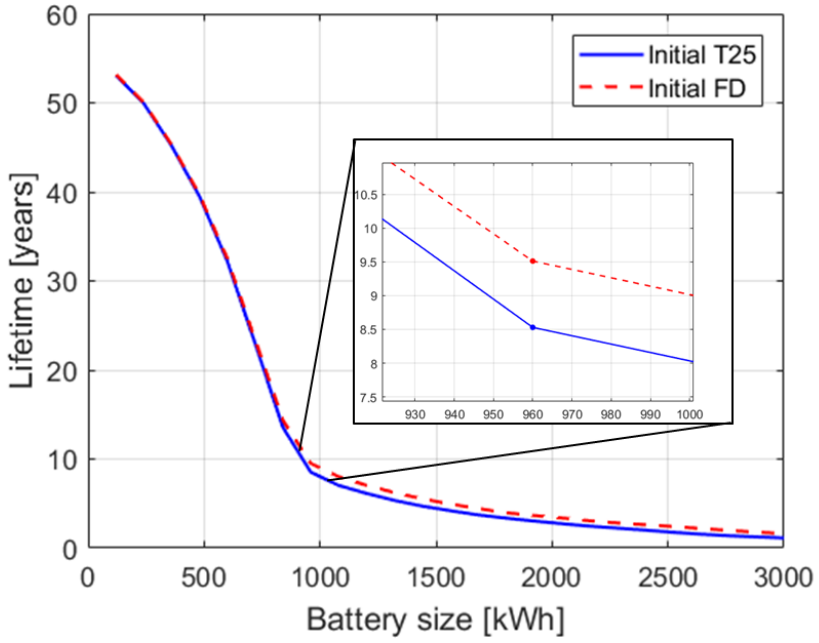

Figure 6.3: SHS sizing methodology based on the LLP variation for various storage sizes and various PV output considerations

Based on the described sizing methodology, the LLP was assessed for various battery sizes as shown in Figure 6.3. The simulation was done with a 330 Wp PV module [66] by considering two different PV power estimation. Firstly, the PV power is estimated by neglecting the thermally induced losses. The other PV power is estimated by considering the thermally induced losses with estimated module temperature using FD model. It can be seen in the figure above, for a low battery size the LLP of both

PV power outputs is closely similar. However, as the higher battery size is used, it results to have a slightly different LLP. Using the FD model, it results to have a slightly higher LLP. It is an economically optimal choice to take the battery size around the knee point. At this point, when a higher battery size is used, it does not make a significant improvement of LLP. This corresponds to an LLP of 9.50% and a battery size of 960 Wh using FD model consideration of PV power output. By neglecting the temperature of the module, an LLP of 8.50% can be achieved by using the same battery size. Both of LLP values are acceptable based on the recommended LLP guide [14]. It is also observed that using 330 Wp rated PV module is considered sufficient enough in providing the load. Thus, based on this result, a 960 Wh battery storage and 330 Wp rated PV module is used.

SHS design components

The system is then evaluated by using two different battery technology: Lithium-ion based battery (LiFeMgPO4 or Li-ion) and Sealed Lead Acid (SLA). based on the data sheet, both of battery banks have different capacity and voltage level. The Li-ion battery bank has 24 V and 20 Ah, while an SLA battery bank has 6 V and 1.1 Ah. Therefore, to fulfill the selected battery size, 960 Wh, and to make an equal comparison, the number of battery banks in parallel might be a decimal number. It can be done due to the assumption of there is no resistance in between the battery bank. Secondly, the minimum and maximum SOC is set to be the same by following the maximum limit of SLA battery technology. Table 6.2 summarized the system design of the SHS, including the size of the PV module and the batteries.

Table 6.2: Design parameter for the SHS

PV Modules		
$P_{pv,rated}$ [Wp]	330	
Batteries		
Technology	Li-ion	SLA
@ $V_{bb,rated}$ [V]	24	6
@ $Ah_{bb,rated}$ [Ah]	20	1.1
Nb_{ser}	2	8
Nb_{par}	1	18.182
Total V_{bb} [V]	48	48
Total Ah_{bb} [Ah]	20	20
Total E_{bb} [Wh]	960	960
SOC limits		
SOC_{max}	80%	80%
SOC_{min}	20%	20%

6.4. Simulation results

6.4.1. Time step consideration

The simulation was done by using 10 minutes (600 s) as the time step. It is due to the computational speed reason in performing multiple years simulation. It is important to know the accuracy/error of the simulation. An LLP for 1 year is estimated under integrated SHS simulation by using different time steps: 60 s, 300 s, 600 s, 1800 s, 3600 s, and 7200 s.

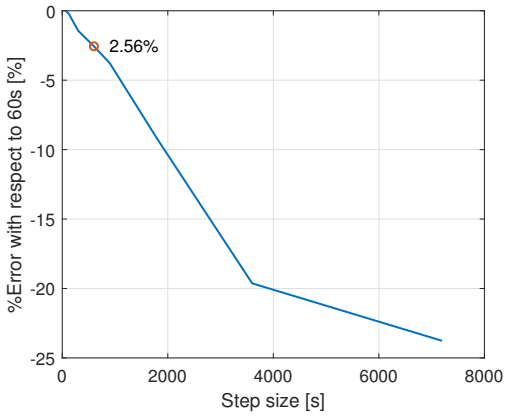

Figure 6.4: Step size error in calculating LLP in the first year with respect to 60s

Figure 6.4 shows the error with respect to the 60 s step size. The result shows that as a higher time step is used, the estimated LLP decreases exponentially. As for 600 s, It can be seen that the simulation results using 600s has 2.56% error in estimating the LLP compared with a 60s time-step simulation.

6.4.2. Typical daily power flow performance

Through the simulation, the characteristics of typical daily power flow can be determined. Figure 6.5 shows a typical power flow of SHS for 2 days. The figure provides the details of PV power, dump or fails power, battery power, and battery SOC level. The positive battery power means that the battery is discharged, while the negative battery power means that the battery is charged. In general, the daily power flow of the SHS can be explained in three modes. These modes can be explained by the battery operation:

1. **The battery charging mode.** It usually occurs between around 7 AM until 12 PM. This is due to the PV generation in which the oversupplied power is stored in the battery. The SOC increases rapidly depending on the PV power magnitude until it achieves the maximum limit of SOC.

2. **The battery peak SOC mode.** It can be observed during the afternoon, from around 12 PM to 5 PM. During this time, the PV module still generates the power to fulfill both the appliances and the storage. However, during this time the load demand is low. The maximum load power can achieve 62 W, as it is shown in Figure 3.7, while the PV power generates around 200 W. Hence most of the time, the battery reaches the maximum SOC limit, and the oversupplied PV power is dumped.

3. **The battery discharging mode.** It occurs during the evening to the early morning at around 5 PM to 5 AM in the next day. At this 12 hours time, the PV power starts to reduce due to the end of the day and the load power dominates the power flow. Due to this, the battery is discharged its power to provide the load. The load is high during the evening to the late night, which can achieve 140 W as it can be seen in Figure 3.7. Moreover, as the battery SOC level decreasing, it can be often found that the battery cannot support the load demand at approximately late night until 5 AM in the next morning.

6.4.3. Temperature influence on daily power flow

The performance of SHS with regard to the temperature depends on the dynamic and aging behavior. The dynamic phenomenon includes the PV power changes, battery maximum capacity, and internal resistance and other parameters from the battery which affects the battery voltage behavior. The degradation phenomenon includes the reduction in PV power, the battery capacity fading, and the battery internal resistance rising. These multiple factors, except the PV power aging, are influenced by temperature, and hence it affects the performance and the lifetime of the SHS. In this analysis, the case of ambient temperature (SF 1.0) and SF 1.2 is used.

PV power

PV power decreases as the ambient temperature increases; it can be seen in Figure 6.5 that the SF1.2 in lower PV power during the first year. As the PV power degrades, the PV power decreases for both temperature profile at the same rate. It is because the aging model of the PV power is not a function of temperature.

Dumped/fail power

When the off-grid energy management control is implemented, the SOC is maintained between 20% to 80%. Therefore, there should be a dumped energy when the upper SOC limit is achieved, and there is still enough PV power. On the other hand, if the lower SOC limit is achieved and there is still load power demanded, the system is considered to fail. Through the figure, the dumped power and the fail power are quantified. It can be observed that overall in the first year, the SHS under ambient temperature resulted to have slightly higher dumped energy as it can be seen during battery peak mode, between the time 12 PM to 5 PM. This is because of the higher output PV power due to the lower ambient temperature than SF1.2 introduced. As the system degrades, at the 18th year (for Li-ion), the dumped/fail power shifts slightly different. A failure can be seen at around time 5 AM on the second day. The result for lead-acid (SLA) battery, as it is illustrated in Figure 6.6, shows a similar phenomenon to fail power. However, a slightly different magnitude of dumped PV energy can be found by using this battery technology when it is in the 7th year. It can be observed that the PV power is still higher compared to the PV power at the 18th year in lithium-ion power flow graph as shown in Figure 6.5.

Battery power

The battery power is divided into two parts: the discharging part (positive value) and the charging part (negative value). Generally speaking, the discharging power of the battery highly depends on the demanded power from the appliances (Figure 6.5). The discharging power has a similar pattern as the battery discharges because the SOC of the battery is still sufficient to satisfy the load during that day. Only at the 18th year and at the time around 30, the battery power drops to zero because the system fails, the system with high temperature gets to zero first because there the SOC has achieved the lower limit. In terms of the charging part, there is a change in the waveform. Generally speaking, the battery with lower temperature is charged with the higher power. This is mainly due to the higher PV power resulted in from a lower temperature. In the 18th year, the charging power decreases as the PV power degraded. A similar characteristic can be found in battery power using SLA battery.

Battery SOC

The SOC behavior of the batteries varies as the temperature profile changes and also as the system is degraded (Figure 6.5. It can be seen that in the first year between the 5 AM to 3 PM, the battery is charging due to the oversupply of the PV power. Two factor affects the battery in which that the battery under ambient temperature increases its SOC with a slightly faster than the higher temperature one. First, as the temperature increases, the PV power increases. Secondly, in the first year, the capacity of the battery at ambient temperature is lower, as it can be seen in Figure 6.9a, which makes the SOC fills the charge quicker. This second phenomenon also explains why the low-temperature battery drops its SOC slightly faster when it is discharged due to the load demand at night, as it can be seen during between 8 PM to 5 AM (Figure 6.5). This phenomenon can also be found in Figure 6.6, in which the SLA battery is used. However, due to the aging (at the 18th year), the battery capacity degrades in which the higher temperature battery degrades more. It explains why during the battery is discharging, the higher temperature battery drops its SOC faster until it hits the lower SOC limit. In the case of SLA battery, the SOC discharge rate for both temperature profile is the same. It is due to the maximum capacity of the battery for SLA battery for both battery is similar under the aging at the 7th year (Figure 6.10a).

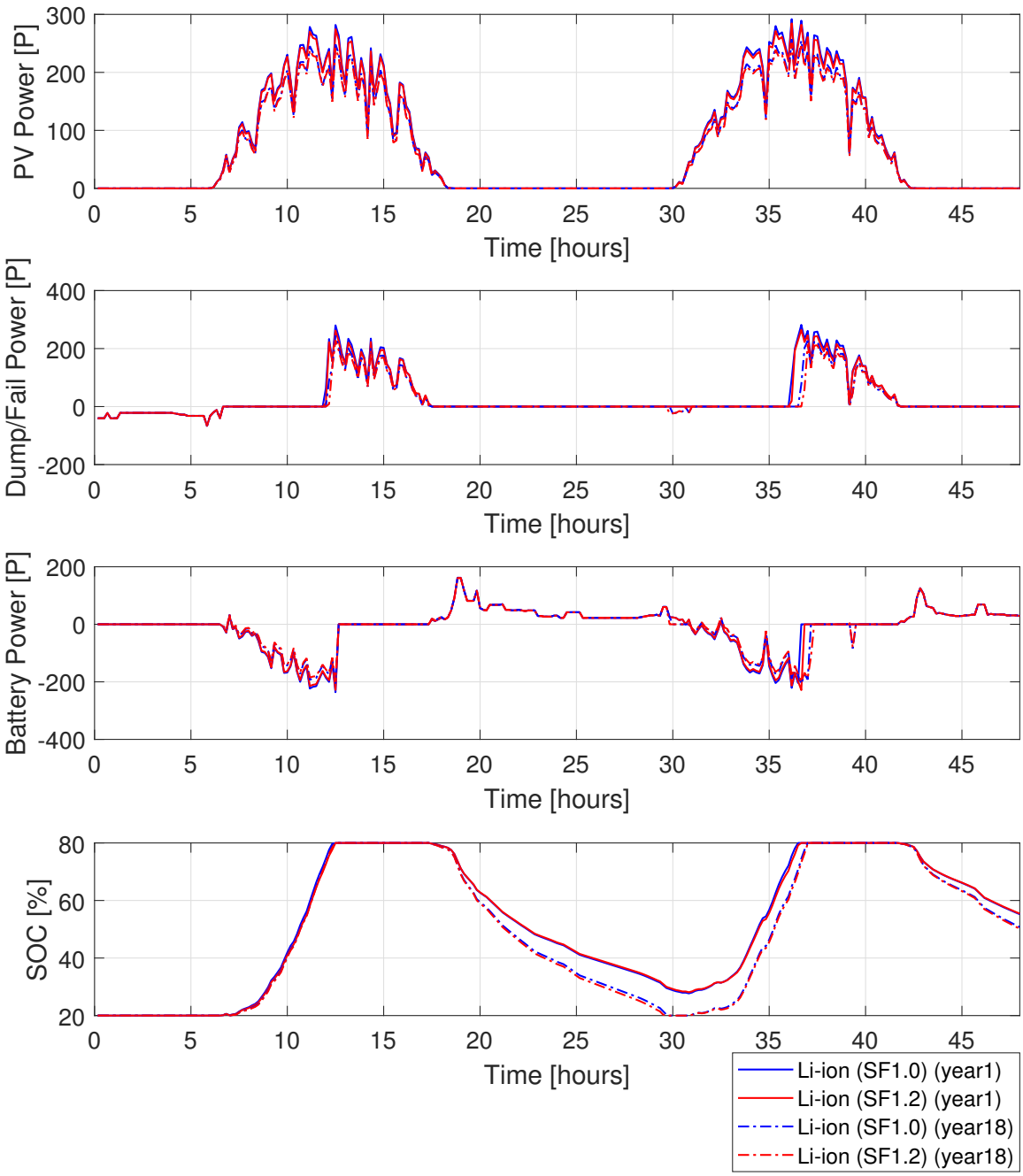

Figure 6.5: SHS power flow under various ambient temperature condition in year 1 and year 18 for 2 days using Lithium-ion battery technology

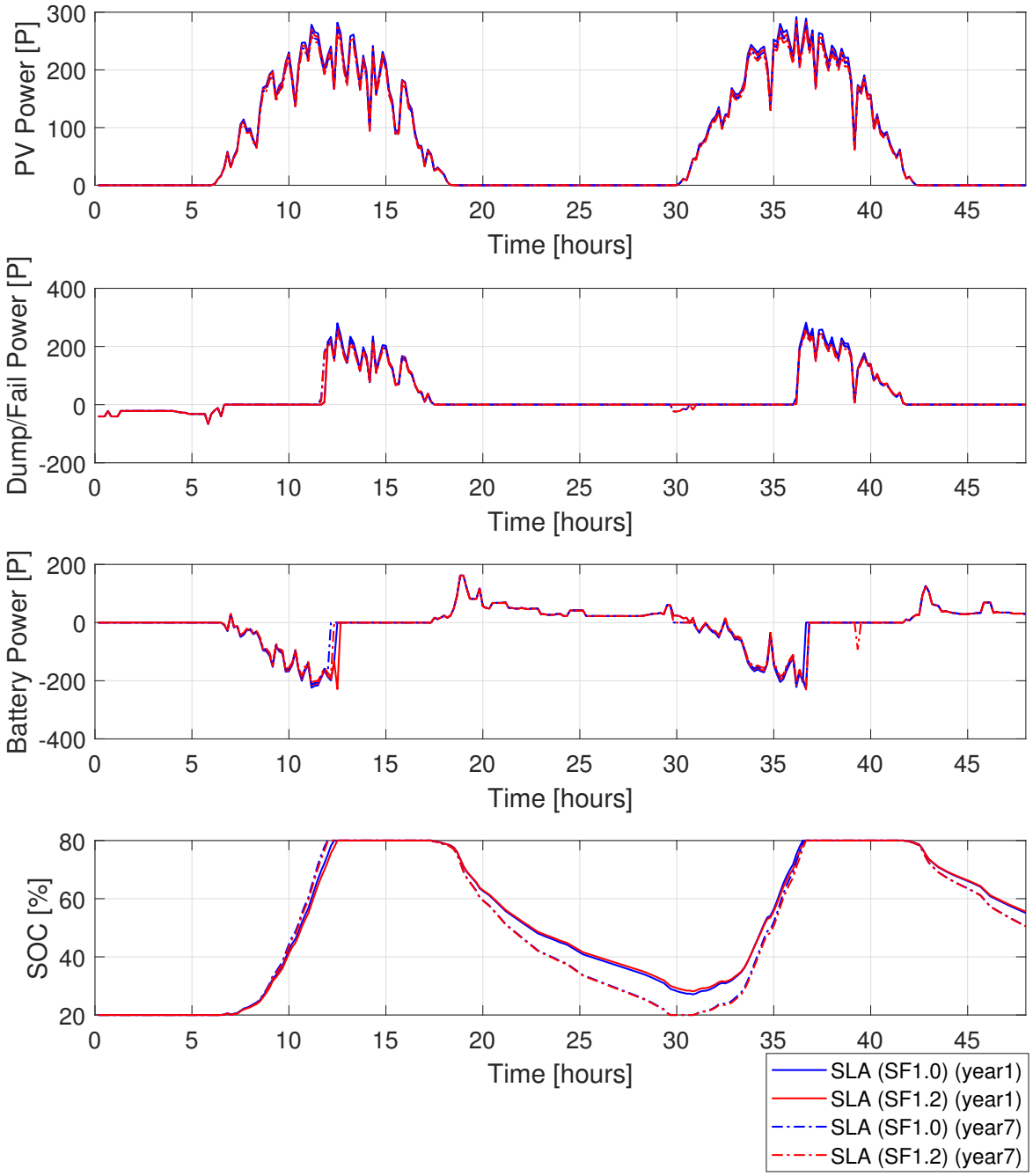

Figure 6.6: SHS power flow under various ambient temperature condition in year 1 and year 7 for 2 days using Sealed Lead-Acid battery technology

Battery voltage and current

In terms of the voltage and current output of the battery, the change in temperature gives an influence during the operation. The voltage of the battery follows the trends based on the discussion in the previous chapter, in which that the battery with higher temperature has an increased voltage when it discharges and charges. As the battery degrades, in which that the capacity decreases and the resistance increases, it has a significant impact on the battery voltage. The temperature stress aging impact is clearly observed when they both are at the same SOC level and they deal with high current. Firstly. it can be seen during the time 5 AM to 10 AM for the Li-ion battery in Figure 6.5. When the

battery is charging, the voltage of the degraded battery increases due to the increase in the internal resistance. It can be observed that the voltage under SF1.2 is higher than the voltage under ambient temperature (SF 1.0). It can be explained in the Figure 6.9b where the degraded internal resistance is higher than the one under SF 1.0.

Secondly, it can be seen during the time 8 PM to 5 AM (next day) for SLA battery as illustrated in Figure 6.6. When the battery is discharging, the voltage of the degraded battery decreases due to the increase in the internal resistance. It can be seen that the voltage under SF1.2 is lower than the voltage under ambient temperature. It can be explained in the Figure 6.10b where the degraded internal resistance is higher than the one under ambient temperature.

The capacity fading, the voltage drop during discharging, and the voltage rise during charging, can be translated into harmful effects. It means that the charge present in the battery will be drawn extremely higher during discharging under the same power. On the other hand, the charge will be stored smaller during charging. Moreover, the capacity stored is going lower as well. This can result in poor performance of the systems.

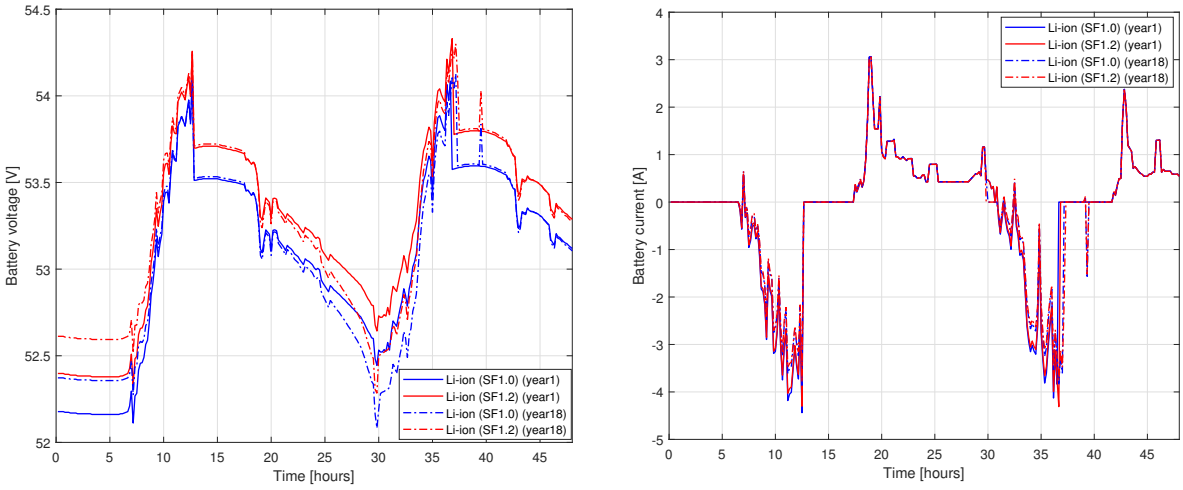

(a) Battery bank voltage

(b) Battery bank current

Figure 6.7: SHS battery SOC and voltage under various ambient temperature and year observed for 2 days using Lithium-ion battery technology

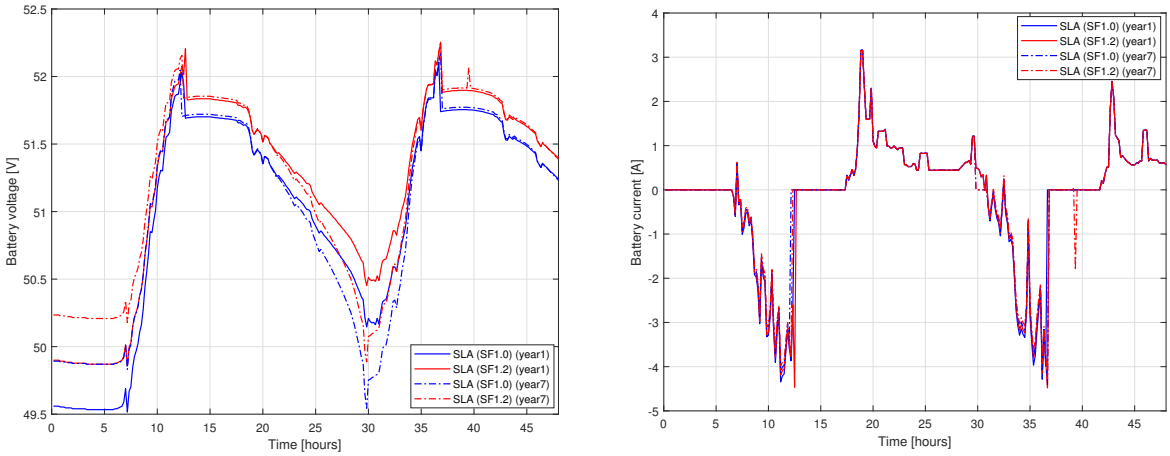

(a) Battery bank voltage

(b) Battery bank current

Figure 6.8: SHS battery SOC and voltage under various ambient temperature and year observed for 2 days using Sealed Lead-acid battery technology

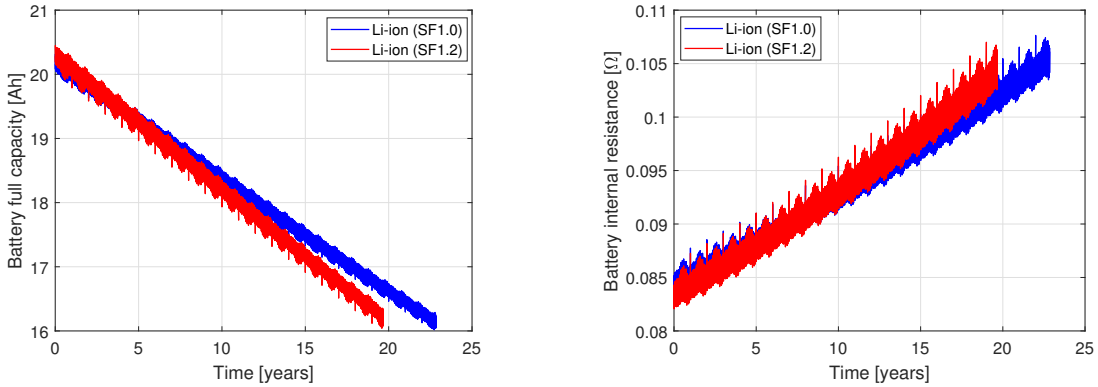

(a) Degraded maximum capacity

(b) Degraded internal resistance

Figure 6.9: SHS batteries maximum capacity and internal resistance under various ambient temperature using Lithium-ion battery technology

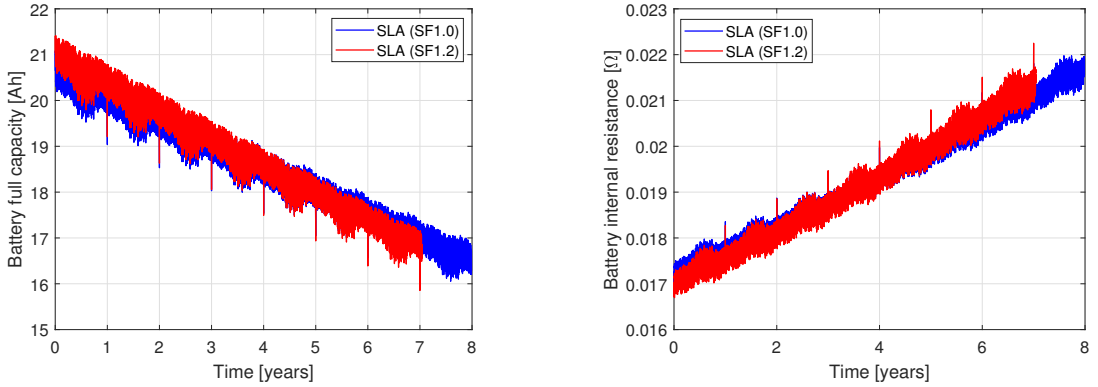

(a) Degraded maximum capacity

(b) Degraded internal resistance

Figure 6.10: SHS batteries maximum capacity and internal resistance under various ambient temperature using Sealed Lead-acid battery technology

6.4.4. Temperature Impact on the LLP

In terms of the performance of the SHS, the assessment is made by evaluating the LLP every year for both Li-ion and SLA battery technologies. In this section, LLP of SHS, by using various battery technologies and temperature profiles (Case 1 - 6), will be discussed. The performance of those conditions are compared with the performance of the initial system sizing (initial FD) as it is described in Figure 6.3.

Comparison with the initial LLP from the system sizing

Figure 6.11 shows the yearly LLP performance until the battery reaches its End Of Life (EOL). First, a comparison between the initial LLP and the simulation result by taking into account the ambient temperature (SF1.0). The simulation shows that 8.8% and 9.1% LLP is achieved for Li-ion and SLA battery respectively. This is 7.4% and 4.2% lower than the initial one. This low LLP is due to the battery model consideration where the voltage varies with the SOC. It is known that the initial FD neglects the battery detail consideration. In other words, the initial FD uses a constant 24 voltage for all the SOC level. While, when the battery model is considered, it boost its voltage to 26 V (Figure 5.14). Thus, it leads to having a more energy content in the battery.

However, as the time goes by the LLP boosts up exponentially as the time goes by, and it achieves 17.8% LLP for Li-ion in 23 years. This is almost doubled the initial LLP on the system sizing. As for SLA battery, the LLP increases rapidly to 14% (LLP) for just in 7 years. This is due to the more rapid aging rate compared with the Li-ion battery which is discussed in the previous chapter.

Comparison between the batteries with the various scaling factor (SF)

Compared to the different temperature profile, it can be seen that the higher temperature always leads to the higher LLP in every year. Even though it is known that the battery has a short term positive effect in terms of capacity and voltage, when the component is combined with the PV modules, the trend is different. Firstly, the de-rating PV power due to the temperature seems to play dominantly. Secondly, as the battery temperature increases, it accelerates the aging rate of the battery. These phenomena play a significant role in the performance of the SHS.

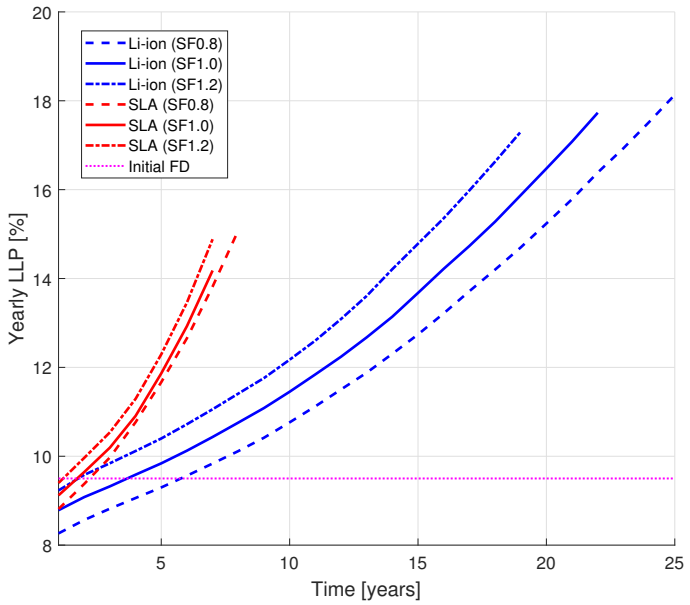

Figure 6.11: Yearly LLP

6.4.5. Temperature impact on SHS lifetime

The temperature impact on SHS lifetime is often seen as the temperature impact on battery lifetime. It is due to the battery lifetime which generally has a short time compared to the PV module lifetime. The lifetime analysis can be shown in two ways. Firstly, it is shown in the battery state of health (SOH)

as a function of time (Figure 6.12a). It can be seen that the SOH decreases overtime due to the aging until it reaches the EOL which is defined as 80%. It can be observed that as the temperature increases, the aging rate increases.

Secondly, the lifetime analysis can be presented in terms of the time to failure as shown in Figure 6.12b. It is shown that the Li-ion battery can operate up to 22.8 years while the SLA battery can work up to 7.99 years under ambient temperature (SF1.0). As the higher temperature is introduced (SF1.2), it leads to having more severe aging, and thus, its makes the lifetime decreases by 14.52% and 12.23% for Li-ion and SLA respectively. It can be concluded that Li-ion battery is slightly more temperature sensitive compared with the SLA battery. However, the lifetime of the battery can surpass the lifetime of the PV modules in the case of Li-ion with lower ambient temperature profile (SF 0.8).

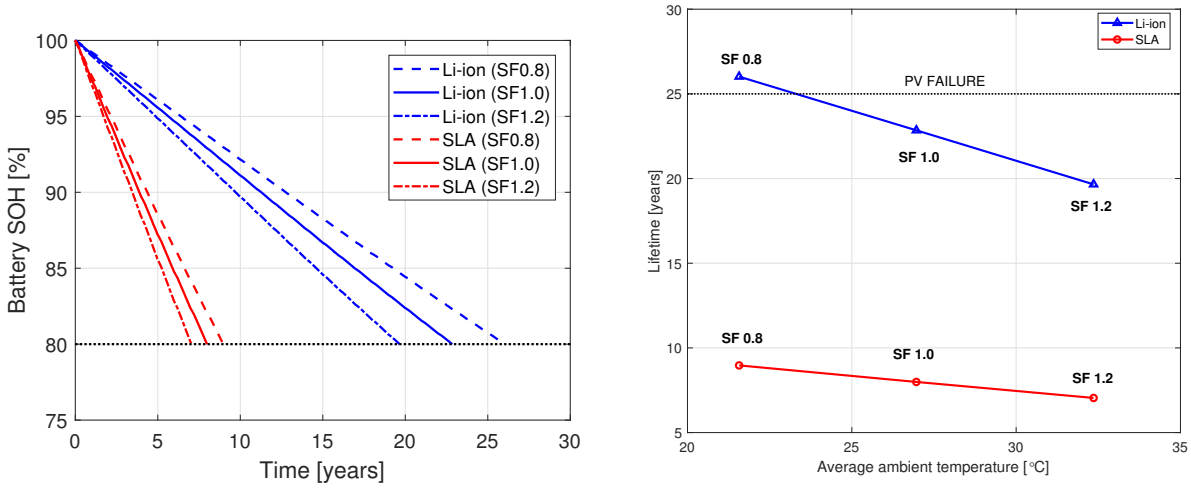

(a) Battery State-of-Health for various Scaling Factor (SF)

(b) Battery lifetime for various Scaling Factor (SF) which can be translated into average ambient temperature

Figure 6.12: Battery SOH and lifetime

6.4.6. Summary

In overall, by taking all behaviors into account, the important results can be summarized into a normalized unit with regard to the average ambient temperature of the location. The overall results comparison consists of: the PV energy yield, the battery lifetime, and the average yearly LLP. In this analysis, the SHS lifetime is denoted as the lifetime of the battery.

It can be observed that the PV energy yield decreases as the average ambient temperature increases as it has been discussed in Chapter 4. This applies to all the battery technologies used. In terms of LLP, it is seen that the LLP of the SHS under higher temperature is always bigger than under the lower temperature. In the first year the LLP increases for both Li-ion and SLA battery. In terms of the lifetime of the battery, the relationship between the battery lifetime and the temperature can be explained linearly by 1.5%/ °C for Li-ion battery and 1.3%/ °C for SLA battery. The lifetime linear rate is slightly different than in the previous chapter. It is due to the fluctuating temperature profile that this simulation uses.

Therefore, with this results, it can be seen that the temperature affects both LLP of the SHS and the lifetime of the battery. It can be concluded that the higher the ambient temperature, it gives a negative impact in terms of LLP, lifetime, and PV energy yield for both battery technologies.

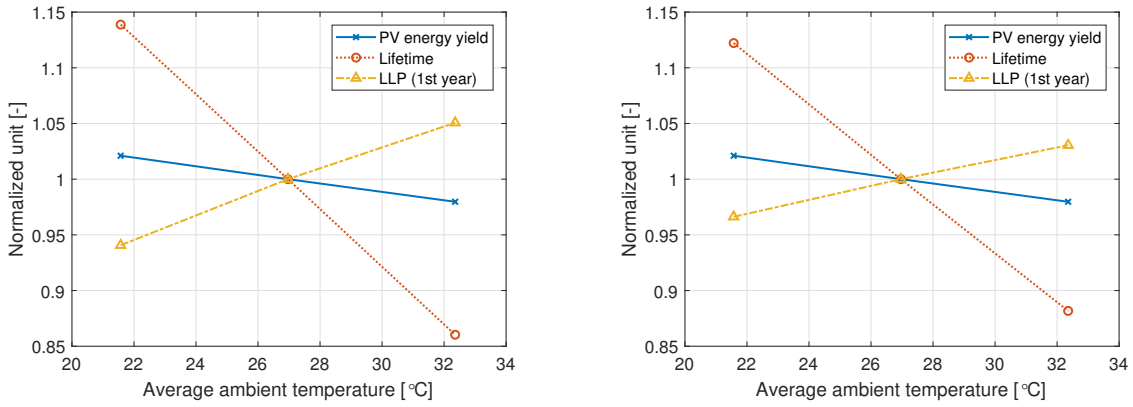

(a) Lithium-ion (Li-ion) battery technology

(b) Lead acid (SLA) battery technology

Figure 6.13: Overall temperature impact on SHS for various battery technology

6.5. Conclusion

Based on the simulation of the integrated system consists of PV model, battery model, power management systems (PMS), and efficiency of converters, the conclusion can be drawn. The following research questions are addressed in this chapter:

How does the temperature affect the performance of the system?

The temperature affects the PV module and the battery during its operations. It also affects the lifetime of the battery as a result of its operational condition and behavior. As for the PV modules, the annual energy yield produced by the PV is affected from 6.69% to 9.36% compared with the STC temperature (25 °C). As the ambient temperature increases, the module gets hotter, which corresponds to a decrease in energy yield by 0.926% / °C linearly.

As for the batteries, the capacity increases and the internal resistance decreases (resulted in having a higher voltage) as the temperature rises non linearly. The battery under higher temperature can store the charged more than the battery under the lower temperature. Hence, it can potentially give a positive influence of the system performance.

By combining the behavior of the components in an integrated SHS system, an increase in ambient temperature deteriorate the performance even in the LLP in the first year. The positive effect of the battery cannot be seen in the yearly LLP. This is due to a negative effect of the PV performance which dominates the other positive effects from the battery as the temperature elevates.

How does the temperature affect the lifetime of the system?

The SHS lifetime generally is determined by the battery lifetime. It is because the batteries are the component that fails the first and has the most significant capital expenses. The rate of aging of batteries varies as a different temperature profile is introduced. By taking the PV aging model from the warranty data sheet into account, both lithium and lead-acid battery decreases its lifetime by 10% to 12% if the temperature profile is increased by 20%.

7

Conclusion and Recommendation

This project involves two different battery technologies: Li-ion and Lead-acid, in evaluating the temperature impact on the SHS. A comprehensive, integrated SHS model was constructed by taking into account the performance and the degradation behavior of both the PV module and the battery. The temperature impact is evaluated through the case study in Sumba Island, Indonesia. This work is done by firstly evaluating each PV module and the battery as the main components. Therefore, each sub-research questions were answered separately in the previous chapters.

7.1. Conclusion

The main aim for this work is to evaluate and quantify the influence of temperature profile on the performance and the lifetime of SHS. The evaluation is addressed by investigating the performance and the lifetime of SHS components. In this work the main research questions are:

How does the temperature affect the performance of the system?

In general, the performance of the SHS is affected by the behavior of the PV module and the battery. It goes the same with the temperature effect, in which the SHS performance is affected by the impact of temperature on the main components.

- From the PV module perspective, the evaluation was done by using the integrated PV model which is described in Chapter 4. As the ambient temperature rises, the IV curve of the PV shift and hence, it leads to having a lower output PV power. By taking into account the irradiance (G_m) and the module temperature estimation (T_m), the annual energy yield produced by the PV in Sumba, Island is affected by 7.45% to 10.41% compared with the STC temperature (25 °C). By introducing the Scaling Factor, it can be concluded that the energy yield decreases as the average ambient temperature rises. The rate of decrease is seen to be a slightly exponential.

- As for the batteries, the investigation was done by performing the proposed integrated battery model which is explained in Chapter 5. A converse behavior is observed with regard to the temperature impact. As the temperature decreases to 0 °C, the capacity decreases exponentially up to 90% and the internal resistance increases exponentially up to 106%. As the temperature rises, the capacity can slightly increase by 5%, and the internal can slightly decrease by 5% compared with the rated capacity. Hence, a high temperature can bring a positive impact in terms of capacity stored and the efficiency. On the other hand, high temperature leads to accelerating the aging rate of the batteries. It affects both the negative impacts in terms of capacity fading and internal resistance rising.

- Through the study case in Chapter 6, the impact of the temperature on the SHS performance has been evaluated. By using the ambient temperature (SF 1.0) and considering PV and battery dynamic performance and aging, the LLP is 4.2% and 7.4% lower compared to the LLP in the initial sizing. It is also found that the increase in ambient temperature deteriorates the LLP from the first year. The LLP increases exponentially in which a higher ambient temperature accelerates faster. This is due to the negative effect of the PV performance which dominates the other positive effects from the battery as the temperature elevates. Therefore, the higher the temperature, the lower the PV power and the faster the aging rate of batteries. Hence, it leads to having a higher LLP.

How does the temperature affect the lifetime of the system?

- The lifetime of the system is limited to the lifetime of the battery. It is because generally, the PV module last much longer than the battery in SHS.

- By using Peck's model which is described in Chapter 4, the lifetime as a function of temperature can be evaluated. By selecting a particular hot and humid location, the ambient temperature is varied: normal ambient temperature and 1.2 higher ambient temperature (SF 1.2). Thus as the average ambient temperature increases by 20% the lifetime decreases by 25%. However, the Peck's model overestimates the degradation rate in which it gives 71% lower lifetime than the warranty. This is due to the water vapor diffusion behavior which is neglected in the Peck's model. Further work should be done by examining the temperature effect on the degradation of the PV precisely.

- The cycle aging model which is described in Chapter 5 is adopted and it is incorporated with the integrated battery model to evaluate the lifetime of the battery. The lifetime of the battery as a function of temperature can be described linearly. By neglecting the PV power aging, both lithium and lead-acid battery decreases its lifetime linearly by 0.59 years/°C and 0.19 years%/°C for Li-ion battery and SLA battery respectively.

- Due to the limitation in determining the PV module lifetime, the SHS lifetime is generally determined by the battery lifetime before it achieves 25 years which is the lifetime of PV modules according to the datasheet. By coupling the battery model, the PV model, and all the input data such as temperature with scaling factor (SF) and load profile, the lifetime can be predicted. The same trend in the battery lifetime is observed through the study case. It also is seen that the battery lifetime can surpass the lifetime of PV module in the case of SF 0.8 using Li-ion battery technologies.

7.2. Recommendation

This work indeed provides a temperature assessment through a comprehensive integrated model, which consists of PV and battery model. There is still further in-depth analysis to be made in resulting more accurate prediction, by incorporating of various elements:

- The temperature and the humidity could be an important factor in predicting the lifetime of the PV module in the SHS application. Peck's model has been introduced to evaluating the degradation behavior of the battery. However, a prediction of the moisture diffusion should be made in determining the relative humidity of the PV module. The other method is to apply the thermal cycling model by taking into account the corrosion of solder joints.
- In this work, the power electronics / converters efficiency is assumed with a constant efficiency throughout the operating condition. However, in the real condition, there should be a minimum and maximum power of the converters in order to operate. It is discussed that the performance of power electronics components are influenced by temperature. Thus, incorporating a dynamic performance model of the power converters with temperature influence, the SHS can be evaluated more accurately. Secondly, it is therefore essential to do a lifetime model of the converters to predict the mean time to failure (MTTF). One of the suggestion is through the life cycle model based on the thermal cycle of the components.
- The future challenge of the battery model lies in three things. Firstly, is related to the battery temperature. It is known that the battery temperature varies as a function of its current flow. Therefore, it is important to do a thermal model of the battery by incorporating the convection and current flow. Therefore, the temperature of the battery can be obtained and hence, it will determine the performance accurately. Secondly, it is related to the precise quantification of the battery lifetime. A calendar aging should be added to the battery model in predicting the capacity fading when the battery is inactive. A battery relaxation periods should be calculated and taken into account when modeling the calendar aging.
- As the lifetime of the SHS main components: PV modules, battery, and power converters, can be determined given the operational condition, further optimization methodology can be drawn. First, a multi-objective optimization can be used by considering the lifetime, the LLP of the systems, and the size of each component. Secondly, a replacing strategy of main components can be proposed in order to minimize the total cost at a given time horizon.

Appendices

A

Photovoltaics Modules Details

The SHS assessment was assumed to use Jinko solar JKM330-72 with 330 Wp rating [66]. The module is based on poly-crystalline silicon technology with an average efficiency of 17.01%. The main module parameters are summarized in Table A.1.

Table A.1: PV module specification of Jinko Solar JKM330P-72 [66]

Name	**Value**
Name	Jinko Solar JKM330P-72
Technology	Poly-crystalline silicon
Pmax STC (W)	330
T_{NocT} (^{o}C)	45
Width (m)	0.992
Length (m)	1.956
Area (m^2)	1.940
Eff. STC (%)	17.01 %
V_{oc} STC (V)	46.9
I_{sc} STC (A)	9.14
Temp. coeff P_{mpp} (%/^{o}C)	-0.41
Temp. coeff V_{oc} (%/^{o}C)	-0.31
Temp. coeff I_{sc} (%/^{o}C)	0.06

Absorptivity and emissivity are the critical inputs for the Fluid-Dynamic model. Absorptivity is defined as the fraction of incident irradiation that gets converted into thermal energy [7], as illustrated in the Equation A.1.

$$\varphi = (1 - R)(1 - \eta_M) \tag{A.1}$$

Moreover the reflectance, absorbance, and emissivity top and back value, for Fluid-Dynamic model intput, were taken from the previous work [7].

Table A.2: Absorptivity and emissivity parameter of the module

Parameter	**Value**
Reflectance of the glass, R [7]	0.07
Absorbance of the glass, A [7]	0.03
Absorptivity, φ	0.772
Emissivity top, ϵ_{top} [7]	0.84
Emissivity back, ϵ_{back} [7]	0.89

B

Other Meteorological Data

This section presents the irradiance meteorological data for Sumba Island, Indonesia. It covers GHI, DHI, and DNI data. The data is obtained from Meteonorm database.

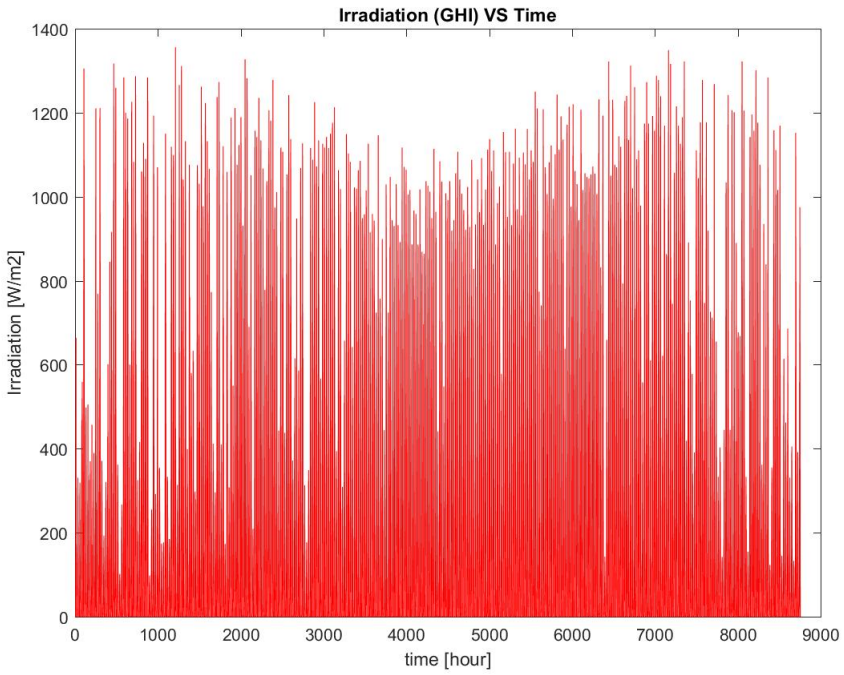

Figure B.1: Global Horizontal Irradiance (GHI) of Sumba Island in a year

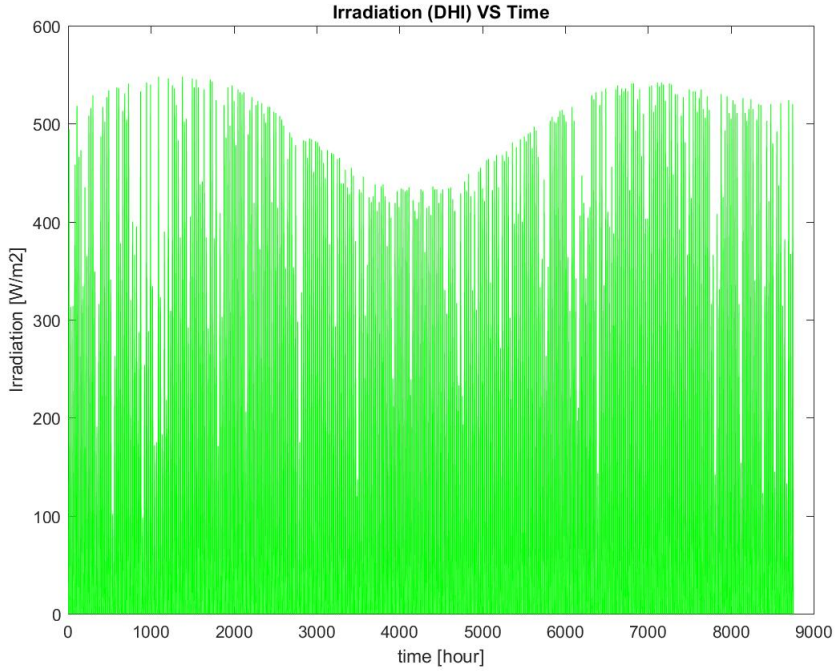

Figure B.2: Diffuse Horizontal Irradiance (DHI) of Sumba Island in a year

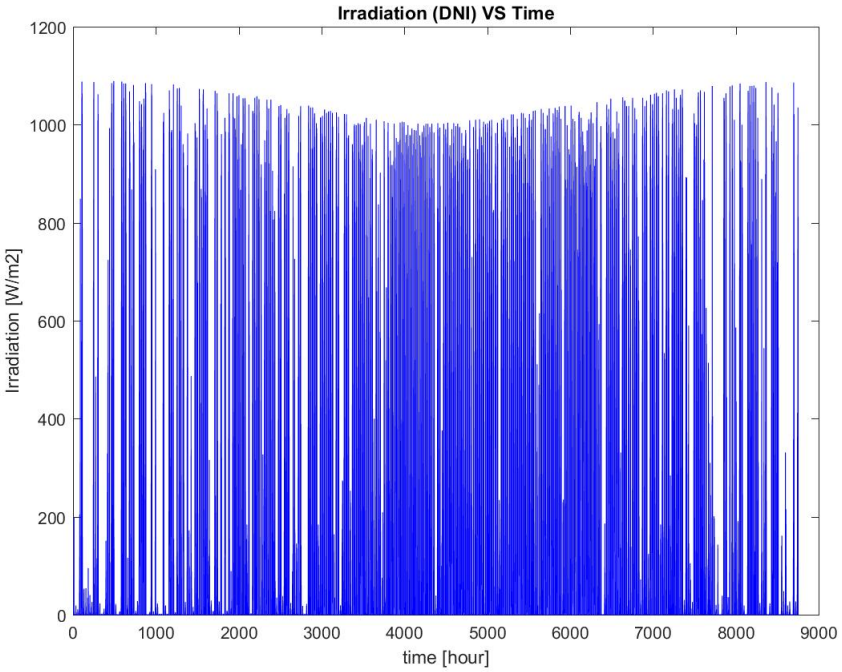

Figure B.3: Direct Normal Irradiance (DNI) of Sumba Island in a year

C

Battery Model Verification and Cycle-life Fitting Coefficients

C.1. Battery model verification

This section explains the verification of dynamic performance battery model as a function of temperature based on the data sheet. Figure C.1a shows the discharge curve generated from the simulation and the discharge curve from the Valence battery datasheet [79]. Figure C.1b shows the discharge curve generated from the simulation and the discharge curve from the Valence battery datasheet [79]. The Li-ion battery is shown to have a nearly fitted curve. However, it can be seen that the curve generated for the lead-acid battery is not fully fitted to the data sheet.

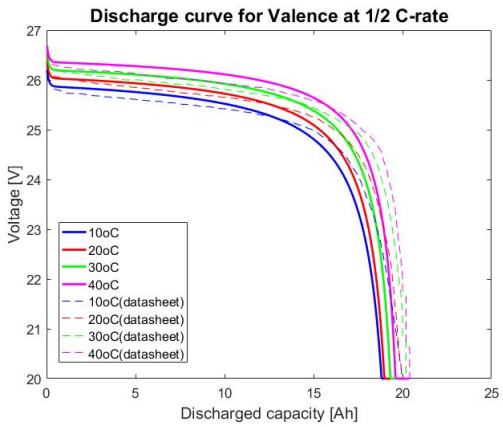

(a) 20Ah Valence LiFeMgPO4 battery discharge curve at various temperature

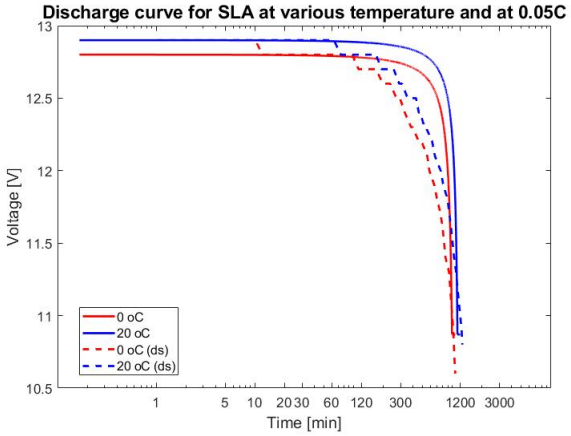

(b) 1.1Ah Power sonic sealed lead acid battery discharge curve at various temperature

Figure C.1: Discharge curve for various battery technologies

C.2. Fitting coefficient of the polynomial functions for calculating battery cycle life

This fitting coefficients are used to calculate the battery cycle life in Sub-section 5.4

Table C.1: Fitting coefficient of the polynomial function for various battery technology, estimated by the previous work [82]

Coefficients	Sealed Lead Acid	LiFePO4
p_0	2.30E+04	4.779e+04
p_1	-1.12E+05	-6.401e+04
p_2	2.53E+05	-1.411e+05
p_3	-2.71E+05	3.233e+05
p_4	1.11E+05	-1.647e+05

Table C.2: Fitting coefficient of the linear difference as a function of temperature for various battery technology, estimated by the previous work [82]

Coefficients	Sealed Lead Acid	LiFePO4
p_{l0}	-3.785774188	-2.80769231
p_{l1}	0.190763893	0.153846154

Table C.3: Fitting coefficient of the curve created when subtracting a temperature curve from the reference one for various battery technology, estimated by the previous work [82]

Coefficients	Sealed Lead Acid	LiFePO4
p_{d0}	2.89E+03	6.49E+03
p_{d1}	-1.58E+04	-9.14E+03
p_{d2}	3.88E+04	-1.69E+04
p_{d3}	-4.44E+04	4.02E+04
p_{d4}	1.91E+04	-2.03E+04

advanced energy storage solutions

U-Charge® U1-24RT

24V Battery Module

Effortlessly replace 24-volt battery applications with the advanced U1-24RT Lithium Iron Magnesium Phosphate module offering 20Ah capacity with a peak load capability of up to 60A.

Overview

The U1-24RT is a 24-volt lithium iron magnesium phosphate battery module incorporating a built-in battery management system. The U1-24RT is ideal for robotics and autonomous vehicles looking for light weight and long runtime.

Over 500,000 Valence batteries are currently in service within numerous industrial products. Excellent float and cycle life results in low operating costs, providing a high return on investment for end user applications.

Specifications		U1-24RT
Voltage		25.6 V
Nominal Capacity (C/5, 23°C)		20 Ah
Weight (approximate) kg		6.4 kg
Weight (approximate) lbs		14.1 lbs
Dimension incl. Terminals LxWxH (mm)		197 x 131 x 183
Dimension incl. Terminals LxWxH (inches)		7.76 x 5.12 x 7.20
BCI Group Number		U1R
Terminals, Female-Threaded		M6x1.0
Specific Energy		80 Wh/kg
Energy Density		110 Wh/l
Standard Discharge @ 23°C	Max. Cont. Current	30 A
	Max. 30 sec. Pulse	60 A
	Cut-off Voltage	20 V
	Run-time @ 10A	120 min
	Run-time @ 30A	40 min
Standard Charge	Charge Voltage	29.2 V
	Float	27.6 V
	Recommended	10 A
	Charge Time*	2.5 hrs
DC Internal Resistance (Max)		43 mΩ
Part Number		1005997

*under recommended conditions

Features

- Built-in automatic protection for over-charge, over-discharge and over-temperature conditions
- No external battery management system required
- Series connection up to two (2) batteries (48 V)
- Automatic module and cell balancing
- LED battery status indicator
- Maintenance-free
- Flame retardant plastics
- Thousands of cycles, under normal conditions
- Can be charged using most 24-volt lead-acid chargers
- Compatible with U-BDI state of charge indicator

advanced energy storage solutions

Common specifications	
Operating temperature	-10°C to +50°C
Storage temperature	-40°C to +50°C
Charge temperature	0°C to +45°C
Operating humidity	5% to 95%, non-condensing
Certifications	FCC Class B, CE IEC 62133, IP56 UL 1642 (cells only)
Module container / cover	flame retardant ABS/PC material (compliant to UL 94-V0, UL 94 5VB, & L.O.I. 32% per ISO 4589 and ASTM D2863)
Shipping classification	UN 3480, Class 9

Accessories

- U-BDI – a wired, remote U-Charge® Battery Discharge Indicator displaying a 10 segment State-of-Charge (SOC).

- Diagnostic Kit allows connection of a PC or laptop to the battery to monitor individual cell voltages and temperatures. Also enables sleep function for long term storage.

U-Charge® Discharge Capacity Performance at 23°C
C/2 cycling, 100% DOD, 42 months

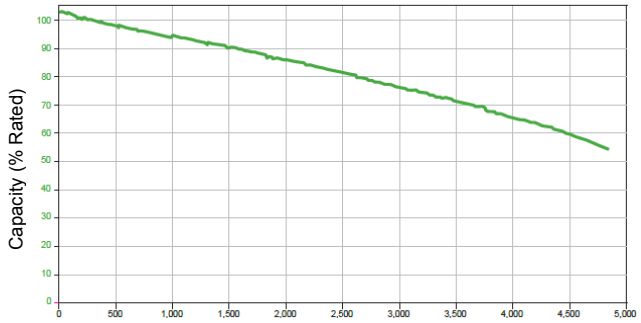

U-Charge® Voltage Profiles at Various Rates
23°C Ambient Temperature

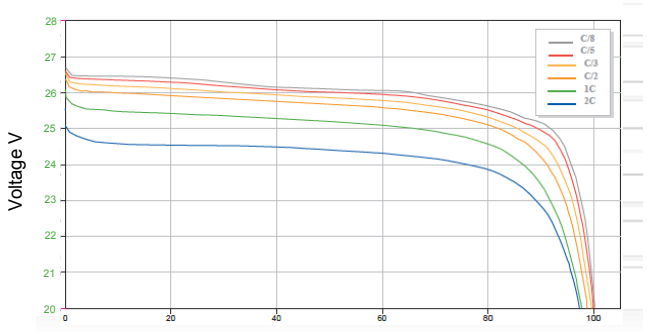

U-Charge® Discharge Voltage Profiles at C/2 Discharge Rate
Various Ambient Temperatures

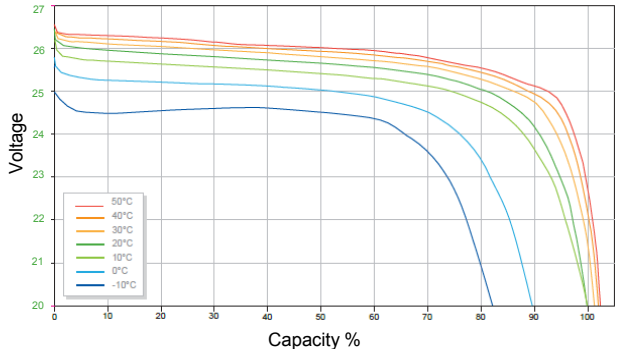

Typical U-Charge® C/2 Charging Voltage and SOC Profiles
23°C Ambient Temperature

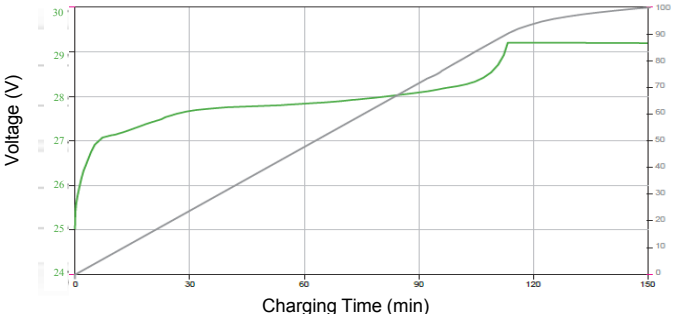

Corporate Headquarters
North America Sales
1807 W. Braker Ln.
Suite 500
Austin, Texas 78758 USA

Tel (888) VALENCE or +1 (512) 527-2900
Fax +1 (512) 527-2910

Europe/Middle East/Africa
Sales
Unit 63 Mallusk Enterprise Park
Mallusk Co.Antrim
Northern Ireland BT36 4GN

Tel +44(0) 28 9084 5400
Fax +44(0) 28 9083 8912

Tell us about your application at www.valence.com/contact

POWER SONIC

SEALED LEAD-ACID BATTERIES

TECHNICAL HANDBOOK

FEATURES

Sealed/Maintenance-Free
The valve regulated, spill-proof construction of the Power-Sonic battery allows trouble-free, safe operation in any position. There is no need to add electrolyte, as gases generated during over-charge are recombined in a unique “oxygen cycle.”

Long Shelf Life
A low self-discharge rate permits storage of fully charged batteries for up to a year at room temperature before charging is required. Lower storage temperatures enhance shelf life characteristics even further.

Design Flexibility
Batteries may be used in series and/or parallel to obtain choice of voltage and capacity. Due to recent design breakthroughs, the same battery may be used in either cyclic or standby applications. Over 50 models are available to choose from.

Deep Discharge Recovery
Special separators, advanced plate composition, and a carefully balanced electrolyte system have greatly improved the ability of recovering from excessively deep discharge.

Economical
The high watt-hour per dollar value is made possible by the materials used in a sealed lead-acid battery: they are readily available and low in cost.

Easy Handling
No special handling precautions or shipping containers — surface or air — are required due to the leak-proof construction. Classified as non-hazardous commodity.

Compact
Power-Sonic batteries use state of the art design, high grade materials, and a carefully controlled plate-making process to provide excellent output per cell. The high energy density results in superior power/volume and power/weight ratios.

High Discharge Rate
Low internal resistance allows discharge currents of up to ten times the rated capacity of the battery. Relatively small batteries may thus be specified in applications requiring high peak currents.

Wide Operating Temperature Range
Power-Sonic batteries may be discharged over a temperature range of -40°C to +60°C (-40°F to +140°F) and charged at temperatures ranging from -20°C to +50°C (4°F to +122°F).

Rugged Construction
The high impact resistant battery case is made either of non-conductive ABS plastic or styrene. Large capacity batteries frequently have polypropylene cases. All of these case materials impart great resistance to shock, vibration, chemicals and heat.

Long Service Life
Under normal operating conditions, four or five years of dependable service life can be expected in stand-by applications, or between 200-1000 charge/discharge cycles depending on average depth of discharge.

CONSTRUCTION

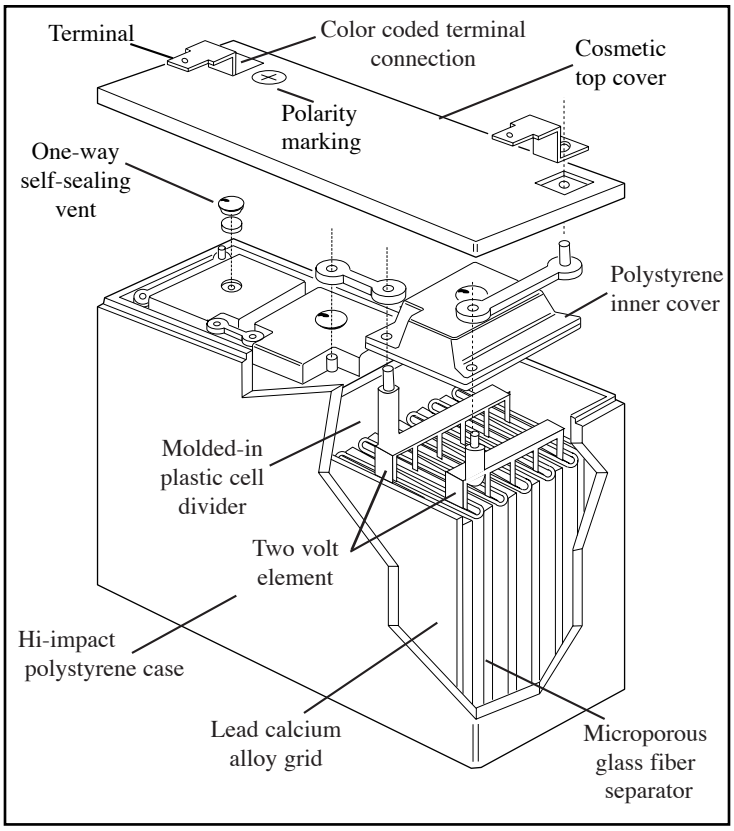

Figure 1

Plates (Electrodes)

Plate construction is the key to producing a good battery. Recognizing this, Power-Sonic utilizes the latest technology and equipment to cast grids from a lead-calcium alloy free of antimony. The small amount of calcium and tin in the grid alloy imparts strength to the plate and guarantees durability even in extensive cycle service. Lead oxide paste is added to the grid to form the electrically active material. In the charged state, the negative plate paste is pure lead and that of the positive lead oxide. Both of these are in a porous or spongy form to optimize surface area and thereby maximize capacity.

Separators

Power-Sonic separators are made of woven glass fiber cloth with high heat and oxidation resistance. The material further offers superior electrolyte absorption and retaining ability, as well as excellent ion conductivity.

Electrolyte

Immobilized dilute sulfuric acid: H_2SO_4.

Container

Case material is either ABS, a high-impact proof plastic resin, styrene, or a polypropylene-polyethylene copolymer with resistance to chemicals and flammability.

Leakproof Design & Operational Safety

Power-Sonic batteries have been approved for shipment by air, both by D.O.T. and I.A.T.A.. U.L.'s component recognition program for emergency lighting and power batteries lists Power-Sonic under file numbers MH14328 and MH14838.

Terminals

Depending on the model, batteries come either with AMP Faston type terminals made of tin plated brass, post type terminals of the same composition with threaded nut and bolt hardware, or heavy duty flag terminals made of lead alloy. A special epoxy is used as sealing material surrounding the terminals.

Relief Valve

In case of excessive gas pressure build-up inside the battery (usually caused by abnormal charging) the relief valve will open and relieve the pressure. The one-way valve not only ensures that no air gets into the battery where the oxygen would react with the plates causing internal discharge, but also represents an important safety device in the event of excessive overcharge. Vent release pressure is between 2-6 psi; the seal ring material is neoprene rubber.

Case Sealing

Depending on model, the case sealing is tongue and groove with polyurethane, epoxy, or heat seal.

THEORY OF OPERATION

The basic electrochemical reaction equation in a lead-acid battery can be written as follows:

Pb	$2H_2SO_4$	PbO_2	Discharging ⇄ Charging	$PbSO_4$	$2H_2O$	$PbSO_4$
(porous lead) active material of negative plate	(sulfuric acid) electrolyte	(porous lead dioxide) active material of positive plate		(lead sulfate) active material of negative plate	(water) electrolyte	(lead sulfate) active material of positive plate

Discharge

During the discharge portion of the reaction, lead dioxide (positive plate) and lead (negative plate) react with sulfuric acid to create lead sulfate, water and energy.

Charge

During the recharge phase of the reaction, the cycle is reversed: the lead sulfate and water are electro-chemically converted to lead, lead oxide and sulfuric acid by an external electrical charging source.

Oxygen Recombination

To produce a truly maintenance-free battery, it is necessary that gases generated during overcharge are recombined in a so-called "oxygen cycle". Should oxygen and hydrogen escape, a gradual drying out would occur, eventually affecting capacity and battery life. During charge, oxygen is generated at the positive and reacts with and partially discharges the sponge lead of the negative. As charging continues, this oxygen recombines with the hydrogen being generated by the negative, forming water. The water content of the electrolyte thus remains unchanged unless the charging rate is too high.

In case of rapid generation of oxygen gas exceeding the absorbing capacity of the negative plate, the pressure relief valve will open to release excessive gas.

Deep Discharge

The Power-Sonic battery is protected against cell shorting by the addition of a buffering agent that insures the presence of acid ions even in a fully discharged state. The need for expensive circuitry in the design of a system to prevent deep discharge and possible cell shorting is thereby reduced considerably.

Power-Sonic defines "deep discharge" as one that allows the battery voltage under load to go below the cut-off (or "final") voltage of a full discharge. The recommended cutoff voltage varies with the discharge rate for a 6 volt battery, for example, it is 5.25V at the 20-hour (0.05C) rate, 5.10V at the 4-hour (0.2C) rate, and 4.5V at the 1/2- hour(1.0C) rate.

It is important to note that deep discharging a battery at high rates for short periods is not nearly as severe as discharging a battery at low rates for long periods of time. To clarify, let's, analyze two examples:

• Battery A is discharged at the 1C rate to zero volts. "C" for a 4 AH battery, for example, is 4 amps. Full discharge is reached after about 30 minutes when the battery voltage drops to 1.5V/cell. At this point, only 50% of rated capacity has been discharged (1C amps x 0.5 hrs = 0.5C Amp. Hrs.) Continuing the discharge to zero volts will bring the total amount of discharged ampere-hours to approximately 75% because the rapidly declining voltage quickly reduces current flow to a trickle. The battery will recover easily from this type of deep discharge.

• Battery B is discharged at the 0.01C rate to zero volts. 0.01C for a 4 AH battery is 40mA. Full discharge is reached after 100+ hours when the terminal voltage drops to 1.75 V/cell. At this point, the battery has already delivered 100% of its rated capacity (0.01 x 100 hrs = 1C Amp. Hrs.). Continuing the discharge to zero volts will keep the battery under load for another 4-5 days(!), squeezing out every bit of stored energy.

This type of "deep" discharge is severe and is likely to damage the battery. The sooner a severely discharged battery is recharged, the better its chances to fully recover.

CAPACITY

The capacity of a battery is the total amount of electrical energy available from a fully charged cell or cells. Its value depends on the discharge current, the temperature during discharge, the final (cut-off) voltage and the general history of the battery.

Capacity, expressed in ampere-hours (AH) is the product of the current discharged and the length of discharge time. The rated capacity (C) of a Power-Sonic battery is measured by its performance over 20 hours of constant current discharge at a temperature of 68°F (20°C) to a cutoff voltage of 1.75 volts.

As an example, Model PS-610, with a rated capacity of 1AH will deliver 50 mA (1/20 of 1AH, or 0.05C) for 20 hours before the voltage drops from 6.45 to 5.25 volts.

By cycling the battery a few times or float charging it for a month or two, the highest level of capacity development is achieved. Power-Sonic batteries are fully charged before leaving the factory, but full capacity is realized only after the battery has been cycled a few times or been on float charge for some time.

The table in *Figure 2* shows capacities for various multiples of the 20-hour discharge current.

Rated Capacity	@ 0.05C rate (20 Hr. Rate.)		@0.1C rate (9 Hr. Rate)		@0.2C rate (4 Hr. Rate)		@0.5C rate (1.3 Hr. Rate)		@1C rate (33 Min. Rate)		@2C rate (12 Min. Rate)		@3C rate (7.2 Min. Rate)	
	Current Amps.	Capacity Amp. Hrs	Current Amps.	Capacity Amp. hrs.	Current Amps.	Capacity Amp.Hrs	Current Amps.	Capacity Amp. Hrs.	Current Amps.	Capacity Amp. hrs.	Current Amps.	Capacity Amp. Hrs.	Current Amps.	Capacity Amp. Hrs.
0.5AH	0.025	0.50	0.05	0.45	0.10	0.40	0.25	0.325	0.50	0.28	1.00	0.20	1.50	0.18
0.8AH	0.04	0.80	0.08	0.72	0.16	0.64	0.40	0.52	0.80	0.44	1.60	0.32	2.40	0.29
1.0AH	0.05	1.00	0.10	0.90	0.20	0.80	0.50	0.65	1.00	0.56	2.00	0.40	3.00	0.36
1.3AH	0.065	1.30	0.13	1.17	0.26	1.04	0.65	0.845	1.30	0.715	2.60	0.52	3.90	0.47
2.3AH	0.115	2.30	0.23	2.07	0.46	1.84	1.15	1.495	2.30	1.288	4.60	0.92	6.90	0.83
3.0AH	0.15	3.00	0.30	2.70	0.60	2.40	1.50	1.95	3.00	1.65	6.00	1.20	9.00	1.08
3.2AH	0.16	3.20	0.32	2.88	0.64	2.56	1.60	2.08	3.20	1.76	6.40	1.28	9.60	1.15
4.5AH	0.22	4.40	0.45	4.05	0.90	3.60	2.25	2.92	4.5	2.47	9.00	1.80	13.50	1.62
5.0AH	0.25	5.00	0.50	4.50	1.00	4.00	2.50	3.25	5.00	2.80	10.00	2.00	15.00	1.80
6.5AH	0.325	6.50	0.65	5.85	1.30	5.20	3.25	4.23	6.50	3.64	13.00	2.60	19.50	2.34
7.0AH	0.35	7.00	0.70	6.30	1.40	5.60	3.50	4.55	7.00	3.85	14.00	2.80	21.00	2.52
8.0AH	0.40	8.00	0.80	7.20	1.60	6.40	4.00	5.20	8.00	4.48	16.00	3.20	24.00	2.88
9.0AH	0.45	9.00	0.90	8.10	1.80	7.20	4.50	5.85	9.00	5.04	18.00	3.60	27.00	3.24
10.0AH	0.50	10.00	1.00	9.00	2.00	8.00	5.00	6.50	10.00	5.60	20.00	4.00	30.00	3.60
12.0AH	0.60	12.00	1.20	10.80	2.40	9.60	6.00	7.80	12.00	6.72	24.00	4.80	36.00	4.32
18.0AH	0.90	18.00	1.80	16.20	3.06	14.40	9.00	11.70	18.00	9.90	36.00	7.20	54.00	6.48
20.0AH	1.00	20.00	2.00	18.00	4.00	16.00	10.00	13.00	20.00	11.20	40.00	8.00	60.00	7.20
26.0AH	1.30	26.00	2.60	23.40	5.20	20.80	13.00	16.90	26.00	14.30	52.00	10.40	78.00	9.36
28.0AH	1.40	28.00	2.80	25.20	5.40	21.60	14.00	18.20	28.00	15.40	54.00	10.88	84.00	10.08
33.0AH	1.65	33.00	3.30	29.70	6.60	26.40	16.50	21.45	33.00	18.15	66.00	13.20	99.00	11.88
40.0AH	2.00	40.00	4.00	36.00	8.00	32.00	20.00	26.00	40.00	22.40	80.00	16.00	120.00	14.40
55.0AH	2.75	55.00	5.50	49.50	11.00	44.00	27.50	35.75	55.00	30.25	110.00	22.00	165.00	19.80
60.0AH	3.00	60.00	6.00	54.00	12.00	48.00	30.00	39.00	60.00	33.60	120.00	24.00	180.00	21.60
75.0AH	3.75	75.00	7.50	67.50	15.00	60.00	37.50	48.75	75.00	41.25	150.00	30.00	225.00	27.00
80.0AH	4.00	80.00	8.00	72.00	16.00	64.00	40.00	52.00	80.00	44.80	160.00	32.00	240.00	28.80
100.0 AH	5.00	100.00	10.00	90.00	20.00	80.00	50.00	65.00	100.00	55.00	200.00	40.00	300.00	36.00

Figure 2

When a battery discharges at a constant rate, its capacity changes according to the amperage load. Capacity increases when the discharge current is less than the 20-hour rate and decreases when the current is higher.

Figure 3 shows capacity curves for major Power-Sonic battery models with different ampere-hour ratings. Amperage is on the horizontal scale and the time elapsed is on the vertical scale; the product of these values is the capacity.

Proper battery selection for a specific application can be made from this graph if the required time and current are known. For example, to determine the proper capacity of a battery providing 3 amps for 20 minutes, locate the intersection of these values on the graph. The curve immediately above that point represents the battery which will meet the requirement.

CAPACITY VARIATION BY CURRENT LOAD

Figure 3

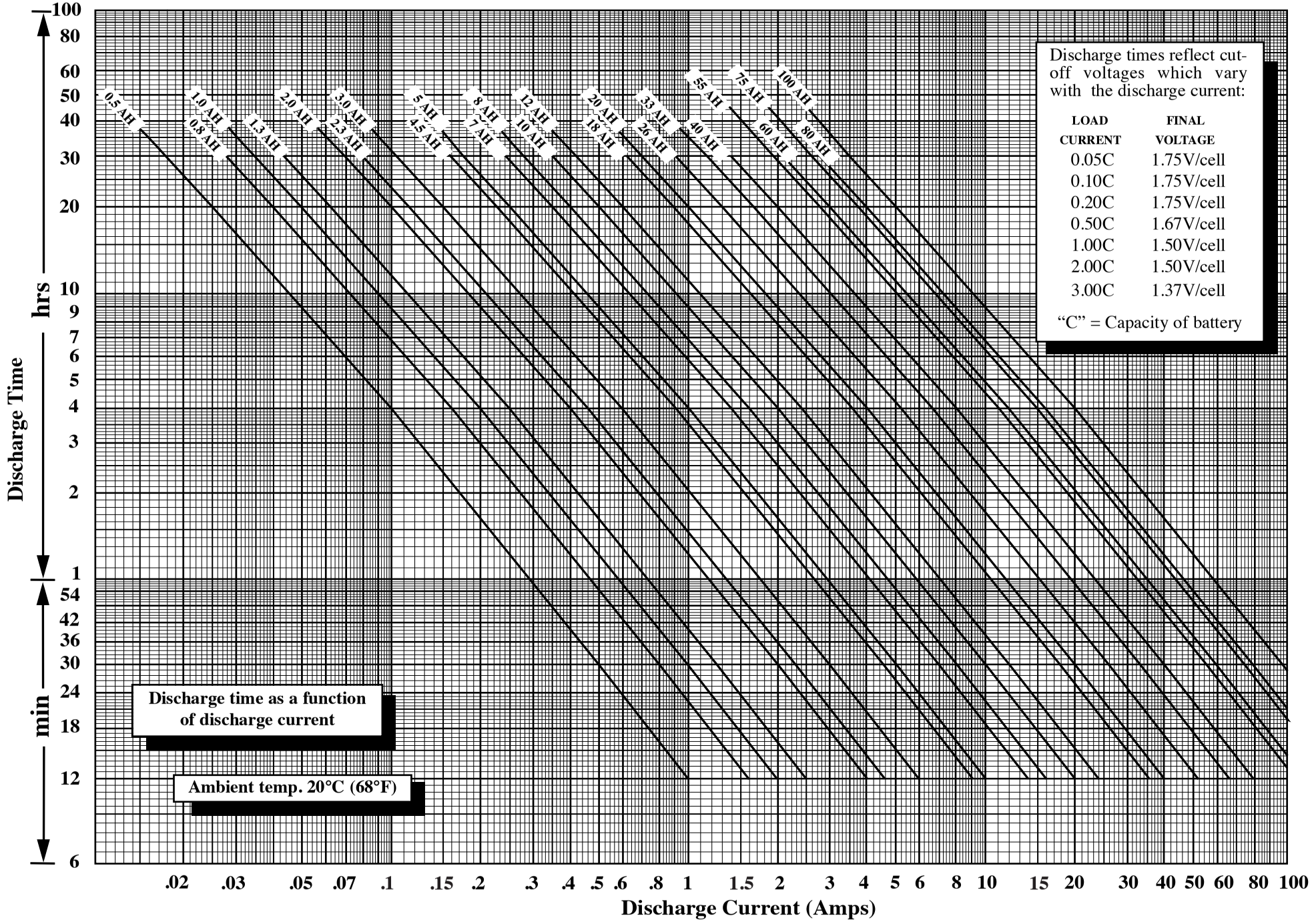

Discharge

During discharge the voltage will decrease. The graphs in *Figure 4* illustrate this for different discharge rates and ambient temperatures. "C" is the rated capacity of a battery: "C" for Model PS-610 (6V - 1AH) is 1AH. By convention, rating of nearly all sealed-lead acid batteries, including Power-Sonic, is based on a 20-hour (0.05C) discharge rate .

An important feature of Power-Sonic batteries is shown in the discharge curves; namely, the voltage tends to remain high and almost constant for a relatively long period before declining to an end voltage.

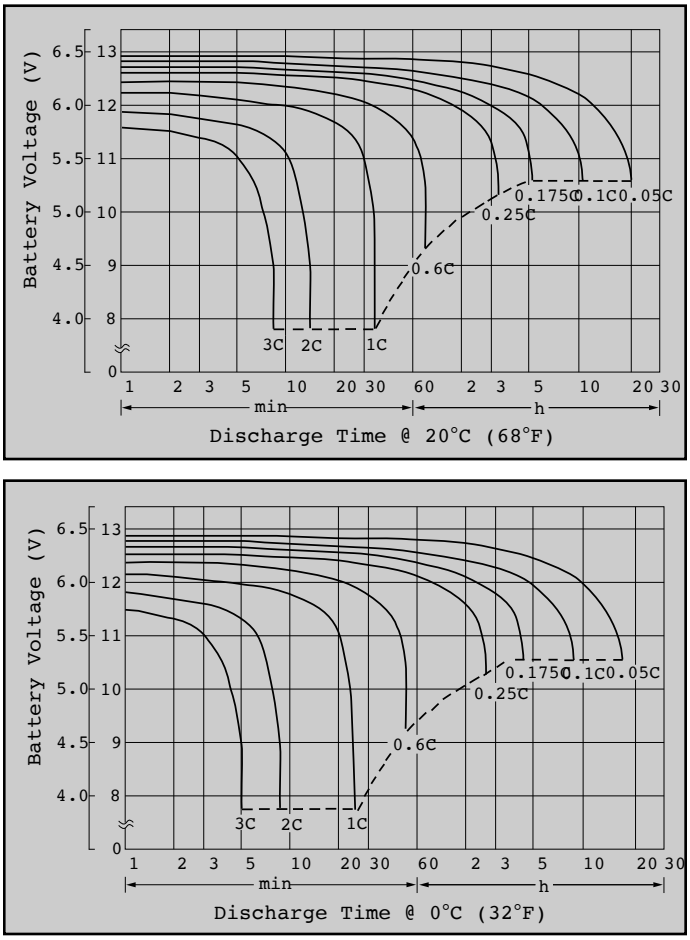

Figure 4: Characteristic Discharge Curves

Open-Circuit Voltage

Open circuit voltage varies according to ambient temperature and the remaining capacity of the battery. Generally, open circuit voltage is determined by the specific gravity of the electrolyte. Discharging a battery lowers the specific gravity. Consequently, it is possible to determine the approximate remaining capacity of a battery from the terminal voltage.

The open circuit voltage of a Power-Sonic battery is 2.15 V/cell when fully charged and 1.94 V/cell when completely discharged.

As seen in *Figure 4,* under load, the battery can deliver useful energy at less than 1.94 V/cell, but after the load is removed the open circuit voltage will "bounce back" to voltages shown in *Figure 5*, dependent upon residual capacity.

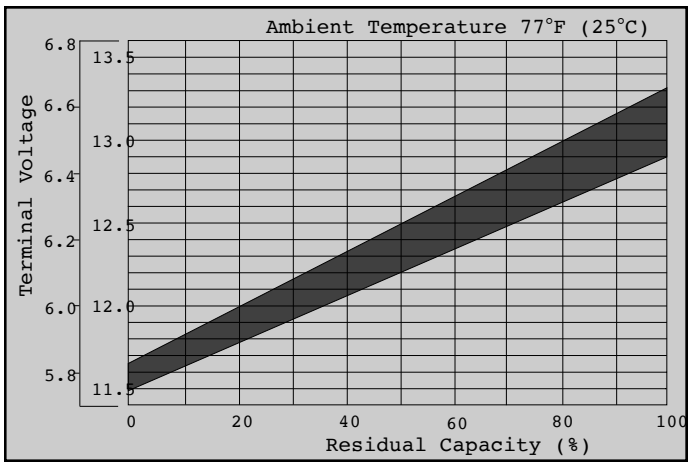

Figure 5: Open-Circuit Voltage Characteristics

Temperature

Actual capacity is a function of ambient temperature and rate of discharge. At 68°F (20°C) rated capacity is 100%. The capacity increases slowly above this temperature and decreases as the temperature falls. Even at -40°F (-40°C), however , the Power-Sonic battery will still function at better than 30% of its rated capacity when discharged at the 20-hour rate (0.05C). At any ambient temperature, the higher the rate of discharge, the lower the available capacity. This relationship is shown in *Figure 6*.

Power-Sonic batteries may be discharged at temperatures ranging from -40°F to 140°F (-40°C to 60°C) and charged at temperatures from -4°F to 122°F (-20°C to 50°C).

While raising ambient temperature increases capacity, it also decreases useful service life. It is estimated that battery life is halved for each 10°C above normal room temperature.

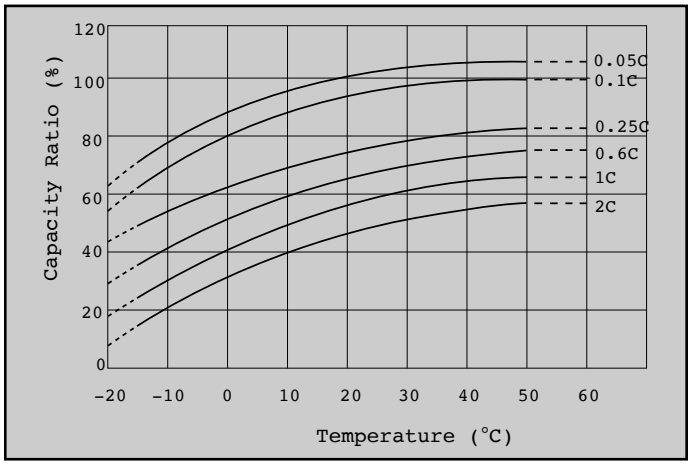

Figure 6: Effect of Temperature on Capacity

Figure 7 shows the relationship between current and discharge time for different ambient temperatures.

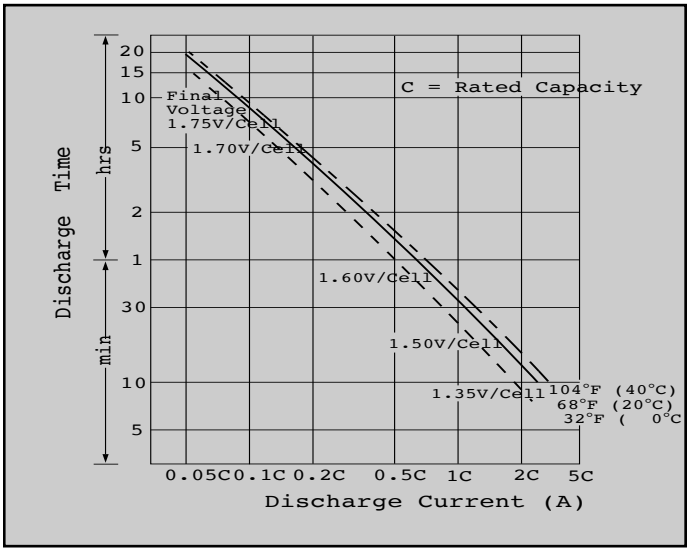

Figure 7: Discharge Time vs. Discharge Current

Shelf Life & Storage

Low internal resistance and special alloys in the electrodes assure a low self discharge rate and, consequently, a long shelf life. If kept at 68°F (20°C), about 60-70% of the nominal capacity remains after one year of storage. One recharge per year is sufficient to maintain the original capacity of a battery not in use.

The rate of self discharge varies with the ambient temperature. At room temperature it is about 3% per month. At low temperatures it is nearly negligible, at higher ambient temperatures self discharge increases.

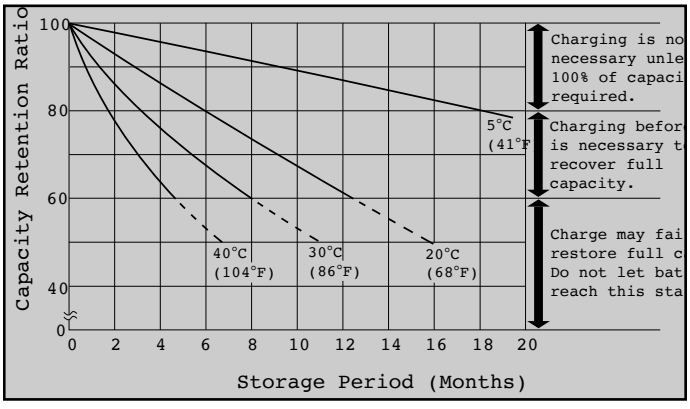

Figure 8: Self Discharge Characteristics

To obtain maximum battery life and performance, batteries should be:

- recharged as soon as possible after each use and not stored in a discharged state;
- stored at 68°F (20°C) or lower, if possible, and
- recharged annually when not used.

Battery Life

Cyclic Use: The number of charge/discharge cycles depends on the capacity taken from the battery (a function of discharge rate and depth of discharge), operating temperature and the charging method.

Figure 9 shows the relationship between depth of discharge and number of cycles as well as increases of capacity during the early cycles.

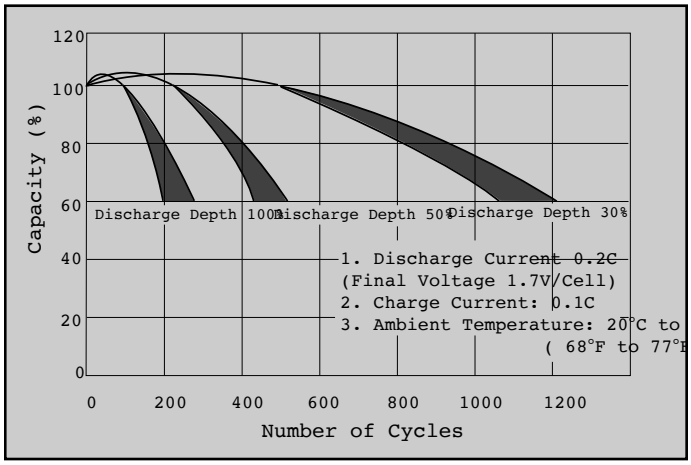

Figure 9: Depth of Discharge vs. Number of Cycles

Standby Use: The float service life, or life expectancy under continuous charge, depends on the frequency and depth of discharge, the charge voltage, and the ambient temperature. At a float voltage of 2.25V to 2.30V/cell and an ambient temperature of 60°F to 77°F (20°C to 25°C) Power-Sonic batteries should last four to five years before the capacity drops to 60% of its original rating.

Figure 10 indicates how capacity changes over time.

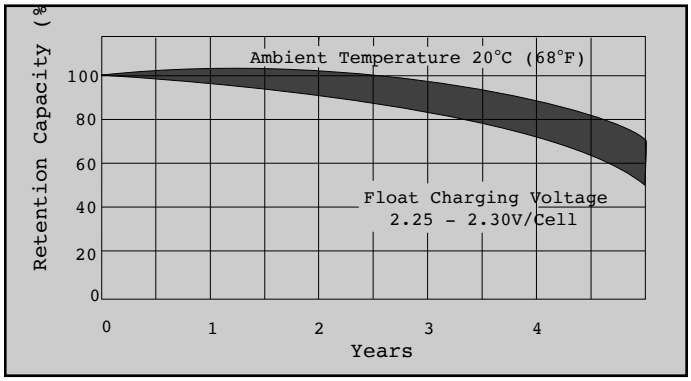

Figure 10: Life Characteristics in Standby Use

PERFORMANCE DATA

The graph in *Figure 11* shows life characteristics in float (standby) service for ambient temperatures ranging from 15°C to 55°C

If prevailing ambient temperatures are well above 20-25°C the life expectancy of this type of battery in float service depends greatly on temperature compensated charging. The typical temperature coefficient is -2mV/cell/°C. The graph shown along side is based on temperature compensated charging.

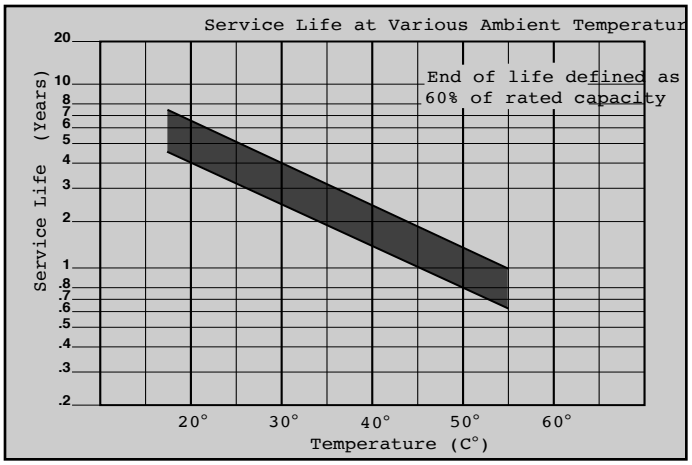

Figure 11: Service Life at Various Ambient Temperatures

OVER-DISCHARGE PROTEC-

To optimize battery life, it is recommended that the battery be disconnected from the load when the end voltage – a function of the discharge rate – is reached. It is the voltage point at which 100% of the usable capacity of the battery has been consumed or continuation of the discharge is useless because of the voltage dropping below useful levels. (see section on Deep Discharge on page 3)

Discharging a sealed lead-acid battery below this voltage or leaving a battery connected to a load will impair the battery's ability to accept a charge. To prevent potential over-discharge problems, voltage cut-off circuits as shown in *Figure 12* may be used.

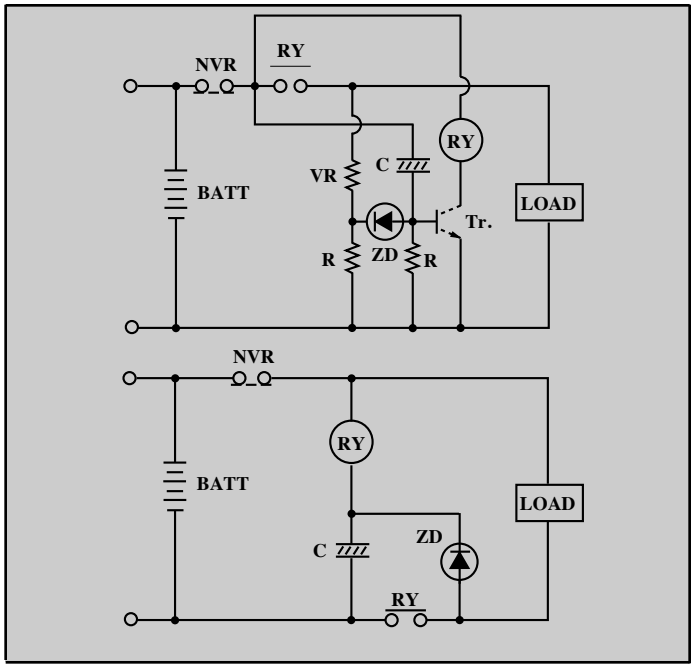

Figure 12: Circuits of Over-Discharge Preventive Device

CHARGING

Dependable performance and long service life depend upon correct charging. Faulty procedures or inadequate charging equipment result in decreased battery life and/or unsatisfactory performance. The selection of suitable charging circuits and methods is as important as choosing the right battery for the application.

General

To charge a Power-Sonic battery, a DC voltage higher than the open-circuit voltage of 2.15 is applied to the terminals of the battery. Depending on the state of charge, the cell may temporarily be lower (after discharge) or higher (right after charging) than 2.15 volts. After some time, however, it should level off at about 2.15 volts per cell.

Power-Sonic batteries may be charged by using any of the conventional charging techniques. To obtain maximum service life and capacity, along with acceptable recharge time and economy, constant voltage-current limited charging is recommended.

During charge, the lead sulfate of the positive plate becomes lead dioxide. As the battery reaches full charge, the positive plate begins generating dioxide causing a sudden rise in voltage. A constant voltage charge, therefore, allows detection of this voltage increase and thus control of the charge amount.

Overcharging: As a result of too high a charge voltage excessive current will flow into the battery after reaching full charge causing decomposition of water in the electrolyte and, hence, premature aging.

At high rates of overcharge a battery will progressively heat up. As it gets hotter, it will accept more current, heating up even further. This is called thermal runaway, and can destroy a battery in as little as a few hours.

Undercharging: If too low a charge voltage is applied, the current flow will essentially stop before the battery is fully charged. This allows some of the lead sulfate to remain on the electrodes which will eventually reduce capacity.

Batteries which are stored in a discharged state, or left on the shelf for too long, may initially appear to be "open circuited" or will accept far less current than normal. This is caused by a phenomenon called "sulfation". When this occurs, leave the charger connected to the battery. Usually, the battery will start to accept increasing amounts of current until a normal current level is reached. If there is no response, even to charge voltages above recommended levels, the battery may have been in a discharged state for too long to recover.

Charging Characteristics

During constant voltage or taper charging, the battery's current acceptance decreases as voltage and state of charge increase. The battery is fully charged once the current stabilizes at a low level for a few hours.

Caution: Never charge or discharge a battery in a hermetically sealed enclosure. Batteries generate a mixture of gases internally. Given the right set of circumstances, such as extreme overcharging or shorting of the battery, these gases might vent into the enclosure and create the potential for an explosion when ignited by a spark.

If in doubt, or concepts of proper use and care are unclear, contact Power-Sonic's department for application engineering at 619-661-2020.

Please note that there are two criteria for determining when a battery is fully charged: (1) the final current level and (2) the peak charging voltage while this current flows.

Figure 13 depicts an example of typical charge characteristics for cycle service where charging is non-continuous and peak voltage can, therefore, be higher.

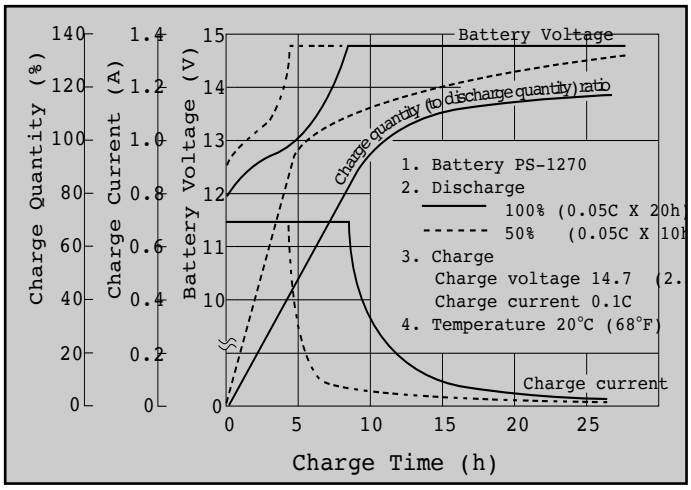

Figure 13: Charge characteristics for 14.7V Constant Voltage

Figure 14 illustrates typical characteristics for standby service type charge. Here, charging is continuous and the peak charge voltage must, therefore, be lower.

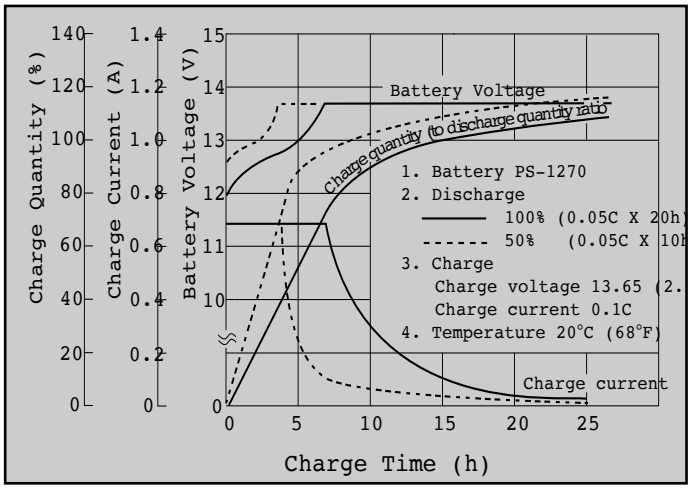

Figure 14: Charge Characteristics for 13.65V Constant Voltage

Charging Methods

Selecting the appropriate charging method depends on the intended use (cyclic or float service), economic considerations, recharge time, anticipated frequency and depth of discharge, and expected service life. The key goal of any charging method is to control the charge current at the end of the charge.

Taper Charging: This is the simplest, least expensive charging method. Either quasi-constant voltage or quasi-constant current characteristics can be built into the charger through combination of transformer, diode and resistance. Of the two, constant potential charging is preferable.

Typical taper chargers are comprised of small transformer-rectifier circuits wherein the transformer is so designed that the current is limited to the maximum initial charge current for the battery. This current is held constant until the terminal voltage and resultant current demand reach a point at which the charge current begins to fall. Although this type of charger can provide a relatively fast recharge, it is basically a constant current device and the charge voltage may be driven too high. Therefore, it must be disconnected, usually within 12-24 hours, or after 100-120% of the preceding discharge has been returned. It is also sensitive to line voltage variations which can cause over- or under-charging. Consequently, this charging method can only be used in cyclic applications

Figure 15 shows an example of a typical diagram and *Figure 16* the resultant charge characteristics for this type of basically unregulated charger.

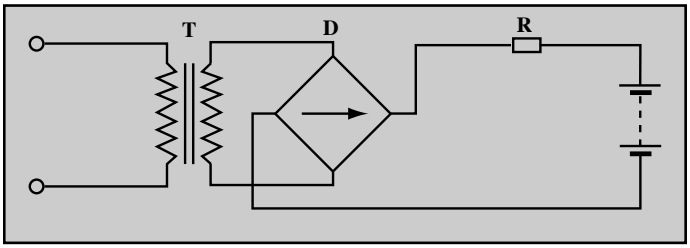

Figure 15: Semi-Constant Current Charging Circuit

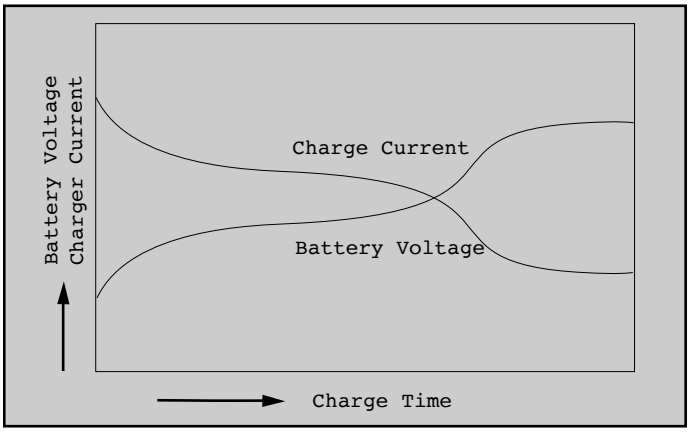

Figure 16: Semi-Constant Current Charge Characteristics

Constant Current Charging: Constant current charging is suited for applications where discharged ampere-hours of the preceding discharge cycle are known. Charge time and charge quantity can easily be calculated, however an expensive circuit is necessary to obtain a highly accurate constant current. Monitoring of charge voltage or limiting of charge time is necessary to avoid excessive overcharge.

While this charging method is very effective for recovering the capacity of a battery that has been stored for an extended period of time, or for occasional overcharging to equalize cell capacities, it lacks specific properties required in today's electronic environment.

An example of a constant current charge circuit is shown in *Figure 17* and the charge characteristics for this type of charger in *Figure 18*.

Figure 17: Constant Current Charging Circuit

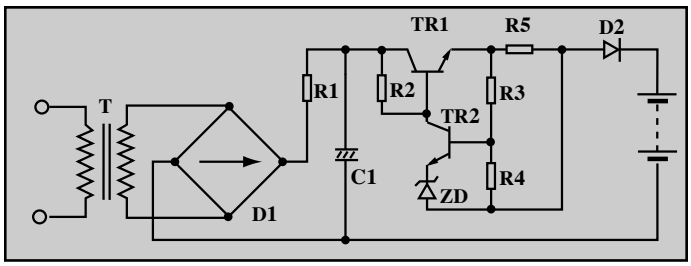

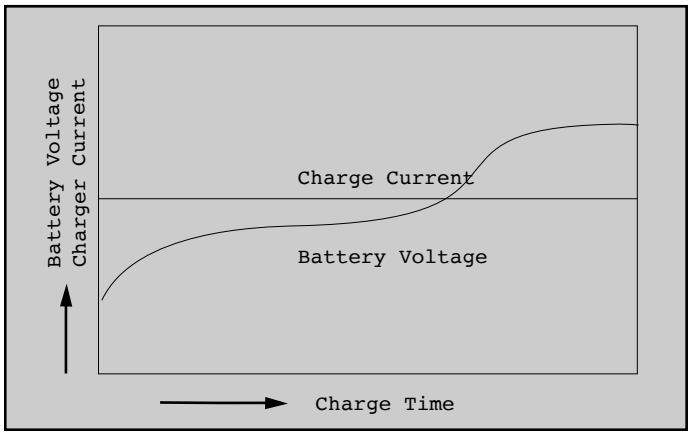

Figure 18: Constant Current Charge Characteristics

Constant Voltage Charging: Constant current/constant voltage charging is the best method to charge Power-Sonic batteries. Depending on the application, batteries may be charged either on a continuous or non-continuous basis. In applications where standby power is required to operate when the AC power has been interrupted, continuous float charging is recommended. Non-continuous cyclic charging is used primarily with portable equipment where charging on an intermittent basis is appropriate.

The constant current/constant voltage charge method applies a constant voltage to the battery and limits the initial charge current. It is necessary to set the charge voltage according to specified charge and temperature characteristics. Inaccurate voltage settings cause over- or under-charge. This charging method can be used for both cyclic and standby applications.

Figures 19 and *20* illustrate examples of a constant current/constant voltage charging circuit and charging characteristics, respectively. The circuit diagram includes a temperature compensation feature for charge voltage to ensure optimum charging conditions regardless of changes in ambient temperature.

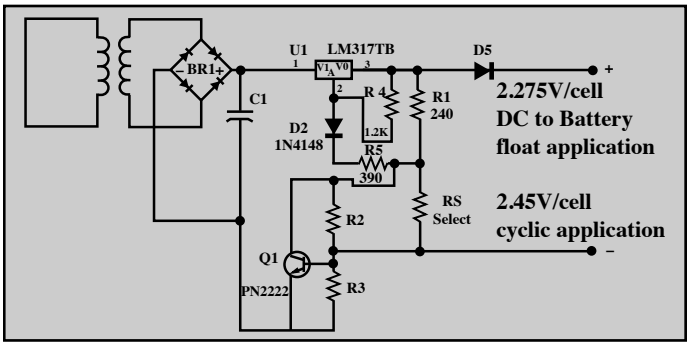

Figure 19: Constant Current/Constant Voltage Charge Circuit

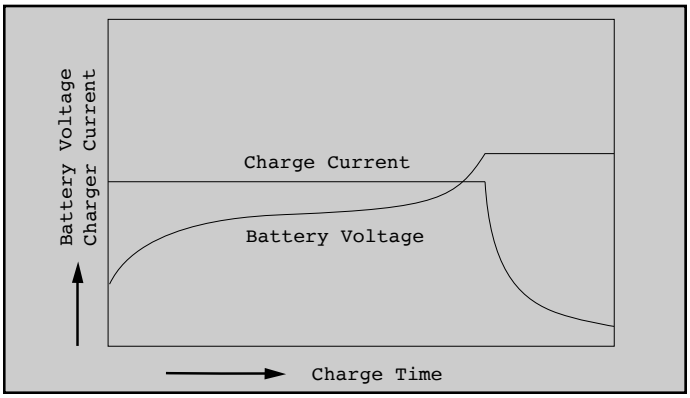

Figure 20: Constant Current/Constant Voltage Charge Characteristics

Charging for Cycle Operation

Cyclic applications generally require that recharging be done in a relatively short time. The initial charge current, however, must not exceed 0.20 x C amps. Just as battery voltage drops during discharge, it slowly rises during charge. Full charge is determined by voltage and inflowing current. When, at a charge voltage of 2.45 ±0.05 volts/cell, the current accepted by the battery drops to less than 0.01 x C amps (1% of rated capacity), the battery is fully charged and the charger should be disconnected or switched to a float voltage of 2.25 to 2.30 volts/cell. The voltage should not be allowed to rise above 2.45 ±0.05 volts/cell.

Charging for Standby Operation

Standby applications generally do not require that the battery be charged as fast or as frequently as in cycle operation. However, the battery must be kept constantly charged to replace the energy that is expended due to internal loss and deterioration of the battery itself. Although these losses are very low in Power-Sonic batteries, they must be replaced at the rate the battery self-discharges; at the same time the battery must not be given more than these losses or it will be overcharged. To accomplish this, a constant voltage method of charging called "float charging" is used.

The recommended constant float voltage is 2.25-2.30 volts per cell. Maintaining this float voltage will allow the battery to define its own current level and remain fully charged without having to disconnect the charger from the battery. The trickle current for a fully charged battery floating at the recommended charge voltage will typically hover around the 0.001C rate (10mA for a 10AH battery, for example.)

The float charger is basically a constant voltage power supply. As in cycle chargers, however, care must be exercised not to exceed the initial charge current of 0.20 x C amperes.

Two-Step Constant Voltage Charging

This method uses two constant voltage devices. In the initial charge phase the high voltage setting is used. When charging is nearly complete and the charge voltage has risen to a specified value (with the charge current decreased), the charger switches the voltage to the lower setting. This method allows rapid charging in cycle or float service without the possibility of overcharging even after extended charging periods.

The graph in *Figure 21* shows charging characteristics, and the diagram in *Figure 22* an example of a charging circuit for this type of charger.

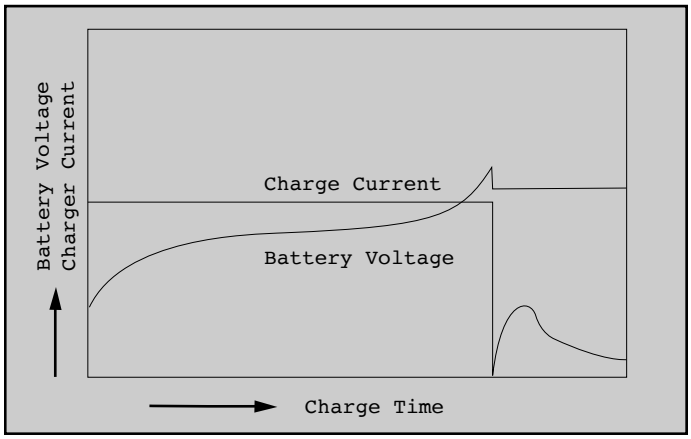

Figure 21: Two-Step Constant Voltage Charge Characteristics

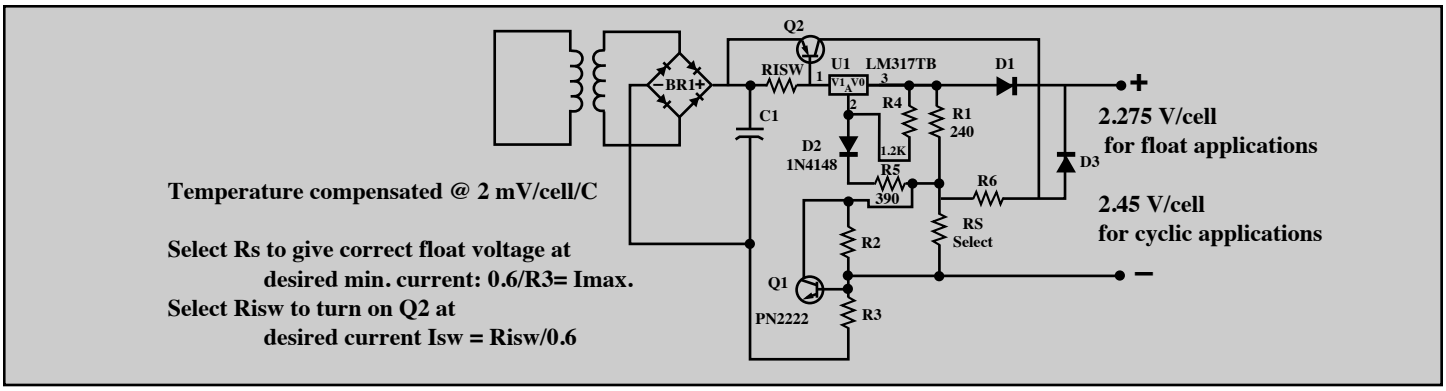

Figure 22: Dual Stage Current Limited Battery Charger

Charging in Series: Lead-acid batteries are strings of 2 volt cells connected in series, commonly 2, 3 ,4 or 6 cells per battery. Strings of Power-Sonic batteries up to 48 volts and higher may be charged in series safely and efficiently. However, as the number of batteries in series increases, so does the possibility of slight differences in capacity. These differences can result from age, storage history, temperature variations or abuse.

When a single constant voltage charger is connected across an entire high voltage string, the same current flows through all cells in the string. Depending on the characteristics of the individual batteries, some may overcharge while others remain in a slightly undercharged condition. When charging high voltage strings this way for extended periods it is generally recommended to use a low input voltage inverter to enhance service life and simplify charging requirements.

If one cell is lower in capacity than the others when discharging a long string in series, it may actually reverse polarity even though the total voltage of the string is at or above the cut-off voltage.

To minimize the effects of individual battery differences, use batteries of the same age and history and, if possible, charge in strings of no greater than 24 or 48 volts.

Charging in Parallel: Power-Sonic batteries may be used in parallel with one or more batteries of equal voltage.

When connected in parallel, the current from a charger will tend to divide almost equally between the batteries. No special matching of batteries is required. If the batteries of unequal capacity are connected in parallel, the current will tend to divide between the batteries in the ratio of capacities (actually, internal resistances).

When charging batteries in parallel, where different ratios of charge are to be expected, it is best to make provisions to assure that the currents will not vary too much between batteries. Holding a small resistance in series with each battery is all that is needed

Temperature Compensation

Power-Sonic batteries perform well both at low and high temperatures. At low temperatures, however, charge efficiency is reduced; at temperatures above 45°C, charge efficiency increases so rapidly that there is a danger of thermal runaway if temperature compensation is not precise.

The effect of temperature on charge voltage is less critical in float applications, than in cyclic use where relatively high charge currents are applied for the purpose of short recharge times.

Temperature effects should definitely be considered when designing or selecting a charging system. As a rule of thumb, temperature compensation is desirable in the charging circuit when operating outside the range of 41°F to 95°F (5°C to 35°C) prevailing ambient. The temperature coefficient is -2mV/cell/°C below 20°C in standby service and -6mV/cell/°C below 20°C in cyclic use. For higher temperatures the charge voltage should be correspondingly decreased.

The table in *Figure 23* lists recommended charge voltages for different temperatures.

AMBIENT TEMPERATURE	CHARGE VOLTAGE PER CELL	
	Cyclic use	Float Use
4°F(–20°C)	2.67–2.77V	2.34–2.39V
14°F(–10°C)	2.61–2.71V	2.32–2.37V
32°F(0°C)	2.55–2.65V	2.30–2.35V
50°F(+10°C)	2.49–2.59V	2.28–2.33V
68°F(+20°C)	2.43–2.53V	2.26–2.31V
77°F(+25°C)	2.40–2.50V	2.25–2.30V
86°F(+30°C)	2.37–2.47V	2.24–2.29V
104°F(+40°C)	2.31–2.41V	2.22–2.27V
122°F(+50°C)	2.25–2.35V	2.20–2.25V

Figure 23: Temperature Compensated Charge Voltage

APPLICATION NOTES

Power-Sonic rechargeable sealed lead-acid batteries are designed to provide years of dependable service. Adherence to the following guidelines in system design will ensure that battery life is maximized and operation is trouble-free.

• Continuous over-or undercharging is the single worst enemy of a lead-acid battery. Caution should be exercised to ensure that the charger is disconnected after cycle charging, or that the float voltage is set correctly.

• Batteries should not be stored in a discharged state or at elevated temperatures. If a battery has been discharged for some time or the load was left on indefinitely, it may not readily take a charge. To overcome this, leave the charger connected and the battery should eventually begin to accept charge.

• Avoid exposing batteries to heat! Care should be taken to place batteries away from heat-emitting components. If close proximity is unavoidable, provide ventilation. Service life is shortened considerably at ambients above 30°C.

• Although Power-Sonic batteries have a low self-discharge rate which permits storage of a fully charged battery for up to a year, it is recommended that a battery be charged 6-9 months after receipt to account for storage from the date of manufacture to the date of purchase. Otherwise, permanent loss of capacity might occur as a result of sulfation. To prolong shelf life without charging, store batteries at 50°F (10°C) or less.

• Fasten batteries tightly and make provisions for shock absorption if exposure to shock or vibration is likely.

• Although it is possible to charge Power-Sonic batteries rapidly, i.e. in 6-7 hrs., it is not normally recommended. Unlimited current charging can cause increased off-gassing and premature drying. It can also produce internal heating and hot spots resulting in shortened service life. Too high a charge current will cause a battery to get progressively hotter. This can lead to "thermal runaway" and can destroy a battery in as little as a few hours.

• Caution: Never charge or discharge a battery in an airtight enclosure. Batteries generate a mixture of gases internally. Given the right set of circumstances such as extreme overcharging or shorting of the battery, these gases might vent into the enclosure and create the potential for an explosion when ignited by a spark. Generally, ventilation inherent in most enclosures is sufficient to avoid problems.

• Do not place batteries in close proximity to objects which can produce sparks or flames, and do not charge batteries in an inverted position.

• When charging batteries in series (positive terminal of one battery is connected to the negative terminal of another), all batteries in the string will receive the same amount of charge current, though individual battery voltages may vary.

• When charging batteries in parallel (positive terminals are connected to the positive terminal and negative terminals to the negative), all batteries in the string will receive the same charge voltage but the charge current each battery receives will vary until equalization is reached.

• High voltage strings of batteries in series should be limited to twenty 6 volt or ten 12 volt batteries when a single constant voltage charger is connected across the entire string . Differences in capacity can cause some batteries to overcharge while others remain undercharged thus causing premature aging of batteries. It is, therefore, not advisable to mix batteries of different capacities, make, or age in a series string.

To minimize the effects of cell or battery differences, charge the string in 24 volt battery groups through a constant current source with zener diode regulation across individual batteries or battery groups.

• To prevent problems arising from heat exchange between batteries connected in series or parallel, it is advisable to provide air space of at least 0.4" (10mm) between batteries.

• Battery containers, made of ABS plastic or styrene, can sustain damage if exposed to organic solvents or adhesives.

• Recharge time depends on the depth of the preceding discharge and the output current of the charger. To determine the approximate recharge time of a fully discharged battery, divide the battery's capacity (amp. hrs.) by the rated output of the charger (amps.) and multiply the resulting number of hours by a factor of 1.75 to compensate for the declining output current during charge. If the amount of amp. hrs. discharged from the battery is known, use it instead of the battery's capacity to make the calculation.

• For best results and generally acceptable performance and longevity, keep operating temperature range between -20°C and +40°C.

• Do not attempt to disassemble batteries. Contact with sulfuric acid may cause harm. Should it occur, wash skin or clothes with liberal amounts of water. Do not throw batteries into fire; batteries so disposed may rupture or explode. Disassembled batteries are hazardous waste and must be treated accordingly. It is unlawful to dispose of batteries except through a recycling center.

GLOSSARY

Ambient Temperature
The prevailing surface temperature to which a battery is exposed.

Ampere
Unit of measurement for electric current.

Ampere-Hour
The product of current (amperes) multiplied by time (hours). Used to indicate the capacity of a battery. Also Amp.Hr. or A.H.

Battery
Two or more cells connected together, most typically in series.

Capacity
The electrical energy available from a cell or battery expressed in ampere-hours.
Available capacity refers to ampere-hours that can be discharged from a battery based on its state of charge, rate of discharge, ambient temperature, and specified cut-off voltage.
Rated capacity ("C") is the discharge capacity the manufacturer says may be obtained at a given discharge rate and temperature.

Cell
The basic building block of a battery. The nominal voltage of a lead-acid battery is 2 volts.
Cell reversal – the act of driving a cell into reverse polarity by excessive discharge.
Primary cell – cell or battery that can be discharged only once.
Secondary cell – the process is reversible so that charging and discharging may be repeated over and over.

Charge
The conversion of electrical energy to chemical energy; the process which restores electrical energy to a cell or battery.
Charge retention refers to a battery's ability to hold a charge. It diminishes during storage.
Charge acceptance quantifies the amount of electric charge which accumulates in a battery.
Float charge maintains the capacity of a cell or battery by applying a constant voltage.
Trickle charge maintains the capacity of a cell or battery by applying a small constant current.
Charge equalization brings all of the cells in a battery or string to the same state of charge.

Discharge
The process of drawing current from a battery.
Deep Discharge – the discharge of a cell or battery to between 80% and 100% of rated capacity.
Depth of Discharge – the mount of capacity – typically expressed as a percentage – removed during discharge.
Self Discharge – the loss of capacity while stored or not in use.
Self Discharge Rate – the percent of capacity lost on open circuit over a specified period of time.

Electrode
Positive or negative plate containing materials capable of reacting with electrolyte to produce or accept current.

Energy Density
Ratio of battery energy to volume or weight expressed in watt-hours per cubic inch or pound.

Gas Recombination
The process by which oxygen gas generated from the positive plate during the final stage of charge is absorbed into the negative plate, preventing loss of water.

Impedance
The resistive value of a battery to an AC current expressed in ohms (Ω). Generally measured at 1000 Hz at full charge.

Internal Resistance
The resistance inside a battery which creates a voltage drop in proportion to the current draw.

Nominal Voltage / Nominal Capacity
The nominal value of rated voltage / the nominal value of rated capacity. The nominal voltage of a lead-acid battery is 2 volts per cell.

Open Circuit Voltage
The voltage of a battery or cell when measured in a no load condition.

Parallel Connection
Connecting a group of batteries or cells by linking all terminals of the same polarity. This increases the capacity of the battery group.

Series Connection
The connection of a group of cells or batteries by linking terminals of opposite polarity. This increases the voltage of the battery group.

Separator
Material isolating positive from negative plates. In sealed lead-acid batteries it normally is absorbent glass fiber to hold the electrolyte in suspension.

SLA Battery
Sealed lead-acid battery, generally having the following characteristics: Maintenance-free, leak-proof, position-insensitive. Batteries of this type have a safety vent to release gas in case of excessive internal pressure build-up. Hence also the term: Valve regulated battery.
"Gel Cells" are SLA batteries whose dilute sulfuric acid electrolyte is immobilized by way of additives which turn the electrolyte into a gel.

Standby Service
An application in which the battery is maintained in a fully charged condition by trickle of float charging.

State of Charge
The available capacity of a battery at a given time expressed as a percentage of rated capacity.

Thermal Runaway
A condition in which a cell or battery on constant potential charge can destroy itself through internal heat generation.

Primary Power

- Portable Tools & Instruments
- Hand-held Lights
- Cordless & Portable Cellular Phones
- Power Packs
- Remote or Portable Data Gathering Devices
- Medical Apparatus
- Battery Powered Wheelchairs, Ride-on Toys
- Engine Starting Devices
- Robotics
- Consumer Electronics
- Hobby Craft

Standby Power

- UPS Systems
- Emergency Lighting
- Fire & Burglar Alarm Systems
- Access Control Devices
- Telecommunications Equipment
- Electronic Equipment Requiring Memory Protection
- Solar Powered Systems
- Automotive Electronics

OPERATIONS & WAREHOUSE
POWER-SONIC CORPORATION
9163 Siempre Viva Road
San Diego, CA 92173
Telephone: (619) 661-2020
Fax: (619) 661-3650

SALES & MARKETING
POWER-SONIC CORPORATION
P.O. Box 5242
Redwood City, CA 94063 USA
Telephone: (650) 364-5001
Fax: (650) 366-3662

EUROPE
POWER-SONIC EUROPE LTD.
3 Buckingham Square, Hurricane way
Wickford, Essex SS11 8YQ, England
Telephone: (1268) 560686
Fax: (1268) 560902

http://www.power-sonic.com
E-mail: battery@power-sonic.com

PRINTED IN USA 25M 6/98

Bibliography

[1] OECD/EIA, *Energy Poverty: How to make modern energy access universal?* Special early excerpt of the World Energy Outlook , 52 (2010).

[2] T. Levin and V. M. Thomas, *Can developing countries leapfrog the centralized electrification paradigm?* Energy for Sustainable Development **31**, 97 (2016).

[3] N. Narayan, J. Popovic, J. C. Diehl, S. Silvester, P. Bauer, and M. Zeman, *Developing for developing nations: Exploring an affordable solar home system design,* GHTC 2016 - IEEE Global Humanitarian Technology Conference: Technology for the Benefit of Humanity, Conference Proceedings , 474 (2016).

[4] T. Den Heeten, N. Narayan, J. C. Diehl, J. Verschelling, S. Silvester, J. Popovic-Gerber, P. Bauer, and M. Zeman, *Understanding the present and the future electricity needs: Consequences for design of future Solar Home Systems for off-grid rural electrification,* Proceedings of the 25th Conference on the Domestic Use of Energy, DUE 2017 , 8 (2017).

[5] N. Narayan, V. Vega-Garita, Z. Qin, J. Popovic-Gerver, P. Bauer, and M. Zeman, *A modeling methodology to evaluate the impact of temperature on Solar Home Systems for rural electrification,* Energy for Sustainable Development (2018).

[6] K. Kawajiri, T. Oozeki, and Y. Genchi, *Effect of temperature on pv potential in the world,* Environmental Science & Technology **45**, 9030 (2011), pMID: 21851102, https://doi.org/10.1021/es200635x .

[7] V. Vega-Garita, A. P. Harsarapama, L. Ramirez-Elizondo, and P. Bauer, *Physical integration of PV-battery system: Advantages, challenges, and thermal model,* 2016 IEEE International Energy Conference, ENERGYCON 2016 (2016), 10.1109/ENERGYCON.2016.7514038.

[8] N. Narayan, T. Papakosta, V. Vega-garita, J. Popovic-gerber, P. Bauer, and M. Zeman, *A simple methodology for estimating battery lifetimes in Solar Home System design,* , 1238 (2017).

[9] C. Kulkarni, G. Biswas, and X. Koutsoukos, *Physics of failure models for capacitor degradation in DC-DC converters,* in *The Maintenance and Reliability Conference* (MARCON, 2010).

[10] D. C. Jordan, R. M. Smith, C. R. Osterwald, E. Gelak, and S. R. Kurtz, *Outdoor PV degradation comparison,* Conference Record of the IEEE Photovoltaic Specialists Conference , 2694 (2010).

[11] R. Adib, H. Murdock, F. Appavou, A. Brown, B. Epp, A. Leidreiter, C. Lins, H. Murdock, E. Musolino, K. Petrichenko, *et al.*, *Renewables 2016 global status report,* Global Status Report RENEWABLE ENERGY POLICY NETWORK FOR THE 21st CENTURY (REN21) (2016).

[12] A. A. Phadke, A. Jacobson, W. Y. Park, G. R. Lee, P. Alstone, and A. Khare, *Powering a Home with Just 25 Watts of Solar PV. Super-Efficient Appliances Can Enable Expanded Off-Grid Energy Service Using Small Solar Power Systems,* (2015), 10.2172/1229861.

[13] T. Urmee, D. Harries, and H.-G. Holtorf, *Photovoltaics for Rural Electrification in Developing Countries: A Road Map* (Springer, 2016).

[14] A. H. Smets, K. Jäger, O. Isabella, R. A. van Swaaij, and M. Zeman, *Solar Energy: The physics and engineering of photovoltaic conversion, technologies and systems* (UIT Cambridge Limited, 2016).

[15] PV Education, *Modules and array,* (2018), Cited 16-06-2018 from: http://www.pveducation.org/.

[16] D. C. Jordan and S. R. Kurtz, *Photovoltaic degradation rates - An Analytical Review,* (2013), arXiv:1303.4604 .

[17] V. Sharma and S. S. Chandel, *Performance and degradation analysis for long term reliability of solar photovoltaic systems: A review,* (2013).

[18] Fraunhofer Institute for Solar Energy SYstems, ISE, *Photovoltaics Report,* (2017).

[19] D. C. Jordan, S. R. Kurtz, K. VanSant, and J. D. Newmiller, *Compendium of photovoltaic degradation rates,* Prog. Photovolt: Res. Appl. **24**, 978 (2016).

[20] batteryuniversity.com, *Can the lead-acid battery compete in modern times?* (2010), Cited 18-08-2018 from: https://batteryuniversity.com/.

[21] J. Hoppmann, J. Volland, T. S. Schmidt, and V. H. Hoffmann, *The economic viability of battery storage for residential solar photovoltaic systems - A review and a simulation model,* Renewable and Sustainable Energy Reviews **39**, 1101 (2014).

[22] J. Yang, C. Hu, H. Wang, K. Yang, J. B. Liu, and H. Yan, *Review on the research of failure modes and mechanism for lead–acid batteries,* International Journal of Energy Research **41**, 336 (2017), arXiv:1011.1669v3 .

[23] S. Zhang, K. Xu, and T. Jow, *The low temperature performance of li-ion batteries,* Journal of Power Sources **115**, 137 (2003).

[24] G. K. A. Pesaran , S.Santhanagopalan, *Addressing the Impact of Temperature Extremes on Large Format Li-Ion Batteries for Vehicle Applications,* 30Th International Battery Seminar (2013).

[25] Power Stream, *Why does battery internal resistance increase over time?* (2017), Cited 19-08-2018 from: https://www.powerstream.com/.

[26] M. Ecker, J. B. Gerschler, J. Vogel, S. K??bitz, F. Hust, P. Dechent, and D. U. Sauer, *Development of a lifetime prediction model for lithium-ion batteries based on extended accelerated aging test data,* Journal of Power Sources (2012), 10.1016/j.jpowsour.2012.05.012.

[27] G. Ning, B. Haran, and B. N. Popov, *Capacity fade study of lithium-ion batteries cycled at high discharge rates,* Journal of Power Sources **117**, 160 (2003).

[28] A. Pesaran, *Battery Pack Thermal Design NREL Energy Storage R & D,* (2016).

[29] G. Graditi, G. Adinolfi, and G. M. Tina, *Photovoltaic optimizer boost converters: Temperature influence and electro-thermal design,* Applied Energy (2014), 10.1016/j.apenergy.2013.10.031.

[30] ST Microelectronics, *Calculation of conduction losses in a power rectifier,* , 1 (2011).

[31] K. Sun, L. Zhang, Y. Xing, and J. M. Guerrero, *A distributed control strategy based on DC bus signaling for modular photovoltaic generation systems with battery energy storage,* IEEE Transactions on Power Electronics **26**, 3032 (2011).

[32] K. Preiser and J. Kuhmann, *Device for testing solar home systems,* (2002), uS Patent 6,351,130.

[33] A. Mellit, M. Benghanem, and S. A. Kalogirou, *Modeling and simulation of a stand-alone photovoltaic system using an adaptive artificial neural network: Proposition for a new sizing procedure,* Renewable Energy **32**, 285 (2007).

[34] A. Joyce, C. Rodrigues, and R. Manso, *Modelling a PV system,* Renewable Energy **22**, 275 (2001).

[35] L. Fara and D. Craciunescu, *Output Analysis of Stand-alone PV Systems: Modeling, Simulation and Control,* Energy Procedia **112**, 595 (2017).

[36] Y. M. Irwan, A. R. Amelia, M. Irwanto, M. Fareq, W. Z. Leow, N. Gomesh, and I. Safwati, *Energy Procedia*, Vol. 79 (Elsevier B.V., 2015) pp. 596–603.

[37] V. Vega-Garita, D. D. Lucia, N. Narayan, L. Ramirez-Elizondo, and P. Bauer, *PV-Battery Integrated Module as a Solution for Off-Grid Applications in the Developing World,* Energycon 2018 , 1 (2018).

[38] H. Mufiaty, *Solar home systems performance in rural area in aceh case study: Deah mamplam village, aceh besar,* Energy Procedia **47**, 133 (2014).

[39] L. Nkhonjera and J.-C. Wu, *Performance Analysis of Battery Based Stand Alone Solar Home Systems in Malawi,* (2015).

[40] Krismadinata, N. A. Rahim, H. W. Ping, and J. Selvaraj, *Photovoltaic Module Modeling using Simulink/Matlab,* Procedia Environmental Sciences **17**, 537 (2013).

[41] M. K. Fuentes, *A Simplified Thermal Model for Flat-Plate Photovoltaic Arrays,* Sandia Report , 60 (1987).

[42] S. Dubey, J. N. Sarvaiya, and B. Seshadri, *Temperature dependent photovoltaic (PV) efficiency and its effect on PV production in the world - A review,* Energy Procedia **33**, 311 (2013).

[43] Simulink, *Generic battery model,* (2016).

[44] Badan Pusat Statistik, *Percentage of poor people by regency/municipality in nusa tenggara timur province, 2015-2017,* (2018), Cited 15-08-2018 from: https://ntt.bps.go.id/.

[45] D. Sasetyaningtyas, *Master's thesis: Sustainable business model for off-grid pv electrification in developing country,* Delft University of Technology (2018).

[46] Winrock, *Fuel independent renewable energy "iconic island",* (2010).

[47] Go100percent, *Sumba iconic island: 100% renewable energy,* (2018), Cited 15-08-2018 from: http://www.go100percent.org/.

[48] Sumba Iconic Island, *Sumba iconic island: 100% renewable energy,* (2016), Cited 15-08-2018 from: http://sumbaiconicisland.org.

[49] Hivos, *Sumba iconic island: Stakeholder leaflet,* (2015).

[50] (software)Meteonorm ver 7.1, *Metrotest,* (2018).

[51] N. Narayan, Z. Qin, and J. P.-g. J.-c. Diehl, *Stochastic load profile construction for the multi-tier framework for household electricity access using off-grid DC appliances,* **2016** (2018).

[52] M. Bhatia and N. Angelou, *Capturing the Multi-Dimensionality of Energy Access,* Livewire , 1 (2014).

[53] A. Jamodkar, *Master's thesis: Energy yield prediction of solar powered e-bike charging station,* Delft University of Technology (2017).

[54] R. Ross Jr and M. Smokler, *Flat-Plate Solar Array Project: Final Report: Volume 6, Engineering Sciences and Reliability*, Tech. Rep. (Jet Propulsion Lab., Pasadena, CA (USA), 1986).

[55] M. Masoudinejad, M. Kamat, J. Emmerich, M. Ten Hompel, and S. Sardesai, *A gray box modeling of a photovoltaic cell under low illumination in materials handling application,* Proceedings of 2015 IEEE International Renewable and Sustainable Energy Conference, IRSEC 2015 (2016), 10.1109/IRSEC.2015.7455081.

[56] A. N. Celik and N. Acikgoz, *Modelling and experimental verification of the operating current of mono-crystalline photovoltaic modules using four- and five-parameter models,* Applied Energy **84**, 1 (2007).

[57] N. C. Park, W. W. Oh, and D. H. Kim, *Effect of temperature and humidity on the degradation rate of multicrystalline silicon photovoltaic module,* International Journal of Photoenergy **2013** (2013), 10.1155/2013/925280.

[58] T. H. Kim, N. C. Park, and D. H. Kim, *The effect of moisture on the degradation mechanism of multi-crystalline silicon photovoltaic module,* in *Microelectronics Reliability* (2013).

[59] P. Loutzenhiser, H. Manz, C. Felsmann, P. Strachan, T. Frank, and G. Maxwell, *Empirical validation of models to compute solar irradiance on inclined surfaces for building energy simulation,* Solar Energy **81**, 254 (2007).

[60] P. Pellikka, *Land use changes in sub-Saharan Africa from local to continental,* (2010).

[61] U. Stutenbaeumer and B. Mesfin, *Equivalent model of monocrystalline, polycrystalline and amorphous silicon solar cells,* Renewable Energy **18**, 501 (1999).

[62] W. Xiao, W. G. Dunford, and A. Capel, *A novel modeling method for photovoltaic cells,* PESC Record - IEEE Annual Power Electronics Specialists Conference **3**, 1950 (2004).

[63] Jinko Solar, *Technical Datasheet (JKM265P),* (2015).

[64] D. S. Peck and C. H. Zierdt, *The Reliability of Semiconductor Devices in the Bell System,* Proceedings of the IEEE **62**, 185 (1974).

[65] L. A. Escobar and W. Q. Meeker, *A Review of Accelerated Test Models,* Statistical Science **21**, 552 (2006), 0708.0369 .

[66] Jinko Solar, *Technical Datasheet (JKM330P),* (2016).

[67] M. D. Kempe, *Modeling of rates of moisture ingress into photovoltaic modules,* Solar Energy Materials and Solar Cells (2006), 10.1016/j.solmat.2006.04.002.

[68] J. Vetter, P. Novák, M. R. Wagner, C. Veit, K. C. Möller, J. O. Besenhard, M. Winter, M. Wohlfahrt-Mehrens, C. Vogler, and A. Hammouche, *Ageing mechanisms in lithium-ion batteries,* Journal of Power Sources **147**, 269 (2005).

[69] P. Ruetschi, *Aging mechanisms and service life of lead-acid batteries,* Journal of Power Sources **127**, 33 (2004).

[70] R. Rao, V. Sarma, and D. N. Rakhmatov, *Battery Modeling for Energy-Aware System Design,* Computer (Long. Beach Calif) **36**, 77 (2003).

[71] O. Tremblay, *Experimental Validation of a Battery Dynamic Model for EV Applications Experimental Validation of a Battery Dynamic Model for EV Applications,* **3**, 289 (2009).

[72] P. Rong and M. Pedram, *An analytical model for predicting the remaining battery capacity of lithium-ion batteries,* IEEE Transactions on Very Large Scale Integration (VLSI) Systems **14**, 441 (2006).

[73] M. Doyle, T. F. Fuller, and J. Newman, *Modeling of galvanostatic charge and discharge of the lithium/polymer/insertion cell,* Journal of the Electrochemical Society **140**, 1526 (1993).

[74] C. M. Shepherd, *Design of Primary and Secondary Cells,* Journal of The Electrochemical Society **112**, 657 (1965).

[75] N. Narayan, T. Papakosta, V. Vega-Garita, Z. Qin, J. Popovic-Gerber, P. Bauer, and M. Zeman, *Estimating battery lifetimes in Solar Home System design using a practical modelling methodology,* Applied Energy **228**, 1629 (2018).

[76] O. Tremblay, L.-a. Dessaint, and A.-I. Dekkiche, *A Generic Battery Model for the Dynamic Simulation of Hybrid Electric Vehicles,* 2007 IEEE Vehicle Power and Propulsion Conference , 284 (2007).

[77] L. H. Saw, K. Somasundaram, Y. Ye, and A. A. Tay, *Electro-thermal analysis of Lithium Iron Phosphate battery for electric vehicles,* Journal of Power Sources **249**, 231 (2014).

[78] E. Raszmann, K. Baker, Y. Shi, and D. Christensen, *Modeling stationary lithium-ion batteries for optimization and predictive control,* 2017 IEEE Power and Energy Conference at Illinois, PECI 2017 (2017), 10.1109/PECI.2017.7935755.

[79] Valence, *U-charge u1-24rt battery module data sheet,* (2016).

[80] Power Sonic, *Ps-610-11 battery module data sheet,* (2011).

[81] A123 Energy Solutions, *Battery pack design, validation and assembly guide using 123 systems amp20hd-a nanophosphate cells,* (2014).

[82] T. Papakosta, *Master's thesis: Investigating hybrid battery configuration for solar home systems,* Delft University of Technology (2018).